THE ANALYSIS OF

INTERCONNECTED SHEAR WALLS

Thesis submitted for the degree of

Doctor of Philosophy

of the

University of Edinburgh

by

Alastair J.M. Soane, B.Sc.

March 1966

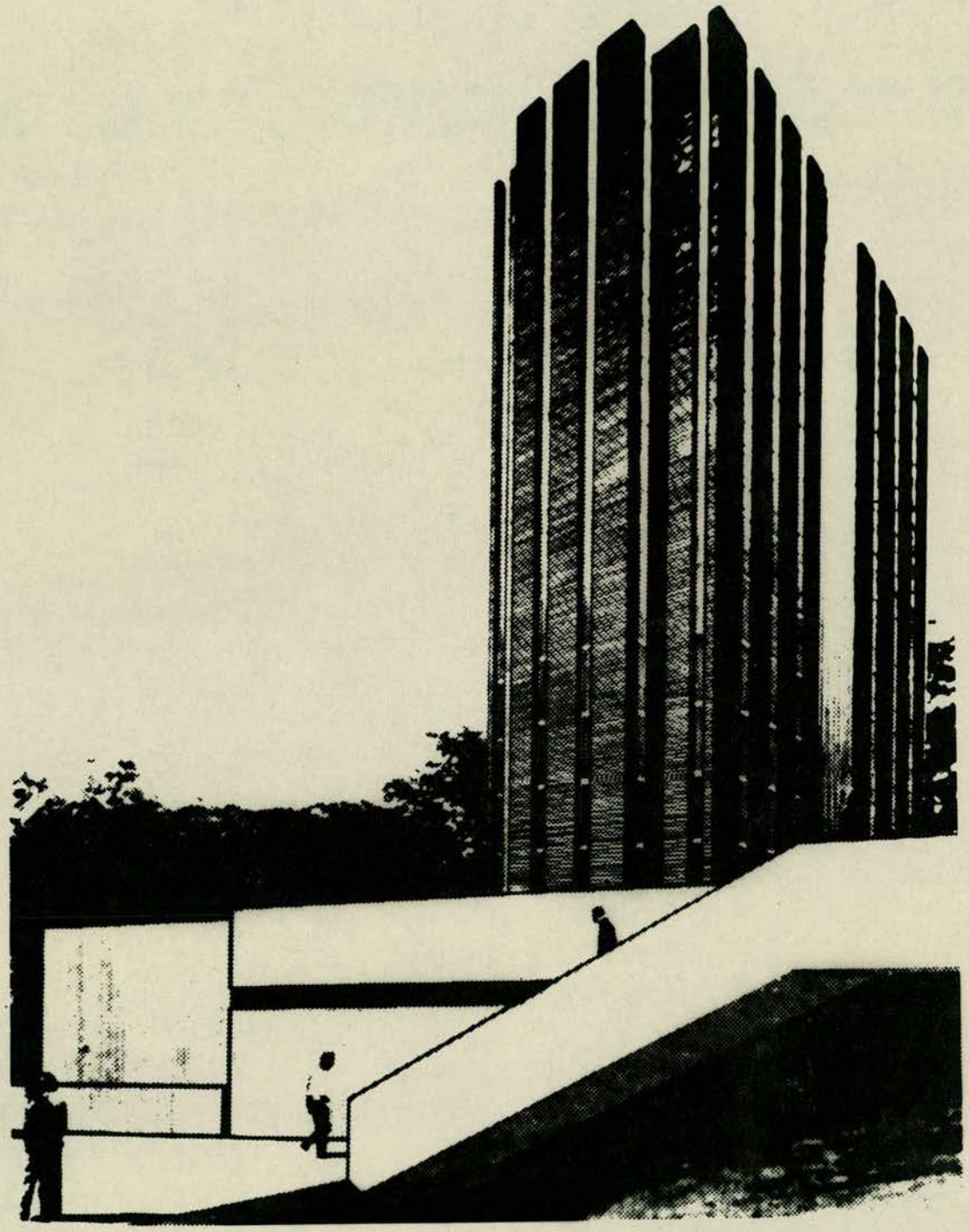

Artists impression of one of the Essex University residence blocks.

CONTENTS

LIST OF FIGURES

SYNOPSIS

It has been known for some time that special methods of lateral load analysis are required for interconnected shear walls and for frameless structures. Current techniques are hence described for the analysis of these problems and the related problems of frames. The continuum approach of replacing the connecting elements between walls by continuous media is discussed, and it is shown that the existing solutions are cumbersome for all for all but the simplest cases.

The derivation is then extended to a general system of plane walls and a new method is postulated for solving the equations - analogue computation. Analogue simulation is described and it is established that a trial and error method is required to find unknown boundary values. To simplify the method a special technique is developed to use analogue memory circuits for iteration purposes. The technique is valuable because the size of structure which can be analysed is now limited by machine capacity only and not, as is often the case, by solution difficulties.

A number of two wall symmetrical structures are treated and typical results are compared with experimental data from models and with digital computer solutions. Non-dimensional design charts are presented and the range of structures is given for which the analysis is valid.

Among the largest load-bearing brickwork structures in this country are the new (1966) residence towers for Essex University. To investigate their behaviour a Perspex model was built and tested and comprehensive experimental data was obtained from stress and deflection measurements. A mathematical model was then devised to simulate the physical model and the solution was found by analogue computation. The theoretical results compare well with the experimental measurements so a further tower block was

analysed by analogue simulation.

The conclusions indicate that the continuum method is a satisfactory basis for analysis and that analogue computation is currently the best technique for obtaining solutions.

Appendix A contains the principal notation while Appendices B and C deal with some detailed aspects of electronic equipment which was used in the course of the work. The last two Appendices are concerned with experimental analyses carried out concurrently with the main topics. In Appendix D the effective width of slabs as beam elements is calculated from the results of a model test. Appendix E covers the investigation, by photo-elasticity, of stress distributions which would be caused by the erection of a proposed building above a section of the Mersey tunnel.

1. INTRODUCTION

This Thesis is concerned with the behaviour of interconnected walls in tall buildings subjected to lateral loading. Lateral loads are most often due to wind action but they may also be caused by earthquakes or explosive blasts. The higher the structure the greater are the magnitudes and importance of such loads.

The earliest high-rise buildings were constructed with load-bearing masonry walls. Some were remarkably tall and one of the finest examples was completed in Chicago in 1891 - the sixteen storey Monadnock building. The 200 ft high walls were designed to carry both vertical and lateral loading and as a result of the approximate methods of analysis then available the walls are 6 ft thick at the base. This structure, however, seemed to be the ultimate in frameless building and a commemoratory plaque declares it to be: "The final triumph of traditional masonry construction".

To build higher it appeared that walls would have to become thicker and hence take up an increasingly large volume of internal space. So, in the search for economy, designers began to pioneer the use of relatively light rectangular frames in the construction of tall buildings. Although these frames can satisfactorily carry vertical loads they are generally inadequate to resist lateral forces. Additional structural elements must therefore be incorporated, the purpose of which is wholly or partially to provide lateral rigidity. An effective stiffening element for this purpose is the cantilever wall.

If the walls are built specifically to carry lateral loading they are normally set out in plane arrays and are interconnected at each storey level by beams or floor slabs. These represent the simplest interconnected shear wall systems. In all residential or commercial structures however, internal and external walls are built for a variety of functional requirements. External walls must be weather proof and provide an adequate measure of thermal and accoustic insulation. Non-structural internal walls must provide accoustic insulation while internal structural walls may be required for lift towers and service ducts. Foremost among the materials for wall construction are reinforced concrete and brickwork, and apart from their insulation properties such walls are capable of resisting lateral forces. It may not therefore be necessary to include special stiffening elements if there are design methods which will permit the use of walls which also have non-structural functions within the frames.

From 1951 onwards frameless blocks in load-bearing brickwork have been erected in several European countries, notably Switzerland. The Continental bricks are generally of the perforated type and the load-bearing walls have thicknesses varying from 39 cm (15.4 in) to 15 cm (6 in). The structures are normally built up from storey height brickwork wall units and reinforced concrete floors, a form which is particularly suitable for residential buildings which have a large number of internal and external walls on a repeated floor plan. Since the walls are combined into units to provide rigidity

in all directions and since the units are interconnected by the floor slabs the result is a partially composite system - an extension of the plane shear wall assembly.

As yet there has been only limited exploitation of highly stressed brickwork in this country, the main reason being a basic lack of knowledge which had led to conservative recommendations in the Code of Practice (C.P.111). Extensive research into the properties of brickwork has been carried out in recent years and much information has been obtained on fundamental and applied problems. As a result of this work the Code of Practice was revised (1964) and engineers and architects are selecting load-bearing brickwork for an increasing number of projects.

Much of the research has been devoted to simple elements such as walls and piers under vertical and lateral loading, and experimental results have been used to establish basic formulae concerning the structural behaviour of the elements. With this information and the necessary conditions of equilibrium and compatability, a system built up from a number of elements may be expressed in terms of a mathematical model, and the solution of this model will provide a basis for design. If however, a real system is so complex that existing mathematical techniques are inadequate then recourse must be made to analysis by means of small scale physical models. Interconnected shear wall problems are beginning to emerge from the latter category (1966). Within the elastic range their inherent properties are known but there is doubt as to the best way

of representing them mathematically. Exact simulation is a formidable problem and approximations are necessary to bring the volume of computation to an acceptable level. The validity of these approximations can only be checked at present with model tests.

The present work is concerned with the analysis of lateral loads in simple and complex shear wall structures. Loading is assumed to be static in accordance with C.P.3 Chapter V, and behaviour is assumed to be ideally elastic. The method which has been adopted is unusual in that it requires analogue simulation for problem solution.

The advantages of modern electronic analogue computers have been largely neglected by structural engineers and this neglect may be attributed to the dominant position occupied by digital computers and the relatively small number of analogue machines. Admittedly there are structural problem which are quite unsuited to analogue simulation, but tall interconnected walls can be conveniently treated.

2. REVIEW OF PREVIOUS WORK

2.1 Summary

Previous work on tall shear walls has followed two main lines of thought. Firstly, approximate methods have been developed which are based on the substitution of the connecting beams by continuous media. Despite this simplification the solutions are difficult to obtain by conventional techniques and the methods have not been extended to deal with general cases. Secondly, plane frame techniques have been adapted to take account of large differences in the stiffnesses of vertical and horizontal members. These methods usually require digital computation for the analysis of tall structures.

Detailed studies have been made on single panels but the results are only of indirect use for multi-storey walls.

2.2 Continuum methods

A convenient analytical device for dealing with arrays of equal discrete members is the use of a continuum. An array of individual members is replaced in a substitute system by a medium which has appropriate stiffness properties per unit length. All variables may then be expressed in terms of continuous functions and the number of redundants is greatly reduced. This approach was extensively used by Pippard (1)* for problems presented by wire wheels, interconnected bridge-girders, and similar structures. His work was followed by Chitty (2) in 1947 who considered a number of interconnected cantilever beams.

---

* Figures in parenthesis denote references at the end of the text.

No restraint is placed on the relative stiffnesses of column and beams, but the method assumes that structures are composed of line elements so that the interconnecting beams bend about the centroids of the columns. Using elementary structural mechanics, sets of 2nd and 4th order differential equations are derived for a variety of cases. In the simplest two column frames, axial deformation of the columns is accounted for, but in general it is neglected. The equations relate forces in terms of continuously differentiable functions of height and their solution follows classical lines. A general solution form is stated and end conditions are applied to evaluate constants of integration.

Two special examples are treated in which the structure has non-uniform properties. In the first the beam properties vary from bay to bay and in the second the columns have continuously varying cross-sections. Particular solutions are given on the basis of inextensible deformation but the form is so complex that evaluation would be most tedious. The method is stated to be applicable to frames in which the stiffnesses of the beams approach those of the columns. The accuracy however is doubtful in such a case and the method has been superseded by techniques which take into account the width of the walls.

Such a technique, using continuous media in place of slender beams, was developed by Eriksson [3] in 1960 in his work on the analysis of wind bracing walls in multi-storey housing. The procedure was applied to buildings with sixteen storeys and a wall to beam inertia ratio of about 600:1.

The derivation will not be given in detail because a similar method is developed in Chapter 3. Briefly however the shear functions at the centres of connecting media are specified as redundants to establish a

2nd order differential equation for each medium. Eriksson's equations are accurate in that they include terms to account for bending and shear deformation of the media, and bending and axial deformation of the walls. The solution is in terms of cosh and sinh functions and once the redundants are known all other forces may be found by statics.

A possible extension of the method for the case of N plane walls is suggested but the volume of computation is so large that it is only practical to calculate maximum values for structures with, at most, three walls. Despite this limitation the work provides a clear and valuable explanation of the fundamental behaviour of simple systems.

Following Eriksson a number of methods were presented which used the same basic techniques. The derivations differed somewhat but a comparative study indicates only minor variations in results. Beck (1962)[4] deals with the symmetrical case of two equal walls as a Vierendeel girder with one free end and one fixed end. A general solution is sought, but for high ratios of wall to beam stiffness simplifications are introduced to cut down the amount of calculation. Some specimen graphs are given in non-dimensional form for the calculation of maximum forces and deflections. under constant horizontal loading.

Rosman[5,6] did similar work but includes factors to allow for either pinned or fixed portal foundations and for foundation movement. In this instance the continuum equation are derived from energy considerations and two solutions are proposed. One is similar to Eriksson's and the other is based on finite difference approximations.

Little experimental evidence has been produced but Arcan (1964)[7] published the results of some photo-elastic work. His theoretical method is similar to those just described and the solutions are applied to two wall structures. Both symmetrical and unsymmetrical cases are treated and

favourable experimental agreement is obtained for edge wall stresses and for connecting beam forces. Non-dimensional graphs are given for the redundant forces at the centre of the connecting medium for uniform, triangular and point loads.

Current developments of the continuum method are proceeding at the Universitites of Southampton (Coull [8]) and Edinburgh.

2.3 Discrete methods

A further approach is to consider interconnected walls as a special type of frame and modify existing techniques. Normal plane frames may be thought of as a regular grid of node points linked by line elements. For a frame in which the stiffnesses of the beams are of the same order as the stiffnesses of the columns it is only necessary to consider bending of the members. If a frame has wall elements however, the importance of axial and shear deformations must be contemplated.

Either forces or displacements may be selected as unknowns. The first choice generally results in fewer equations but the second is simpler to deal with in a systematic manner. Both methods have been used for some time for multi-storey skeletal frames by, for example, Kani [9], Livesley [10], and Brotton [11].

Zbirokowski-Koscia [12] in 1958 dealt with a single cross wall, with one row of openings, as an approximate frame. He considers two type of foundation, the first being infinitely rigid. The moment area method is used to find the slope for each storey and hence give a set of N linear equations for an N storey building. These are solved by standard algebraic methods so the volume of computation is large. For very tall frames an interpolation process is suggested to group together numbers of cross beams.

The second type of foundation material is assumed to be capable of exhibiting elastic settlements proportional to the applied pressure.

Although the technique is sound it would be difficult to decide on site values for K_1, the coefficient characteristic of the soil. Data is reproduced from German and Russian soil tests but these are unconfirmed.

Green (13) (1952) suggested a procedure based on the portal method for frames for the analysis of bracing walls in multi-storey buildings. The assumptions here included inextensible deformations of walls and beams, and the existence of points of inflection at the mid-points of all wall and beam spans. The number of redundants is thus reduced and shear forces and bending moments can be calculated with the aid of stiffness factors. Overall deflection is found for an equivalent cantilever whose moment of inertia is the sum of the inertias of the individual walls with a correction factor to allow for the increased rigidity given by the beams.

In those cases where the relative stiffnesses of the members are similar, the stress conditions given by this method would be approximately correct but the shape of the deflection curve would be inaccurate. For a system with wide walls and relatively flexible beams the analysis would be spurious because the assumptions concerning the wall behaviour are fundamentally incorrect.

More valid assumptions were made by Clark (14) when he considered the deflection of laminated beams. Each beam was composed of two leaves riveted together at a number of points. Loading was at right angles to the direction of lamination so the rivets served to resist shear forces and distribute axial forces to the leaves. Although the method of solution provides insight into the behaviour of connected beams it is too cumbersome to be extended to buildings.

An analogous beam was used by Deschapelles (15) (1962) to represent a symmetric pair of walls. He assumed that the walls are inextensible and

that the effective beam length is the centroid to centroid distance between the walls.

Slope deflection is used to find the shear in the cross beams in terms of elastic joint rotations. It is then demonstrated that the real structure may be replaced by a continuous beam with suitable hinges and supports. The analogous beam can be solved by discrete or continuum methods.

Frischmann Prabhu and Toppler (1963) [16] have described two methods.

(i) An approximate solution based on an equivalent column, and,

(ii) An "exact" method employing influence coefficients.

In the first of these (i) the inertias of all columns and walls are summed, as are the stiffnesses of all beams, at each storey level. The resulting equivalent structure is a single column subject to the externally applied load and a series of bending moments from the beams. In many aspects the solution of this is similar to the continuum approaches but is somewhat simpler because bending only is considered.

The degree of redundancy of a frame is expressed as:

$$n_s = 3(M - N + 1) - r$$

where n_s is the degree of statical indeterminacy,

M is the number of members,

N is the number of nodes,

r is the number of releases already present.

The second method (ii) involves making n_s releases on the structure. Superposition is used, together with tabulated coefficients, to set up a matrix whose solution requires digital computation. In both methods the width of a shear wall is taken into account by assuming an infinitely stiff connection between the centroid of the wall and its face.

The combination formed from one full height shear wall and a number of frames was studied by Rosenblueth and Holtz [17] in 1960.

They consider the wall as a cantilever beam supported elastically by the surrounding frames, and two methods of successive approximations are developed for analysing the system. It is assumed that the shear in a given storey is proportional to the average slope in the storey and that the stiffnesses of a number of plane frames may be summed to give the equivalent stiffness for a single frame. By considering the interaction of this frame and a wall, a set of 1st order equations can be set up relating slopes, shears, and moments on the wall. An initial estimate is then made of the shear force distribution and the estimate is refined by iteration cycles until there is a satisfactory degree of convergence.

The second method is adapted from Newmark's work on buckling and produces a nonhomogeneous differential equation in terms of slope. Again iteration is used for the solution although preliminary results may be obtained from prepared tables. However, the theories only apply when the frame is very much less stiff than the wall and is hence not directly applicable to the problems of a number of interconnected walls. Similar systems were studied by Cardan [18] in 1961.

A most comprehensive paper was presented by Khan and Sbarounis [19] in 1964 on the interaction of walls and frames. Their aim was to provide designers with a direct method and they include a number of graphs and tables for this purpose. The method is applicable to any number of frames connected to any number of shear walls. A structure is divided into two basic parts, an equivalent frame and an equivalent shear wall. The stiffness properties of the various elements are summed to give the stiffnesses of the simplified system. Such a substitution introduces errors but the authors consider these to be insignificant for typical buildings.

The first step in analysis is to determine the lateral load distributed

on the walls and frame at each storey. The second phase is an iterative solution to conform with equilibrium and compatability conditions between the frame and the wall. The number of cycles required depends on the type of structure, the accuracy of the first estimates, and the desired final accuracy. Techniques are developed for "forced -convergence-corrections", and using these the equations for a structure with very stiff walls can be solved in three cycles. In general, however, ten or twenty cycles are required and a digital computer is essential. Forces and moments in the equivalent structure are then re-distributed in the real one. Also dealt with are foundation rotations and plastic hinges in the walls. Tentative recommendations are made on the effectiveness of slabs as beam elements.

The merits of power series solutions were advocated by Bandel (20) in 1962 for the problems of frames combined with shear trusses or shear walls. Virtual work is used to establish the series for joint rotations in a general frame connected to a truss, or a wall which can be replaced by an equivalent truss. The equations are set up to minimise the number of the redundants but notwithstanding this the evaluation is lengthy, particularly if there is no axis of symmetry. A sixty storey tower is analysed and the important influence of axial deformations is demonstrated. When axial effects are included the lateral deflections are three times as large as when they are neglected.

By 1964 the use of large digital computers was well established for the analysis of large frames and Clough, King and Wilson (21) produced a systematic method for setting up stiffness equations. The method is exact, subject to certain restrictions about the regularity of the system.

The stiffness of each storey element is expressed in matrix form with 10 degress of freedom. The stiffness of the complete frame is then obtained by superposition to give a tri-diagonal matrix which may be solved with the aid of a FORTRAN programme. If the programme is available this method is most powerful and is particularly suited to very large regular frames with a limited number of walls.

A slightly different approach was adopted by Tezcan[22], also in 1964, for frame problems. In this case the moment coefficient matrix is used rather than a stiffness or flexibility matrix. The author claims that these are more readily generated on a computer and solution time is thereby reduced. A necessary simplification is to neglect the changes in lengths of all members.

Some of the discrete methods described have been programmed by Batchelor and Cranston of the Cement and Concrete Research Association (see also Chapter 5). A refined technique using finite elements is currently being developed by McLeod[23] at the University of Glasgow.

2.4 Single panels

Much of the practical work on walls has been devoted to single storey units. Their height to width ratio is approximately 1:1 so the behaviour is not of the same type as the tall cantilever walls already discussed.

Benjamin and Williams[24,25, 26, 27] have conducted many tests on single panels, with and without openings, in reinforced concrete, brickwork, and masonry. All specimens were loaded to failure, generally by racking tests but in some cases by direct exposure to atomic blasts. The results have been extended to a theoretical level by Benjamin[28] who gives a method for calculating the forces in an array of walls interconnected by a diaphragm. The procedure is complex because both bending and shear

compatability must be satisfied. It has only been applied to one and two storey buildings and is unsuitable for tall blocks.

Single infilled panels have been tested by Holmes [29, 30], Wood [31] and Smith [32]. The reinforced concrete or steel frames were loaded vertically and then jacked laterally. Holmes equated the infilling to an equivalent diagonal strut and has given empirical formulae. The stiffness imparted by the infilling is demonstrated by a typical case examined by Wood. The frame alone failed at a racking load of 9.3 tons, but with $4\frac{1}{2}$" brickwork infilling it took 49 tons, and with $13\frac{1}{2}$" brickwork, the failure load was 135 tons.

Full scale tests have been performed at the Building Research Station [33,34] on single brick panels and on the interaction of floors and beams. The panel tests with and without openings are compared with solutions from a biharmonic stress function.

The Structural Ceramics Research Unit [35] has been set up at the University of Edinburgh to investigate all aspects of load bearing brickwork. Full scale panels have been tested under vertical loads only but a technique has been developed for lateral loading tests on model brickwork. Murthy [36] has examined model brick structures up to three storeys in height and provided data for combined vertical and horizontal loading. The work has been considerably extended by Sinha [37] who is testing interconnected shear panel models up to five storeys high. The experiments are supported by theoretical solutions for stress distributions and modes of failure.

Photo-elastic experiments have been carried out by Amaratunga [38] and Liauw [37] on panels. They were concerned with stress distribution around openings and theoretical solutions are presented for equivalent grid frames and by stress functions.

3. CONTINUUM THEORY

3.1 Assumptions

A combination of walls and floor slabs or beams forms a statically indeterminate structure which, because of the large number of redundancies, is difficult to analyse by exact methods. If, however, the discrete connecting elements are replaced in a mathematical model by continuous media, having appropriate stiffness properties, the system can be expressed approximately in terms of continuously varying functions. The number of redundancies is reduced to one per medium.

In this Chapter a general plane structure with K walls and n(= K-1) interconnecting sets of beams or slabs will be considered from basic structural concepts in order to derive the necessary differential equations. The notation is introduced as required and is also given in Appendix A.

So that the volume of computation can be brought to a manageable level the following assumptions will be made:

1. All behaviour is elastic.
2. The boundary conditions are known at foundation level.
3. Moments and shears from the external lateral load are distributed among the walls in proportion to their moments of inertia.
4. The points of inflection of connecting elements in the real system, and connecting media in the equivalent system, are at their centres.
5. The connecting elements are inextensible so that the lateral deformations of the walls are the same at any given level.

The validity of (1) is dependent on the construction material but for reinforced concrete or for brickwork it is approximately correct within the range of stresses normally used for design purposes. Assumption (2) can allow for differential settlement but to avoid the large stresses which this

could induce, the foundations would normally be designed as rigid rafts and a correction would be added for deflections caused by body rotation.

In the process of derivation a statically reduced system is introduced which is equivalent to a row of cantilevers interconnected with pinned struts and the distribution of moments in this is proportional to the flexural stiffnesses of the walls. The assumption concerning shear distribution is only an approximation but since bending deflections of the walls are considerably greater than shear distortions it will not give serious errors.

The existence of central points of inflection is only true for a symmetric structure with two walls, but where the stiffnesses of all the walls are of similar orders of magnitude the points of inflection can be assumed to be so near the centres that errors from this cause are negligible.

Assumption (5) has been verified experimentally to be valid for the type of structure considered here. The substitution of a continuous medium requires that the stiffnesses of the beams in any vertical row are constant throughout the height of the structure. An exception is the topmost beam which is assumed to have half the inertia and half the area of the others.

3.2 Equilibrium conditions

A typical array of plane walls is shown in Fig. 3.1 and the first step is to replace the connecting beams with continuous media whose moment of inertia per unit height is I_h/d, where I_h is the moment of inertia of a beam and d is the storey height. To make the system statically determinate the media are cut through their points of inflection and the free body forces to restore equilibrium are shown in Fig. 3.2 for two of the walls in a general system. The vertical shear force per unit height at the cut edges

of medium is dR_m/dx or R'_m where the prime denotes differentiation with respect to the height co-ordinate x measured from the top of the building.

If free distortion is permitted then the cut edges at any given height will be a distance Δ_m apart (Fig. 3.3) and a shear constant K_m is expressed as:

$$K_m = \frac{R'_m}{\Delta_m} \qquad (3.1)$$

A section in the medium of unit thickness and length e/2 may be considered as a cantilever fixed to the wall and with a force R'_m applied to the free end. The tip deflection will be:

$$\delta = \frac{R'_m \cdot d}{3.E_s \cdot I_h} \left(\frac{e_m}{2}\right)^3 + \frac{R'_m \cdot \chi \cdot d}{G \cdot b \cdot h} \left(\frac{e_m}{2}\right) \qquad (3.2)$$

The first term on the right hand side is deflection due to bending and the second is due to shear.

where d is the storey height,

e is the clear span between the walls,

E_s is the modulus of elasticity of the connecting elements,

G is the modulus of rigidity of the connecting elements,

h is the depth of a beam,

I_h is the moment of inertia of a beam ($bh^3/12$)

χ is the shear distribution constant for a rectangle (1.2)

Since $\Delta = 2\delta$ for a central point of inflection, equation 3.2 may be re-arranged and substituted into equations 3.1 to yield:

$$K_m = \frac{12\ E_m \cdot I_h}{d_m \cdot e_m^3 \left(1 + \chi \frac{E_m}{G_m} \left(\frac{h_m}{e_m}\right)^2\right)} \qquad (3.3)$$

The shear force R_m is defined as:

$$R_m = \int_o^x R'_m \, . \, dx \qquad (3.4)$$

Lateral compressive forces in the media can be divided into two components.

1. The compression which would occur if the beams were pin-connected to the walls, and
2. The additional compression which occurs as a result of the beams being fixed between walls of different stiffnesses.

Component (1) is inherent in the argument for assumption (3) to give the distribution of statically determinate moments. Component (2) is denoted dt/dx per unit height and the moment which this applies to wall m is:

$$M_{t',m} = \int_o^x t'_m \, . \, x \, . \, dx \qquad (3.5)$$

Since the wall moments from the external load in the statically determinate system (M_{oa}, M_{ob}, ... M_{oj}, M_{ok}) are those which would apply to the walls as a row of simple cantilevers, they are proportional to the flexural stiffnesses of the walls.

$$M_{oj} = M_o \frac{I_j}{I_o} \qquad (3.6)$$

where M_o is the total external moment from the lateral load at any given level,

I_j is the moment of inertia of wall J,

I_o is the sum of the moments of inertia of all the walls,

($I_o = I_a + I_b + I_c + ... I_k$)

Therefore at any distance x below the top the net moments on the walls (M_a, M_b, ... M_j, M_k) are: (see also Fig. 3.2)

$$M_a = M_{oa} - R_1 c_{1a} - M_{t',1}$$

$$M_b = M_{ob} - R_1 c_{1b} - R_2 c_{2b} + M_{t',1} - M_{t',2} \qquad (3.7)$$

.....

$$M_j = M_{oj} - R_m c_{mj} - R_n c_{nj} + M_{t',m} - M_{t',n}$$

It has been assumed that the deflected profile of all walls is the same, so:

$$y_a = y_b = y_c \quad ..... = y_j = y_k \qquad (3.8)$$

where y is the deflection measured from the deflected position

For simple bending of the walls,

$$\frac{d^2 y_a}{dx^2} = \frac{M_a}{E_w I_a}, \qquad \frac{d^2 y_b}{dx^2} = \frac{M_b}{E_w I_b} \qquad \text{etc.}$$

where E_w is the modulus of elasticity of the walls.

Therefore:

$$\frac{M_a}{E_w I_a} = \frac{M_b}{E_w I_b} = ... = \frac{M_j}{E_w I_j} = \text{constant.} \qquad (3.9)$$

The equations in set 3.7 can hence be divided by the appropriate EI values to give j simultaneous equations all equal to the above constant. The unknown $M_{t'}$ quantities may be found by normal algebraic processes in terms of known dimensional constants and the R functions.

$$M_{t',1} = -\frac{I_a}{I_o} R_1 \left(c_{1a} \left(\frac{I_o}{I_a} - 1\right) - c_{1b} \right) + \frac{I_a}{I_o} \left(R_2c_2 + R_3c_3 + \ldots\ldots + R_nc_n\right)$$

$$M_{t',2} = -\frac{I_o - I_a - I_b}{I_o} R_1c_1 - \frac{(I_a + I_b)}{I_o} R_2 \left(c_{2b} \left(\frac{I_o}{I_a + I_b} - 1\right) - c_{2c} \right)$$

$$+ \frac{(I_a + I_b)}{I_o} \left(R_3c_3 + R_4c_4 + \ldots\ldots\ldots + R_nc_n\right)$$

$$M_{t',3} = -\frac{I_o - I_a - I_b - I_c}{I_o} \left(R_1c_1 - R_2c_2\right)$$

$$- \frac{(I_a + I_b + I_c)}{I_o} R_3 \left(c_{3c} \left(\frac{I_o}{I_a + I_b + I_c} - 1\right) - c_{3d} \right)$$

$$+ \frac{(I_a + I_b + I_c)}{I_o} \left(R_4c_4 + R_5c_5 + \ldots\ldots\ldots + R_nc_n\right)$$

etc. equations (3.10)

3.3 Continuity conditions

By assuming that the points of inflection of the media are at their centres the only criterion of continuity is zero relative movement between adjacent cut edges of the media. Figure 3.3 shows the free displacements of walls I and J under the action of the net moments M_i and M_j and the axial forces R_l, R_m, and R_n. The displacements of any element of media n between these walls at a distance x below the top can be set out in tabular form.

TABLE 3.1

Relative displacements of the mth medium

force component	displacement
axial force R_l on wall I	$+ \int_x^L \frac{R_l}{E_w A_i} dx$
axial force R_m on wall I	$- \int_x^L \frac{R_m}{E_w A_i} dx$
axial force R_m on wall J	$- \int_x^L \frac{R_m}{E_w A_j} dx$
axial force R_n on wall J	$+ \int_x^L \frac{R_n}{E_w A_j} dx$
bending moment M_i on wall I	$+ \int_x^L \frac{M_i \cdot c_{mi}}{E_w I_i} dx$
bending moment M_j on wall J	$+ \int_x^L \frac{M_j \cdot c_{mj}}{E_w I_j} dx$

The sum of these must be equal the unrestrained displacement Δ_m which has already been defined as:

$$\Delta_m = \frac{R'_m}{K_m}.$$

Differentiating with respect to x.

$$\frac{R''_m}{K_m} = \frac{1}{E_w} \left(\frac{R_l}{A_i} - \frac{R_m}{A_i} - \frac{R_m}{A_j} + \frac{R_n}{A_j} + \frac{M_i \cdot c_{mi}}{I_i} + \frac{M_j \cdot c_{mj}}{I_j} \right) \qquad (3.11)$$

The form of equation 3.11 applies to all media with the exception of the two outermost ones which must have one less axial deformation term.

A complete set is given below:

$$\frac{R''_1}{K_1} = \frac{1}{E_w}\left(-\frac{R_1}{A_a} - \frac{R_1}{A_b} + \frac{R_2}{A_b} + \frac{M_a \cdot c_{1a}}{I_a} + \frac{M_b \cdot c_{1b}}{I_b} \right)$$

$$\frac{R''_2}{K_2} = \frac{1}{E_w}\left(+\frac{R_1}{A_b} - \frac{R_2}{A_b} - \frac{R_2}{A_c} + \frac{R_3}{A_c} + \frac{M_b \cdot c_{2b}}{I_b} + \frac{M_c \cdot c_{2c}}{I_c} \right)$$

.....

$$\frac{R''_m}{K_m} = \frac{1}{E_w}\left(+\frac{R_l}{A_i} - \frac{R_m}{A_i} - \frac{R_m}{A_j} + \frac{R_n}{A_j} + \frac{M_i \cdot c_{mi}}{I_i} + \frac{M_j \cdot c_{mj}}{I_j} \right)$$

equations (3.12)

3.4 Differential equations

The expressions for M_t, given in equations 3.10 may now be substituted in equations 3.7 to give the wall moments M in terms of the R functions and the external moment M_o. These, in turn, may be substituted into equations 3.12 to give a set of differential equations incorporating the redundant R functions, their second derivatives R", the external moment, and constants.

Their form is as follows:

$$R''_1 = R_1 \alpha^2_{11} + R_2 \alpha^2_{21} + R_3 \alpha^2_{31} + ... + R_m \alpha^2_{m1} - M_o \beta_1$$

$$R''_2 = R_1 \alpha^2_{12} + R_2 \alpha^2_{22} + R_3 \alpha^2_{32} + ... + R_m \alpha^2_{m2} - M_o \beta_2 \qquad (3.13)$$

.....

$$R''_m = R_1 \alpha^2_{1m} + R_2 \alpha^2_{2m} + R_3 \alpha^2_{3m} + ... + R_m \alpha^2_{mm} - M_o \beta_m$$

The α^2 and β constants which emerge from the substitution depend only on the geometry of the structure and the elastic moduli of the walls and beams. They are stated for the general case in an abbreviated manner.

$$\alpha^2_{11} = \frac{K_1}{E_w I_o} \left(c_1^2 + \frac{I_o}{A_a} + \frac{I_o}{A_b} \right)$$

$$\alpha^2_{21} = \frac{K_1}{E_w I_o} \left(c_1 c_2 - \frac{I_o}{A_b} \right)$$

$$\alpha^2_{31} = \frac{K_1}{E_w I_o} \, c_1 c_3$$

.....

$$\alpha^2_{n1} = \frac{K_1}{E_w I_o} \, c_1 c_n$$

$$\alpha^2_{12} = \frac{K_2}{K_1} \, \alpha^2_{21}$$

$$\alpha^2_{22} = \frac{K_2}{E_w I_o} \left(c_2^2 + \frac{I_o}{A_b} + \frac{I_o}{A_c} \right)$$

$$\alpha^2_{32} = \frac{K_2}{E_w I_o} \left(c_2 c_3 - \frac{I_o}{A_c} \right)$$

$$\alpha^2_{42} = \frac{K_2}{E_w I_o} \, c_2 c_4$$

.....

$$\alpha^2_{n2} = \frac{K_2}{E_w I_o} \, c_2 c_n$$

$$\alpha^2_{1n} = \frac{K_n}{K_1} \, \alpha^2_{n1}$$

$$\alpha_{2n}^2 = \frac{K_n}{K_2} \alpha_{n2}^2$$

.....

$$\alpha_{nn}^2 = \frac{K_n}{E_w I_o} \left(c_n^2 + \frac{I_o}{A_j} + \frac{I_o}{A_k} \right)$$

$$\beta_1 = \frac{K_1}{E_w I_o} c_1$$

$$\beta_2 = \frac{K_2}{E_w I_o} c_2$$

.....

$$\beta_n = \frac{K_n}{E_w I_o} c_n$$

equations (3.14)

3.5 Boundary conditions

Equations 3.13 are simultaneous 2nd order differential equations with constant coefficients. There is one independent variable, height x, and n(= K - 1) dependent variables R_1, R_2, ... R_n for a structure with K plane walls. Their solution is governed by boundary conditions.

At the free end (x = 0) the R functions are zero and the R' functions, in general, have finite values. At foundation level (x = L), R is finite and R' is approximately zero if the depth of the beams is small compared with the storey height.

The conditions may be stated for any medium as:

x = 0 R = 0

R is unknown

x = L R is unknown

R' = 0 (ideal structure)

These are of the mixed variety and particular solutions of the equations can only be found when the unknown conditions are ascertained for all media at the same boundary.

3.6 Deflection equations

Lateral deflection of the structure will be principally due to bending since shear distortion is small in the walls of a multi-storey building. For the case of inextensible beams the bending deflection can be found by a double integration of any of the bending functions.

$$\frac{d^2y}{dx^2} = \frac{M_a}{E_w I_a} = \frac{M_b}{E_w I_b} = \ldots\ldots\ldots = \frac{M_k}{E_w I_k} \qquad (3.15)$$

Again the analysis is dependent on boundary conditions.

$x = 0$ $\quad$ $y = 0$ (origin at deflected position)

$\quad$ $\quad$ y' is unknown

$x = L$ $\quad$ y is unknown

$\quad$ $\quad$ $y' = 0$ (rigid foundation)

Finding one of the unknowns will be sufficient to furnish a solution.

An approximate shear deflection function is:

$$y_v = \frac{cQ}{2G}(L^2 - x^2) \qquad (3.16)$$

where y_v is the shear distortion

c is a shape factor

Q is the shear force function on a wall.

With the assumptions made however it is not possible to ensure shear deflection compatability of the walls.

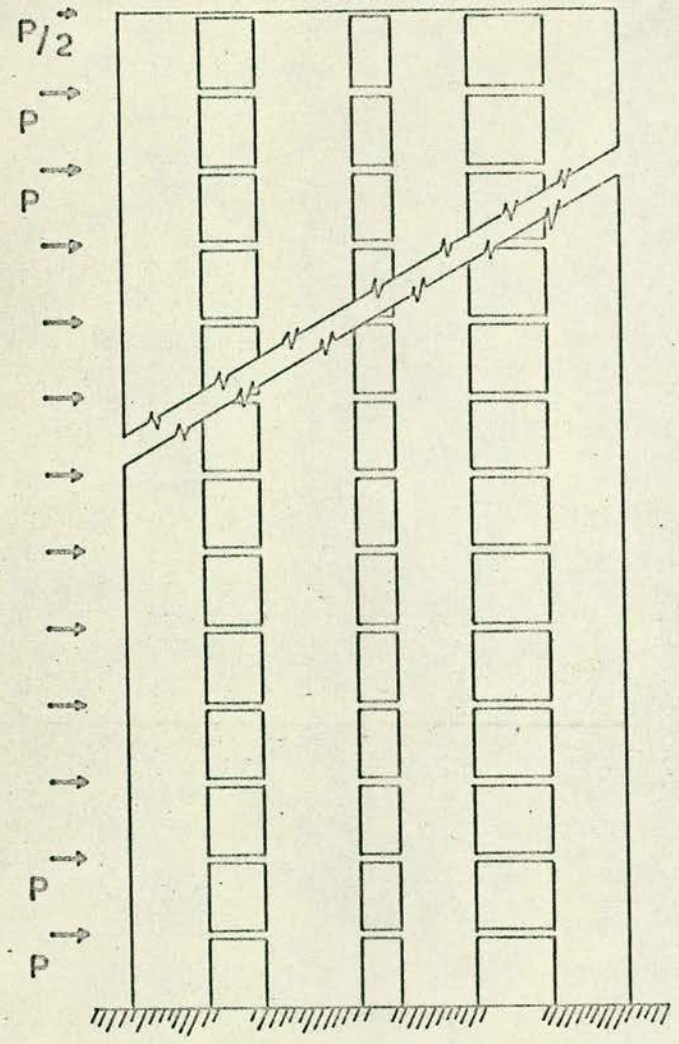

typical system of
shear walls interconnected
by thin slabs

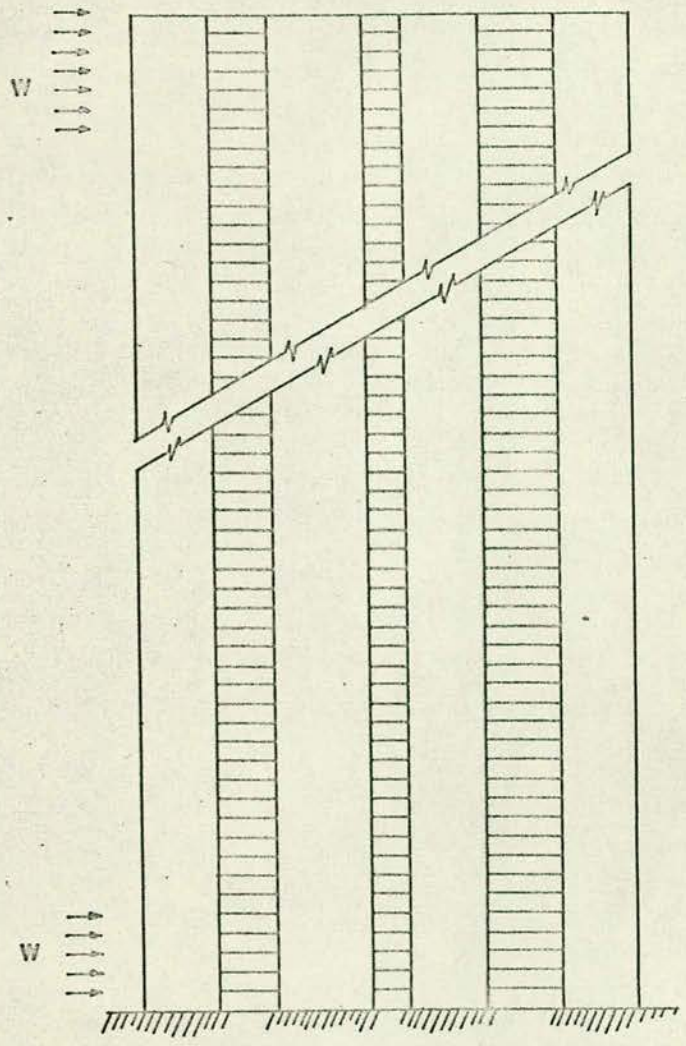

equivalent system of
shear walls interconnected
by continuous media

FIG. 3.1 PLANE ARRAY OF WALLS

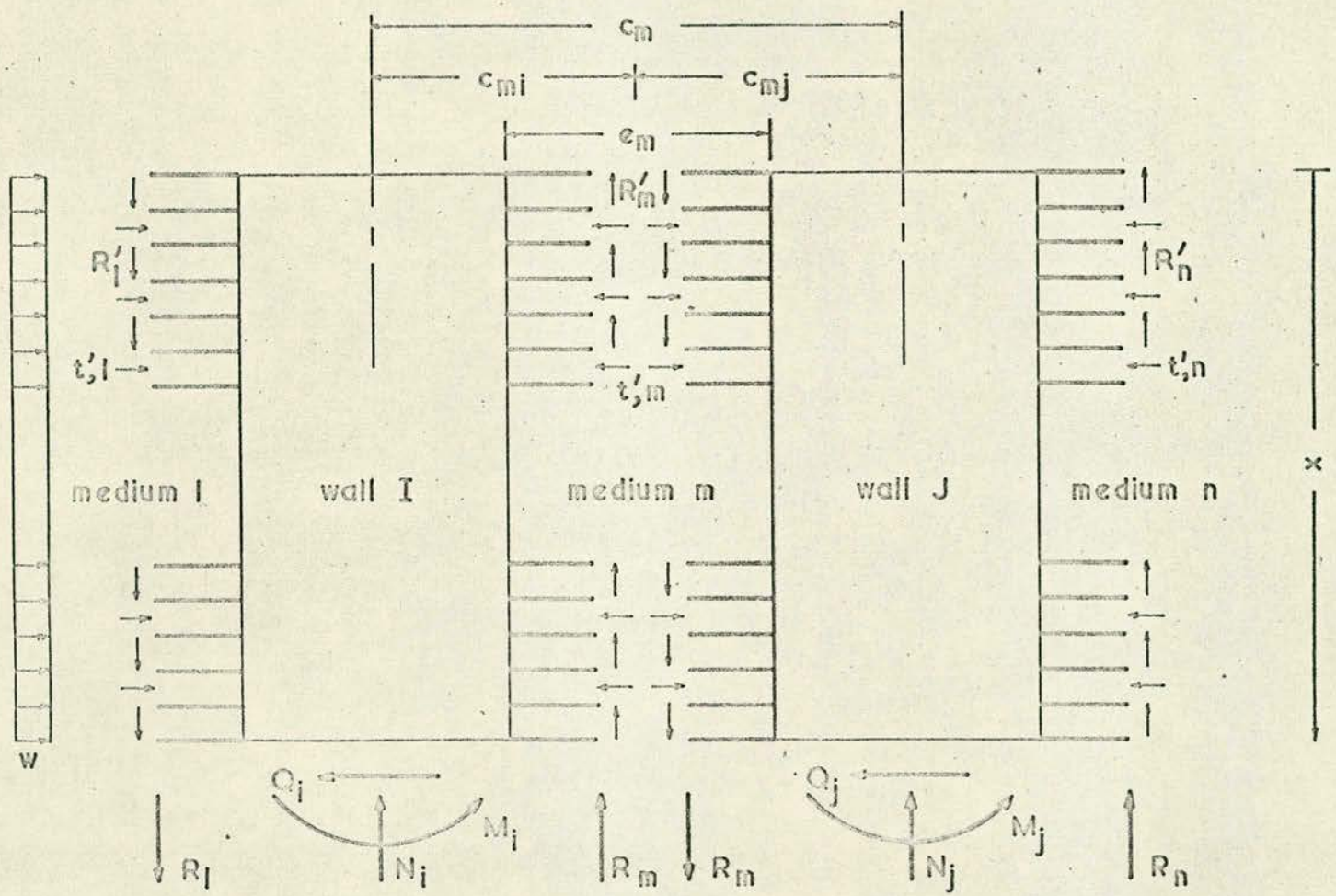

FIG 3.2 FREE BODY DIAGRAM

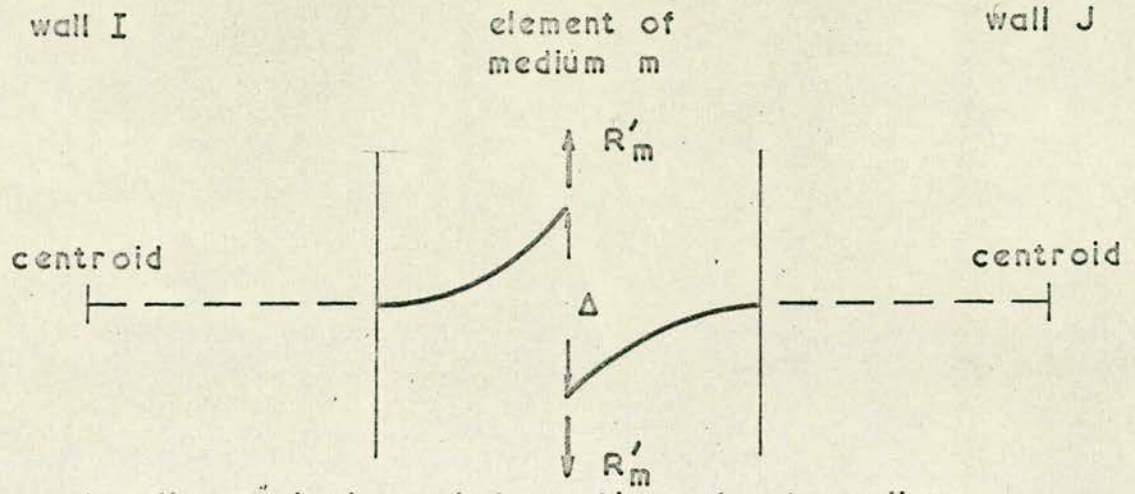

bending and shear deformation of cut medium

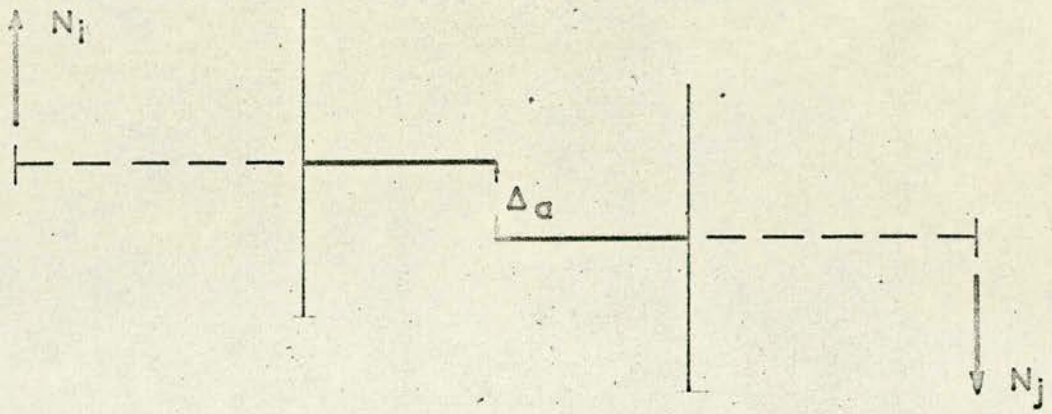

axial deformation of walls

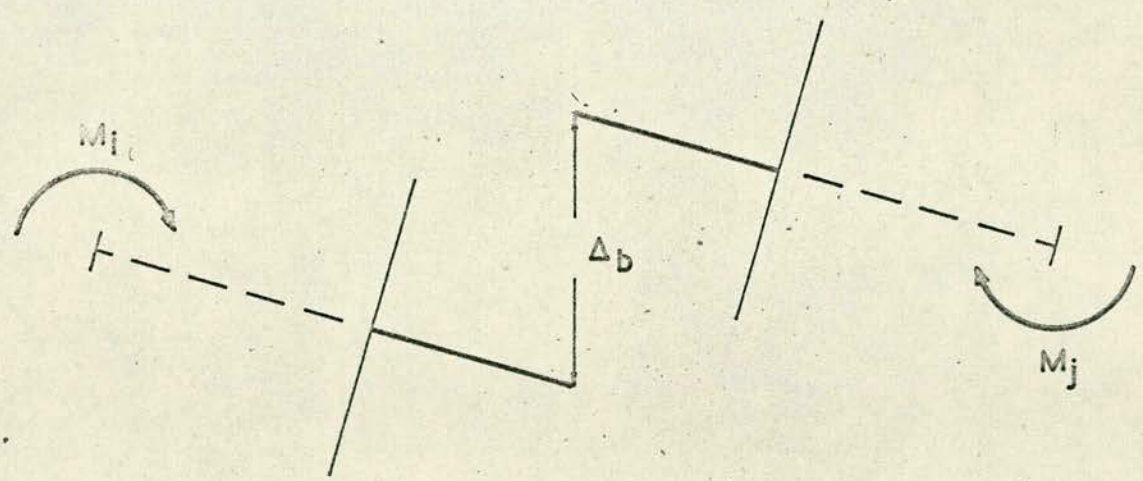

bending deformation of walls

compatability condition:

$$\Delta = \Delta_b - \Delta_a$$

FIG. 3.3 COMPATABILITY OF CUT MEDIUM

4. ANALOGUE COMPUTATION METHODS

4.1 Basic theory

Electronic analogue computers can be used to simulate certain mathematical models by representing physical quantities as D.C. voltages. The voltages may be constant or continuously varying, and they can be added, integrated or multiplied; each operation being done by a separate sub-circuit.

The basic computing element is the high gain D.C. amplifier which, with a resistance feedback becomes a summer, and with a capacitance feedback becomes an integrator. These also have the property of reversing the signs of all inputs and of changing them by certain constant multiples of ten. Multiplication of a variable by a constant smaller than unity is done with linear potentiometers. These can be pre-set with standard reference voltages.

The various amplifiers and associated sub-circuits are arranged within the machine so that all inputs and outputs are brought to a common patch panel. Links on the panel may be used to connect the units in any desired manner. Modes of operation are determined by push button switches.

Time is the only independent variable on the computer and static problems must therefore be scaled to make time represent a length parameter. For the structural systemsdescribed in the present work the fundamental scaling equation is $x = \lambda\tau$ where x is the vertical distance from the free end of a building (an independent variable), λ is a constant, and τ is computer time. Most machines have τ as a variable within the range $1 \leqslant \tau \leqslant 100$ seconds for accurate work. The dependent variables must be appropriately scaled so that the output at any point

does not exceed the maxima of ± 100 volts. The use of analogue computers is discussed more fully in standard references (40, 41, 42).

As a first step in problem solution the differential equations defining a system between two fixed boundaries must be written down to comply with the above scaling requirements. A flow chart is then laid out to establish the manner and sequence of the operations which have to be carried out to simulate the system. From this the inputs and outputs of the units which are required (summers, integrators, potentiometers etc.) can be linked on the patch panel. The gains of the summers (0.1, 1 or 10) and the integrators (1, 10 or 100) can then be selected and with the computer in the "Pot. Set" mode the coefficient potentiometers can be set.

By switching to the "Problem Check" mode and putting appropriate initial conditions on the integrators the computer is made to satisfy the equations at one boundary. On going into the "Compute" mode the machine will begin to traverse the region between the boundaries. Since the integrators operate in a continuous manner voltages will normally be changing continuously at all points in the circuit, and will do so until the computer is instructed to stop in the "Hold" mode, thereby indicating that the far boundary has been reached.

If the problem has mixed boundary conditions so that all the conditions are not known at either boundary there are computational difficulties and these will be discussed in Section 4.3.

4.2 Equipment

Two Solartron computers were used, an SC30 and a 247, which could be operated independently or as a master-slave system. Each of these contains thirty operational amplifiers, most of which can operate either as summers

or integrators. There are a total of one hundred and twenty potentiometers fifteen servo and electronic multipliers, and four diode function generators, as well as a number of auxiliary components. They are shown in Fig. 4.1.

Several types of computation cycle are avaiable, notably "single shot", in which the machine scans once and holds all final voltages until reset, and "repetitive", in which the machine resets automatically and the cycles are continual. The length of each cycle is goverened by a timer which is manually pre-set. The 247 has twin timers and a specialised use of these is described in Appendix B.

Voltages were monitored on the computers' digital voltmeters and on oscilloscopes which included an Aero Equipment display unit (type 279) with four traces and a long persistence screen. So that each computer run could be readily viewed it was found convenient to disconnect the internal time bases on the oscilloscopes and feed the X inputs with a voltage from the computer which was proportional to computer time. A suitable output was the independent variable x.

Permanent records were made with a Digital Measurements electric typewriter, giving outputs at discrete points, or a Bryans X-Y plotting table giving continuous graphs.

4.3 Scaling

Equations 3.13 have one independent variable x and n (R_1, R_2 .....R_n) dependent variables so they are suitable for simulation on an analogue computer. There is also a non-linear function of x contained in the external bending moment term ($M_o = f(x)$). The simplest load case, and the one most often employed is practical design, is a uniform wind

pressure on the face of a structure. This can be stated as a line load w on a plane array of walls. The external moment is then $M_o = wx^2/2$, a function which may be readily obtained on the computer by integrating x and multiplying the result by w. Any function, however, that represents a given wind pressure distribution can be fed in with a diode function generator, a plotting table with curve following attachments, or on hybrid installations, a memory unit.

The basic time scaling equation has already been given as:

$$x = \lambda\tau$$

and the derivatives will hence become:

$$dx = \lambda\, d\tau$$
$$dx^2 = \lambda^2\, d\tau^2$$

Equations (3.13) are modified to the form:

$$\frac{d^2R_1}{d\tau^2}\ \lambda^{-2} = R_1\ \alpha_{11}^2 + R_2\ \alpha_{21}^2 + \ldots\ldots + R_m\ \alpha_{m1}^2 + \ldots - \frac{w\lambda^2\tau^2}{2}\ \beta_1 \qquad (4.1)$$

$$\text{or}\quad R_1''\ \lambda^{-2} = R_1\ \alpha_{11}^2 + R_2\ \alpha_{21}^2 + \ldots\ldots + R_m\ \alpha_{m1}^2 + \ldots - \frac{w\lambda^2\tau^2}{2}\ \beta_1$$

Similarly equations (3.7) after differentiation become:

$$\frac{dM_a}{d\tau}\ \lambda^{-1} = Q_a\lambda^{-1} = w\lambda\tau\ \frac{I_a}{I_o} - \frac{dR_1}{d\tau}\ \lambda^{-1}c_{1a} - \frac{d}{d\tau}\ (M_{t',1})\ \lambda^{-1} \qquad (4.2)$$

$$\text{or}\quad M_a' = w\lambda^2\ \tau\ \frac{I_a}{I_o} - R_1'c_{1a} - M'_{t',1}$$

Primes now denote differentiation with respect to τ.

Deflection is found from the scaled equation:

$$y''\ \lambda^{-2} = \frac{M_a}{E_w I_a} = \frac{M_b}{E_w I_b} = \ldots\ldots = \frac{M_j}{E_w I_j} \qquad (4.3)$$

The choice of λ is restricted by practical considerations but a computation time of about one second is convenient for the initial stages of finding the solutions. This time can be extended on the computer for recording results on the X-Y plotter.

4.4 Methods of solution

Typical flow diagrams for structures with one, and three redundants are shown in Figs. 5.3, 5.4, and 8.2. From these it may be noted that the external load is supplied through an integrator to the loops of summers and integrators which generate each redundant R' shear function in accordance with equations 4.1.

Computations were always started at the free end of the structure which meant that all R functions had zero initital conditions and all R' functions had unknown initial conditions. Once these R' functions were known, the unique solution of equations 4.1 had been found since there is only one initial pair of boundary conditions for any R' and R functions which will give the required final conditions.

To determine the unknowns one computer run was insufficient and some form of iteration had to be used. There were two possible approaches, superposition or trial and error. The former involved scanning the structure a number of time with arbitrary initial conditions, noting the resultant final conditions, and using the data to form simultaneous algebraic equations. These had to be solved for the required initial conditions. However, the process is both unwieldy and indirect and it was found that trial and error was much more satisfactory.

To do this the computer was put in a fast repetitive mode and the unknown initial conditions were given arbitrary values. For the first

high speed runs the compution time was cut down so that the fixed boundary (foundation level) was close to the free boundary (top level) and the computer simulated a short structure. This prevents the overloads which may well occur for the full-height case when the chosen initial conditions differ significantly from the correct ones. The R' functions were monitored on the multi-channel oscilloscope and their initial condition potentiometers were manually adjusted to make the final conditions for this intermediate height approach zero.

Computation time was then increased slightly so that the boundaries widened and the conditions were corrected again. The procedure was repeated in stages until the computation period represented the total structure height ($x = L, \tau = \tau$ final) and fine adjustments were made to force the final conditions of R' to zero. The computer was then simulating the mathematical model in all respects since the prescribed boundary conditions were satisfied.

During this phase the operator had to observe the direction and magnitude of the final R' values and decide which initial condition should be altered to produce the best result at each stage. Since all the R' functions are mutually dependent a change in the initial condition of one alters all final conditions. When dealing with a multi-wall case difficulties can arise because experience is required to assess the changes which will give good convergence.

Some problems were repeated using an improved technique which obviated manual trial and error. This was an automatic iteration process and required special sub-circuits as described in Appendix B. These were designed to sample conditions at the end of a run and then change

the initial conditions in an appropriate manner before the start of the next cycle. It may be simplest to consider the method applied to a structure with one redundant R function.

The computer was put in a repetitive mode and set with the initial R' condition as zero. At the end of the first run there was therefore a large positive error on the far boundary. This positive value was sampled and then integrated for a short time interval. The output of this integration was fed back to the main circuit as a negative initial condition for the second run. Depending on the rate and time of integration the second cycle could result in a smaller positive error or a negative error. This error in turn was integrated and either added or subtracted to the existing initial condition according to whether the new error was negative or positive.

The special sub-circuit thus acted as an analogue memory; the information in it being an R' initial condition. The level of this condition changed with each new cycle by an amount proportional to the final error in the last one.

The process normally repeated itself with smaller and smaller corrections until the final condition was zero and consequently the initial condition remained constant. The explanation may be clarified by referring to Fig. 4.2 which shows typical steps in obtaining a solution.

With very small integrator gains in the automatic sub-circuit the number of cycles to reach equilibrium was large, but with high gains the errors could oscillate divergently and result in instability and overloading. To calculate the gain for an exact solution in two cycles would be tantamount to solving the basic differential equations. During the experiments the gain was judiciously set on the low side at the start of a new problem and gradually increased if it became apparent that

convergence was going to take more than a few seconds. For a complex case with n simultaneous R' functions, n sub-circuits were needed. These sub-circuits were independent of each other so that each function sought its own solution.

As with manual trial and error the boundaries were always widened discretely, and simultaneously the gain in the memory units had to be reduced because of increasing sensitivity of final conditions to initial conditions. The operator had only to check, on the oscilloscope display, that the R' functions were convergent, and special skill was not needed. This technique is a considerable step forward from manual trial and error because it means that there is no theoretical limit to the number of simultaneous equations which can be solved. In fact, the number was limited to four because of the size of the machine, but this was sufficient for any of the practical structures which were encountered.

Computational difficulties only occured in the equations just described. The shear functions in the walls, M', were found by multiplying the external shear by a constant and then adding the product to an appropriate fraction of the R' functions. Bending moments, M, were found by passing each M' through an integrator. Circuits incorporating two integrators gave slope, y' and deflection y. It might be argued that one such circuit is sufficient. It was, however, found useful to have a circuit for each wall since it was assumed in setting up the equations that all deflection profiles would be the same. If, therefore, the computed deflections were equal for each wall it was positive proof that the equations had been correctly solved.

At the free end of a structure the slope was unknown so this also had to be adjusted by trial and error, either manual or automatic, until the slope at the fixed end was zero. The operation was simple because the same condition applied to all walls and it was done after the R' functions were found. In this connection it may be noted that although all parts of the circuit were computing simultaneously the outputs for M', M, y' and y were meaningless until the R' solutions were correct.

It may also be noted that circuits could be set up to calculate stresses directly from the force functions. This however seemed unnecessary because in practice it is sufficient to know the stresses at a few discrete points. The extra circuits would decrease the number of amplifiers available for more complex operations.

Working on a new structure meant that the magnitudes of the various outputs were largely unknown and scaling changes were often necessary during the solution process. Overloading could occur at an intermediate stage or some outputs could be very small and hence inaccurate. Such cases could generally be improved by altering the inputs of the amplifiers by integer factors such as 2, 5 or 10 to use as much as possible of the full $\pm$ 100 volts range.

With this accomplished the integrator gains were stepped down by a factor of 10 and the computation time was increased by a factor of 10. The computer then ran at a tenth of its previous rate and permanent records were taken on the X-Y plotter.

4.5 Errors and instability

There are two types of error associated with the analogue simulation of a system.

1) The validity of the equations to represent the real system, and

2) imperfections in equipment.

The first of these depends upon assumptions made in formulating the equations. They can be tested experimentally and can be controlled to a large degree although their magnitude is open to doubt. The second depends on the quality of the electronic components within the computer. In most machines the tolerances are small and the cumulative error in a circuit is not more than a few per cent. It does however vary because, for example, multipliers are less accurate than summers or integrators. The size of this error in a structural analysis may be found by static equilibrium checks and for all the shear wall buildings the sum of the internal moments was within 3% of the external moment.

Instability can be divided to three categories.

1) Fundamental instability of the physical structure,

2) instability of the equivalent structure, and

3) instability of the computer circuits.

If a physical structure is unstable then both the equivalent system and the computer circuits will certainly be unstable and a solution is impossible.

The existence of the second type means that the equations of the simulated system, representing the real structure, are invalid. This occurs if the assumptions are incorrect and is a structural rather than a computing problem. Thirdly the circuits may be unstable because of the imperfect nature of the computing equipment.

A combination of the last two was encountered. The real structures were certainly stable but the equivalent sytems were not. This was demonstrated by extreme sensitivity of final conditions to small changes

in initial conditions and non-repeatability of the solutions. In physical terms these phenomena appeared when the stiffnesses of the beams approached those of the walls so that full frame behaviour could be expected. The assumption of zero R' at foundation level also becomes incorrect. The mathematical definition of such instability is beyond the scope of this work. It was found however that the computer was stable when dealing with structures which had typical wall dimensions and relatively flexible connecting elements. The possible range is discussed further in Chapter 5.

Errors are intimately related to stability since an unstable system is prone to large errors but these become obvious if the solution varies significantly from cycle to cycle.

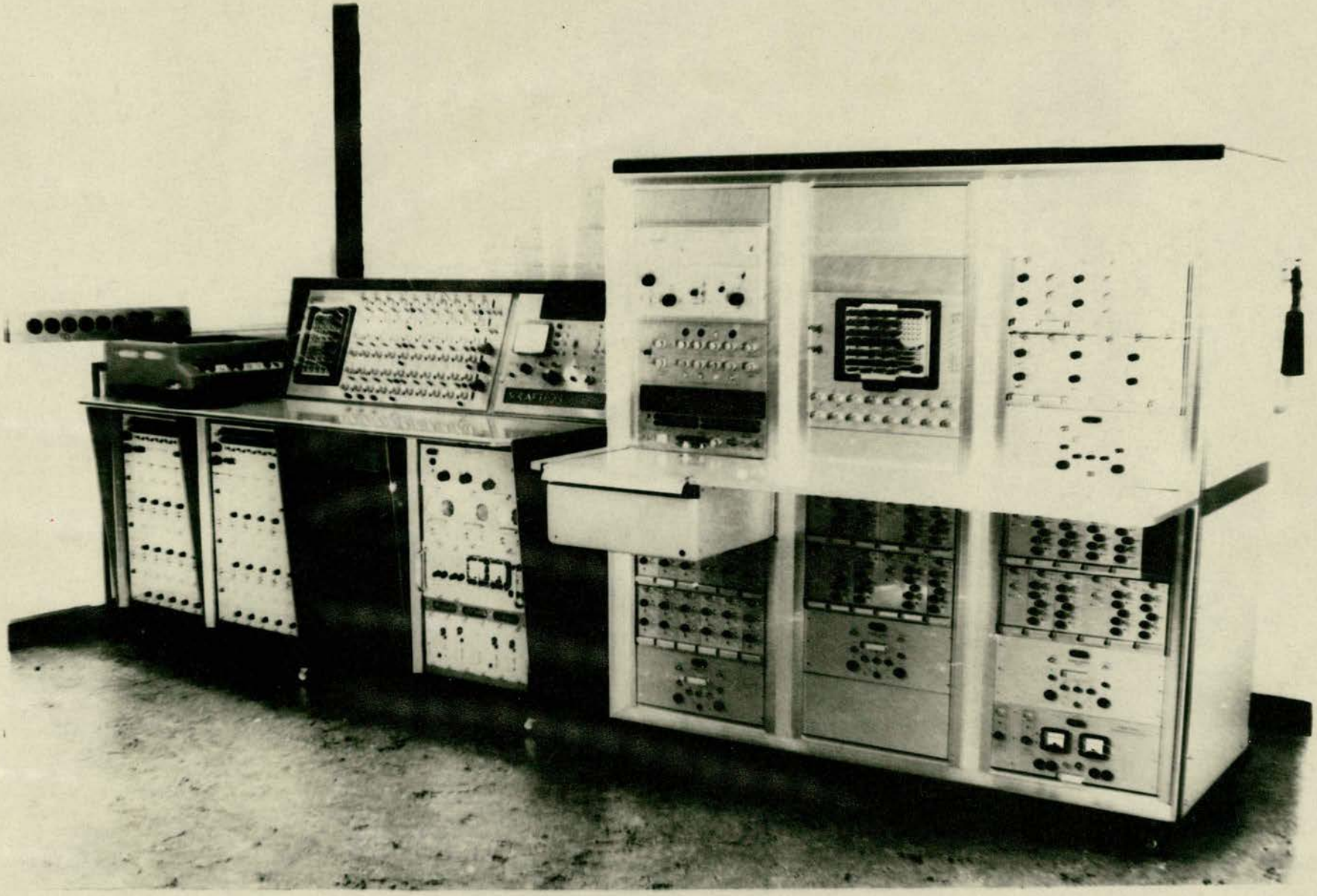

FIG. 4.1 Solartron analogue computers showing, on the left the SC30, and on the right the 247.

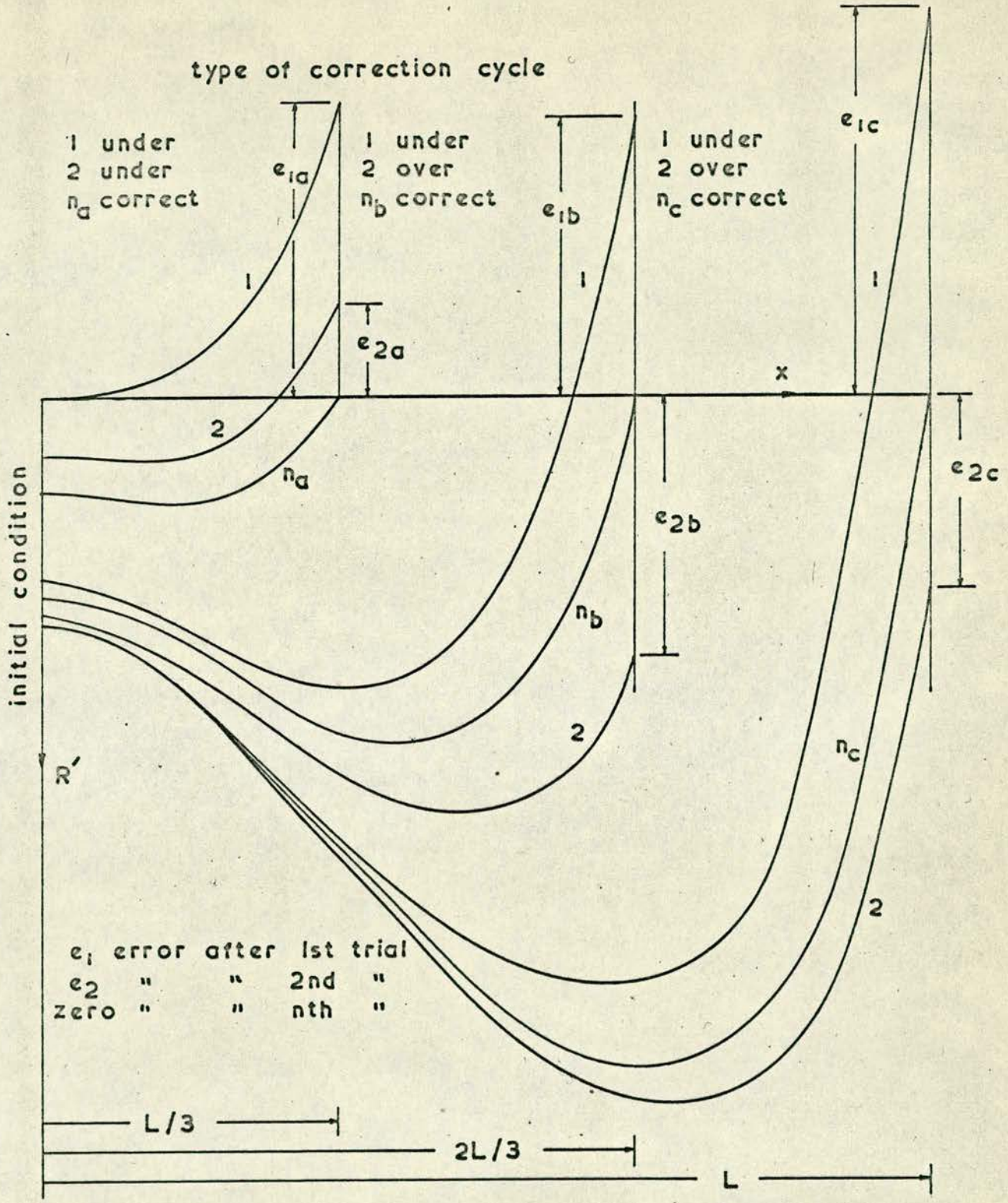

a. stable under corrections $e_{2a} < e_{1a}$

b. unstable oscillations $e_{2b} > -e_{1b}$

c. stable convergent corrections $e_{2c} < -e_{1c}$

final solution for structure of height L is case n_c

FIG. 4.2 AUTOMATIC CORRECTION PROCEDURE

5. TWO WALL STRUCTURES BY ANALOGUE COMPUTATION

5.1 Cases examined

Analogue computation was used in the investigation of a number of two wall structures; the main purpose being to establish relationships between structural dimensions and behaviour patterns, and hence produce design recommendations. In certain cases the results were tested with model work and with digital computer solutions.

The examples can be divided into four basic groups.

1. Thirteen concrete structures each with twenty storeys and 200ft high. They are denoted as Series A.
2. Three Perspex models, each with twenty storeys and 20in high.
3. An eight storey Araldite model 16in high.
4. A series of hypothetical structures which were analysed in non-dimensional form to give design charts.

5.2 Description of concrete structures

With the co-operation of the Cement and Concrete Association a typical two wall concrete structure was chosen for detailed analysis. The walls were plane, with no flanges, and the beams were of the same width as the walls representing the gable end of an actual block of flats. Dimensions are given in Table 5.2 and Fig. 5.1.

Batchelor and Cranston (43) of the Research and Development Department of C. & C.A. have been working (1966) with digital computer programmes based on a number of current methods of analysis to test the importance of different assumptions.

The methods they used for this example were.

1) Continuous medium equations adapted from Eriksson.
2) Equivalent column method of Frishmann, Prabhu and Toppler.

3) Influence co-efficient method of the above authors.

4) Renton's general space frame programme.

Methods (1), (2) and (3) were programmed for Sirius computer. It was found however, that the continuum approach was not ideal for a digital machine because of difficulties with the boundary conditions. Method (4) was run on "Edsac II" by Livesly at Cambridge and he considered the structure as a line element frame with rigid gussets between the column centres (representing the central axes of the walls) and the fixed ends of the beams (the inner edges of the walls). The equivalent column method and the influence co-efficient methods neglect axial deformation of the walls and shear deformation of the beams so Eriksson's equations were subsequently modified to ignore these terms and provide a comparison.

The bending moment distributions found from three of the above analyses for each wall section are given in Fig. 5.2. They all agree well at the base and this is important because the maximum wall stresses are at foundation level. The true zig-zag nature of the moments between floors is not, of course, reproduced by the continuum approximations. Differences are noticeable further up the structure between those methods which include axial and shear effects and those which do not. In this example the discrepancies are unimportant but for the other configurations there might be serious errors. Such errors are particularly liable to occur when shear deformation of the beams is of the same order as bending deformation.

Analogue computations were also carried on a further twelve cases. Each of these was a modification of the one just described and the dimensions of the walls and beams were changed in turn as shown

in Table 5.1. Complete physical data is in Table 5.2 and the evaluated constants are in Table 5.3.

5.3 Analogue computation for two walls

The continuum equations for two walls are a simplification of the general equations in Chapter 3.

$$R_1'' = R_1 \alpha_{11}^2 - M_o \beta_1$$

$$M_{t',1} = -\frac{R_1}{I_o}(c_{1a} I_b - c_{1b} I_a) = 0 \text{ for equal walls} \qquad (5.1)$$

$$M_a' = M_{oa}' - R_1' c_{1a} - M_{t',1}'$$

$$y'' = \frac{M_a}{E_w I_a}$$

If the walls are equal the constants are:

$$\alpha_{11}^2 = \frac{K_1}{2E I_a}\left(c^2 + \frac{4I_a}{A_a}\right)$$

$$\beta_1 = \frac{K_1}{2E I_a} c \qquad (5.2)$$

The total height was 200 ft and the time scale was chosen as:

$x = 10^3 \tau$ so equations 5.1 become:

$$R_1'' = R_1 \alpha_{11}^2 - \beta_1 \cdot \frac{w}{2} \cdot 10^6 \tau^2$$

$$M_a' = 0.5 \times w.10^3 \tau - R_1' \cdot \frac{c}{2} \qquad (5.3)$$

$$y'' = 10^6 \frac{M_a}{E_w I_a}$$

Primes now denote differentiation with respect to τ. Taking the dimensions of the standard structure from the first row of Tables 5.2 and 5.3 and putting in the constants:

$$R_1'' \cdot 5 \cdot 10^{-2} = 0.8325\ (0.5R_1 \times 0.3861 - 10\tau^2)$$

$$M_a' \cdot 4. \ 10^{-3} = 40\tau - 0.5R_1' \times 0.7200 \qquad (5.4)$$

$$y'' \cdot 5 \cdot 10^{3} = 4 \cdot 10^{-3} M_a \times 0.5272$$

The general analogue computer circuit for equations 5.3 is shown in Fig. 5.3 and the circuit for equations 5.4 is shown in Fig. 5.4. The methods described in Chapter 4 were used to find the solutions. The basic circuit remainded unchanged for all cases but the potentiometers were set each time to the values given in Table 5.4 . Initial condition voltages are also shown.

Table 5.1

Dimensional changes in structures A1-A13

case	modification
A1	standard
A2	wall widths decreased by 24 in
A3	" " " " 12 in
A4	" " increased " 12 in
A5	" " " " 24 in
A6	beam lengths decreased by 24 in
A7	" " " " 12 in
A8	" " increased " 12 in
A9	" " " " 24 in
A10	beam depth decreased by 4 in
A11	" " " " 2 in
A12	" " increased " 2 in
A13	" " " " 4 in

Table 5.2

Dimensions of structures A1-A13

Case	wall width a (in)	wall thick-ness t (in)	distance apart e (in)	moment arm c_{1a} (in)	storey height d (in)	beam depth h (in)	M. of I. of wall I_a (in^4)	M. of I. of beams I_h (in^4)	$\frac{I_a}{I_h}$
A1	84	12	96	90	120	10	592,704	1,000	593
A2	60	12	96	78	120	10	216,000	1,000	216
A3	72	12	96	84	120	10	373,248	1,000	373
A4	96	12	96	96	120	10	884,736	1,000	885
A5	108	12	96	102	120	10	1,259,712	1,000	1,260
A6	84	12	72	78	120	10	592,704	1,000	593
A7	84	12	84	84	120	10	592,704	1,000	593
A8	84	12	108	96	120	10	592,704	1,000	593
A9	84	12	120	102	120	10	592,704	1,000	593
A10	84	12	96	90	120	6	592,704	216	2,745
A11	84	12	96	90	120	8	592,704	512	1,160
A12	84	12	96	90	120	12	592,704	1,728	344
A13	84	12	96	90	120	14	592,704	2,744	216

Table 5.3

Constants for structures A1-A13

($E = 4 \times 10^6$ lb/in^2, $G = 1.7 \times 10^6$ lb/in^2)

case	α_{11}^2 / β_1 (in)	$\beta_1 \times 10^7$ (in^{-3})	$2c_1 \times 10^{-3}$ (in)
A1	193.07	0.1765	0.360
A2	169.39	0.3959	0.312
A3	178.29	0.2469	0.336
A4	218.00	0.1189	0.384
A5	223.10	0.0883	0.408
A6	171.08	0.3345	0.312
A7	182.00	0.2299	0.336
A8	204.25	0.1255	0.384
A9	215.53	0.0977	0.408
A10	193.07	0.0367	0.360
A11	193.07	0.0862	0.360
A12	193.07	0.2841	0.360
A13	193.07	0.4442	0.360

Table 5.4

Potentiometer settings and initial conditions for structures A1-A13

Case	amp. 1 setting	pot. 1	pot. 2	pot. 3	pot. 4	I.C. amp. 1 (volts)	I.C. amp. 2 (volts)
A1	x10	0.3861	0.8325	0.7200	0.5272	-25.50	-51.25
A2	x100	0.1637	0.3959	0.6240	0.1447	-23.89	-93.70
A3	x100	0.1793	0.2469	0.6720	0.8372	-25.61	-70.65
A4	x10	0.4360	0.5945	0.7680	0.3532	-24.39	-76.89
A5	x10	0.4462	0.4415	0.8160	0.2481	-24.77	-44.09
A6	x100	0.1711	0.3345	0.6240	0.5272	-24.05	-53.75
A7	x100	0.1820	0.2299	0.6720	0.5272	-25.61	-46.71
A8	x10	0.4085	0.6275	0.6780	0.5272	-25.74	-59.96
A9	x10	0.4311	0.4885	0.8160	0.5272	-25.71	-79.08
A10	x10	0.3801	0.1835	0.7200	0.5272	-26.61	-89.00 (x2)
A11	x10	0.3861	0.4310	0.7200	0.5272	-28.61	-74.47
A12	x100	0.1930	0.2841	0.7200	0.5272	-21.89	-31.82
A13	x100	0.1930	0.4442	0.7200	0.5272	-17.50	-35.21

5.4 Calculation of forces and stresses

Forces and stresses can readily be calculated from the computer output. Voltage levels must be converted to physical quantities by going through the scaling process in reverse. Derivatives of τ must be changed to derivatives of x and all outputs must be divided by the scale factors given on the computer flow diagram.

If this is done for structure A1 the shear forces in the medium are as shown in Fig. 5.5 and the wall forces at foundation level are found to be:

$$M_a = 5.71 \times 10^5 \quad \text{lb in}$$

$$R = 9.50 \times 10^3 \quad \text{lb}$$

for a load of w = 1 lb/in.

The moment of inertia of the wall is $I_a = 592{,}704$ in^4, the distance from the centre to the edge is 42 in, and the area is 1008 in^2. If the wall is isotropic the maximum bending stress is therefore:

$$\sigma_b = \pm \frac{M_a}{I_a} \cdot \bar{y} = \pm 40.5 \text{ lb/in}^2$$

and direct stress is:

$$\sigma_d = \pm \frac{R}{A} = \pm 9.4 \text{ lb/in}^2$$

At the outside edges the net stress is therefore,

$$\sigma_{max.} = \sigma_b + \sigma_d = \pm 49.9 \text{ lb/in}^2$$

and at the inside edges the net stress is,

$$\sigma_{min.} = -\sigma_b + \sigma_d = \mp 31.1 \text{ lb/in}^2$$

A static equilibrium check can be made by taking the sum of the internal moments :

$$\Sigma M = 2M_a + R.c$$
$$= 2.85 \times 10^6 \text{ lb in}$$

the external moment being:

$$M_o = \frac{wL^2}{2} = 2.88 \times 10^6 \text{ lb in}$$

Forces in the beams are found by integrating R' over the storey height. The maximum value of R' occurs at the seventh floor:

$$R'_{max.} = 5.2 \text{ lb/in}$$

The shear force in this beam is approximately:

$$R'.d = 5.2 \times 120 = 624 \text{ lb}$$

and with a parabolic distribution the maximum shear stress is :

$$\frac{3}{2} \cdot \frac{R'.d}{h.b} = 7.8 \text{ lb/in}^2$$

At the wall to beam junction the bending moment is:

$$R'.d. \frac{e}{2} = 29,950 \text{ lb in}$$

so the area of reinforcing steel can hence be calculated.

The complete results of the above calculations for structures A1-A13 are shown in Table 5.5 (walls) and Table 5.6 (beams). These are not comprehensive because they refer only to one basic structure, but they demonstrate the order of stress change which can be achieved by altering wall and beam dimensions.

Table 5.5

Results of computations on A1-A13 (walls)

Case	B.M. at base $\times 10^{-5}$ (lb in)	R at base $\times 10^{-3}$ (lb)	M' at base $\times 10^{-3}$ (lb)	σ bending at base ($\pm$ lb/in^2)	σ direct at base ($\pm$ lb/in^2)	$\sigma_b + \sigma_d$ max. (lb/in^2)	$-\sigma_b + \sigma_d$ min. (lb/in^2)	σ shear max. (lb/in^2)	sum of moments at base (external = 2.880×10^6) (lb/in)
A1	5.71	9.5	1.2	40.5	9.4	+49.9	-31.1	1.8	2.853
A2	4.37	12.4	"	60.7	17.2	+77.9	-43.5	2.5	2.814
A3	4.87	10.0	"	46.7	11.7	+58.6	-35.2	2.4	2.654
A4	6.25	7.4	"	33.8	6.4	+40.2	-27.4	1.6	2.670
A5	7.00	7.2	"	30.0	5.9	+35.9	-24.1	1.5	2.870
A6	5.00	11.6	"	35.4	11.5	+46.9	-23.9	1.8	2.810
A7	5.13	9.8	"	36.2	9.7	+46.9	-26.5	1.8	2.676
A8	6.00	8.0	"	42.4	7.9	+50.3	-34.5	1.8	2.735
A9	6.75	7.6	"	47.7	7.5	+55.2	-40.2	1.8	2.900
A10	8.86	5.8	"	62.6	5.7	+68.3	-56.9	1.8	2.817
A11	5.57	7.9	"	40.6	7.8	+48.4	-32.8	1.8	2.535
A12	4.62	10.4	"	32.6	10.3	+43.9	-21.3	1.8	2.797
A13	4.13	10.8	"	19.2	10.3	+39.5	-18.9	1.8	2.771

Table 5.6

Results of computations A1-A13 (beams)

Case	R' max. (lb/in)	max. shear force in a beam (R'.d) (lb)	height above base of this beam (ft)	max. shear stress (lb/in^2)
A1	5.2	624	70	7.8
A2	7.8	936	60	11.7
A3	6.2	744	60	9.3
A4	4.3	516	80	6.4
A5	4.0	480	80	6.0
A6	7.1	852	60	10.7
A7	5.9	707	70	8.8
A8	4.5	540	70	6.8
A9	4.2	504	80	6.3
A10	3.0	360	100	7.5
A11	4.2	504	90	7.9
A12	6.4	768	60	8.0
A13	6.9	828	60	7.4

Deflection curves are given in Figs. 5.6 and 5.7 for different wall and beam inertias. Points of inflection are clearly seen in each case and these correspond to the change in sign of the bending moment functions.

Tip deflection has been plotted against the parameter α^2 in Fig. 5.8 to show how a given overall stiffness can be produced by selecting either wall sizes or beam sizes; provided the clear span between the wall is kept constant. Suppose for example that it is necessary to reduce the tip deflection from 0.2 in to 0.1 in . When the beams are retained to a depth of 10in the wall widths must be increased from 84in to 138in. If the wall widths are retained at 84in the beam depths must

be increased from 10in to 14.5in to achieve the same result. In terms of volume of material the ratio is:

$$\frac{\text{Increase in volume of walls}}{\text{Increase in volume of beams}} = 30$$

In all cases if the relative costs of shuttering and reinforcement are ignored it is more economical to change the total stiffness by altering the beams rather than the walls.

5.5 Perspex models

Three simple Perspex models were tested experimentally. Details are given in Chapter 6. They are analysed theoretically with the analogue computer and checked by the methods of Eriksson and Beck. A solution was also obtained from McLeod who used his wide column frame analysis technique on an English Electric KDF9 digital computer.

One model was built with slabs and the other two had beams. The moments of inertia of the beams and slabs were the same so that any differences in theoretical solution would be due to shear deformation only. It was also thought that the slabs might transfer forces more effectively to the walls than the beams whereas the theory takes no account of this possibility. The moment of inertia of the topmost connections was half that of the others to comply with the requirements of a continuous even medium.

Dimensions are given in Fig. 5.9 and the flanges shown were included in calculating equivalent wall areas and inertias. The constants are given below with all dimensions in inches units.

Table 5.7

Dimensions of Perspex models

	slab connected	beam connected
no. of storeys	20	20
length of wall including flange	1.525	1.525
flange thickness	0.125	0.125
wall thickness b	0.125	0.125
flange width	0.500	0.500
beam width b		0.125
beam thickness h		0.125
slab width b_s	1.000	
slab thickness h	0.0625	
storey height d	1.000	1.000
clear distance between walls e	0.500	0.500
moment arm c_{1a}, c_{1b}	1.1506	1.1506
wall area A	0.2375	0.2375
wall inertia I_a	0.05544	0.05544
beam, slab, inertia I_h	0.20344×10^{-4}	0.20344×10^{-4}
modulus of elasticity E	0.42×10^6	0.42×10^6
ω^2_{11}	0.10445	0.09129
β_1	0.03858	0.03372

With a storey height of 1in the total height was 20in and the time scale was chosen as $x = 2\tau$. An equivalent load of 2 lb/in was applied

to give satisfactory voltage levels. The scaled equations for the redundants are:

slab connected:

$$0.5\ R'' = 0.3088\ (5R \times 0.1353 - \tau^2)$$

beam connected: (5.5)

$$0.5\ R'' = 0.2698\ (5R \times 0.1353 - \tau^2)$$

moment equations are the same for both:

$$M'_a = 4\tau - 5R' \times 0.2031$$

(5.6)

$$y''.10^3 = M_a \times 0.1718$$

The normal two wall circuit was used and within the limits of computer accuracy there was no difference between the slab and beam connected systems. Model stresses were measured on the flanges at second floor level and they were 482 lb/in^2 (slab connected) and 505 lb/in^2 (beam connected) compared with the computed value of 462 lb/in^2.

Deflection profiles are shown in Fig. 5.10. The results from those models with cantilever foundations were 74% larger than the computed values indicating a foundation rotation of 0.0017 radians for a test load of w = 0.5 lb/in.

The discrepancy was eliminated by constructing a "mirror-image" model with a central support, and loading it simultaneously on both sides. The deflections from this closely approach the theoretical curve for bending only (Table 5.8).

It would be possible to find shear distortions of the walls on an analogue computer, but the equipment which this would require was not available. An estimate however, was made by considering each wall web

as a simple cantilever taking half of the external load.

Eriksson and Beck give formulae for the tip deflection under bending, and in the usual notation:

$$y_{tip} = \frac{wL^4}{8E_w I_t}\left\{\frac{I_t}{I_o} - c_{1a}\cdot\frac{\beta}{\alpha^2}\cdot\frac{I_t}{I_a}\left(1 - \frac{8}{(\alpha L)^2}\left(\frac{1}{2} - \frac{1}{\alpha L} + \frac{1}{(\alpha L)^2}\right)\right)\right\} \qquad (5.7)$$

where I_t is the moment of inertia of the total cross section about its centroid.

A comparison of results is shown in Table 5.8.

Table 5.8

Tip deflection of Perspex model

method	tip deflection (in)
experimental (mirror image model)	0.101
analogue (bending only)	0.090
analogue (bending and shear)	0.094
Eriksson and Beck	0.090
wide column frame (McLeod)	0.093

5.6 Araldite model

The same type of analysis described in Sections 5.3, 5.4 and 5.5 was applied to an eight storey Araldite model. Photo-elastic experiments were conducted by the frozen stress technique (Chapter 6) and these gave boundary stresses on walls and shear stresses at the points of inflection of the beams.

The form of the model is as shown in Fig. 5.1 and the dimensions and constants are given below in inches units.

Table 5.9

Dimensions of Araldite model

no. of storeys	8
length of wall	2.00
wall and beam width b	0.25
beam thickness h	0.25
storey height d	2.00
clear distance between walls e	1.00
moment arm c_{1a}, c_{1b}	1.50
wall area A	0.50
wall inertia I_a	0.333
beam inertia I_h	0.326×10^{-3}
modulus of elasticity	1900 (approx.)
α_{11}^2	0.0576
β_1	0.01677

For a maximum computer time of 0.8 seconds, $x = 2\tau$ (with integrator gains of 10) and the equations are:

$$R'' = 0.2670\ (R \times 0.8610 - \tau^2)$$

$$M_a' = 4\tau - R' \times 1.500 \qquad (5.8)$$

$$y''.10 = M_a \times 0.1263$$

Stress distribution from foundation level to the first floor is shown

in Fig. 5.11 while shear forces in the connecting beams are in Table 5.10 for a load of w = 1 lb/in.

Table 5.10

Shear forces in connecting beams of Araldite model

storey	experimental (lb)	computed (lb)
1	2.81	2.00
2	3.40	3.68
3	3.12	3.79
4	3.12	3.60
5	2.95	3.25
6	2.81	2.70
7	2.50	2.25
8	0.75	1.00

5.7 Non-dimensional design charts

The redundant R function is the only one which cannot be calculated by simple formulae and if this is known then the maximum forces in both the cross beams and the walls can be established without difficulty. The stiffness properties of a symmetric two wall case can be expressed as the constant α which was derived in Chapter 3.

$$\alpha^2 = \frac{12\, E\, I_h}{de^3 \left(1 + \frac{E}{G}\left(\frac{h}{e}\right)^2\right)} \cdot \frac{1}{E_w I_o} \cdot \left(c^2 + \frac{2I_o}{A}\right) \qquad (5.9)$$

For any value of αL a non-dimensional function ψ can be plotted where ψ is connected to dR/dx by a formula giving the relationship

between external load and shear at the centre of a composite cantilever beam:

$$\frac{dR}{dx} = \psi \cdot w \cdot L \cdot \frac{S}{I_t} \qquad (5.10)$$

w is the lateral load,

L is the total structure height,

S is the static moment of one wall about the centroid of the whole cross-section,

I_t is the moment of inertia of the whole cross-section about its centroid.

A further function ϕ is defined as:

$$\phi = \int_0^x \psi \cdot dx \qquad (5.11)$$

and the total shear force R is hence given by:

$$R = \phi \cdot w \cdot L^2 \cdot \frac{S}{I_t} \qquad (5.12)$$

For αL within the range $2 \leq \alpha L \leq 6$, ψ and ϕ are shown in Figs. 5.12 and 5.13. If $\alpha L < 2$ the behaviour is almost that of a pair of cantilevers with pinned interconnections. For $\alpha L > 6$ the equations tend towards instability thereby indicating that the assumption $dR/dx = 0$ at the fixed end is becoming invalid, and frame type action may be expected. When $\alpha L = \infty$ there are no openings in the wall and the structure acts as a solid cantilever.

The largest force in a beam is found by integrating the maximum dR/dx over one storey.

Bending moments in the walls are given by:

$$M_a = \frac{M_o}{2} - R_1 c_{1a} \qquad (5.13)$$

and the axial force is simply R.

The shapes of the deflection curves for the upper and lower limits of $2 \leqslant \alpha L \leqslant 6$ have been plotted non-dimensionally in Fig. 5.14. The smaller the value of α L the more the deflected shape tends towards that of a simple cantilever, and as α L increases the point of inflection becomes marked. The value of the tip deflection can be calculated from Eriksson's formulae in Section 5.5.

Any symmetrical pair of shear walls within the given range of αL can thus be rapidly analysed using the charts in Figs. 5.12, 5.13, and 5.14, and equations 5.10 to 5.13.

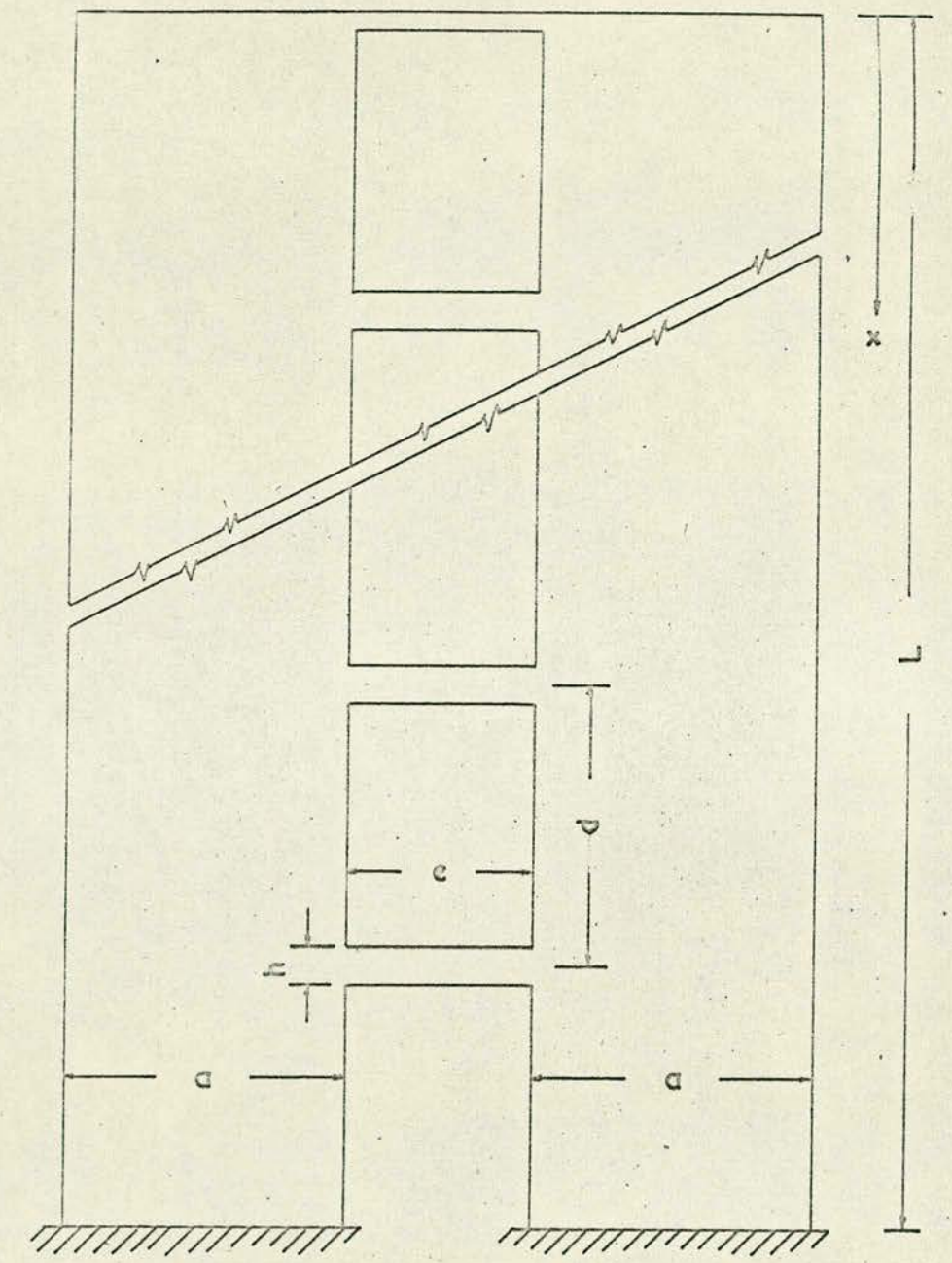

FIG. 5.1 TWO WALL STRUCTURE

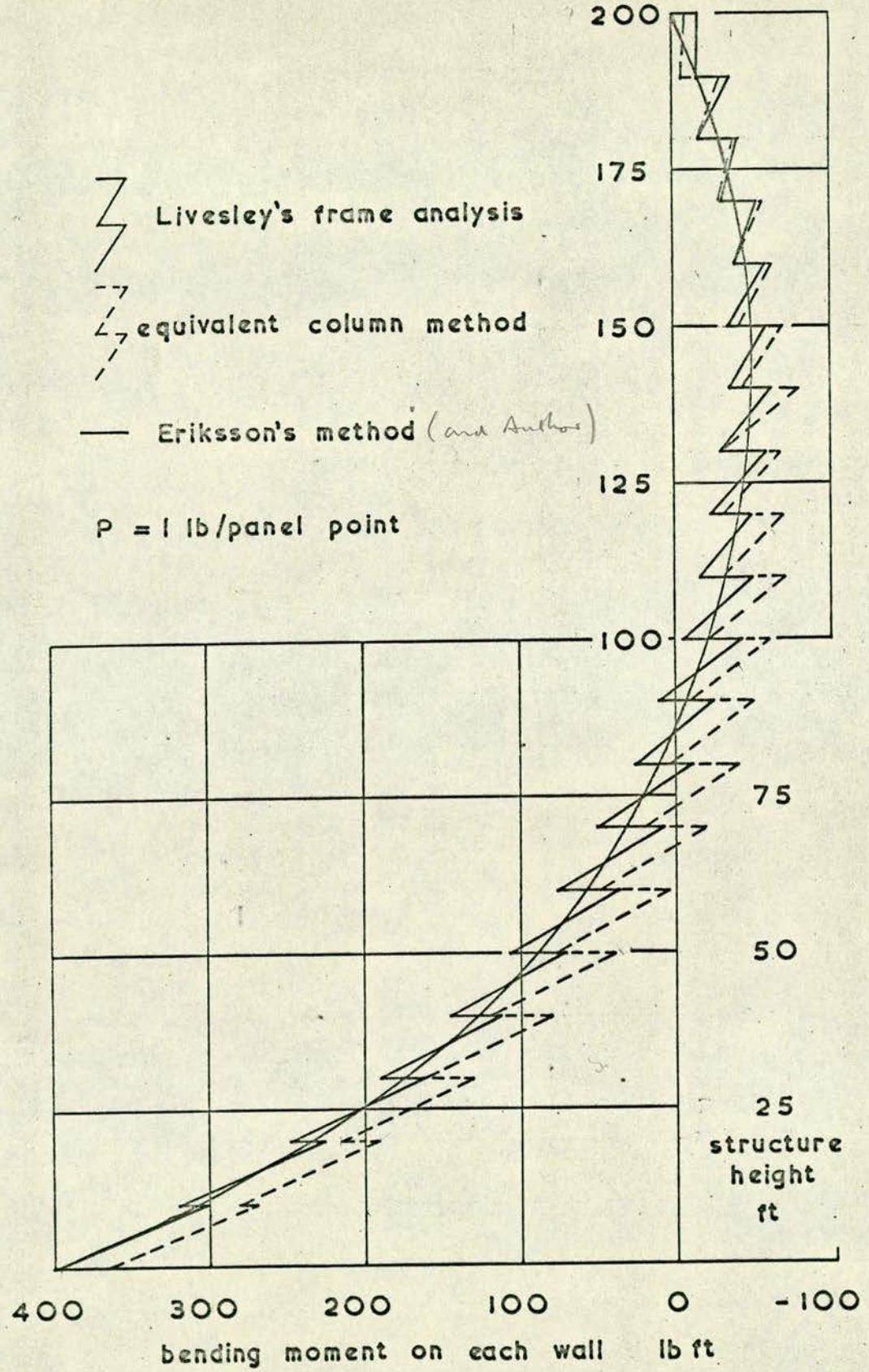

FIG. 5.2 WALL MOMENTS ON CONCRETE STRUCTURE A1

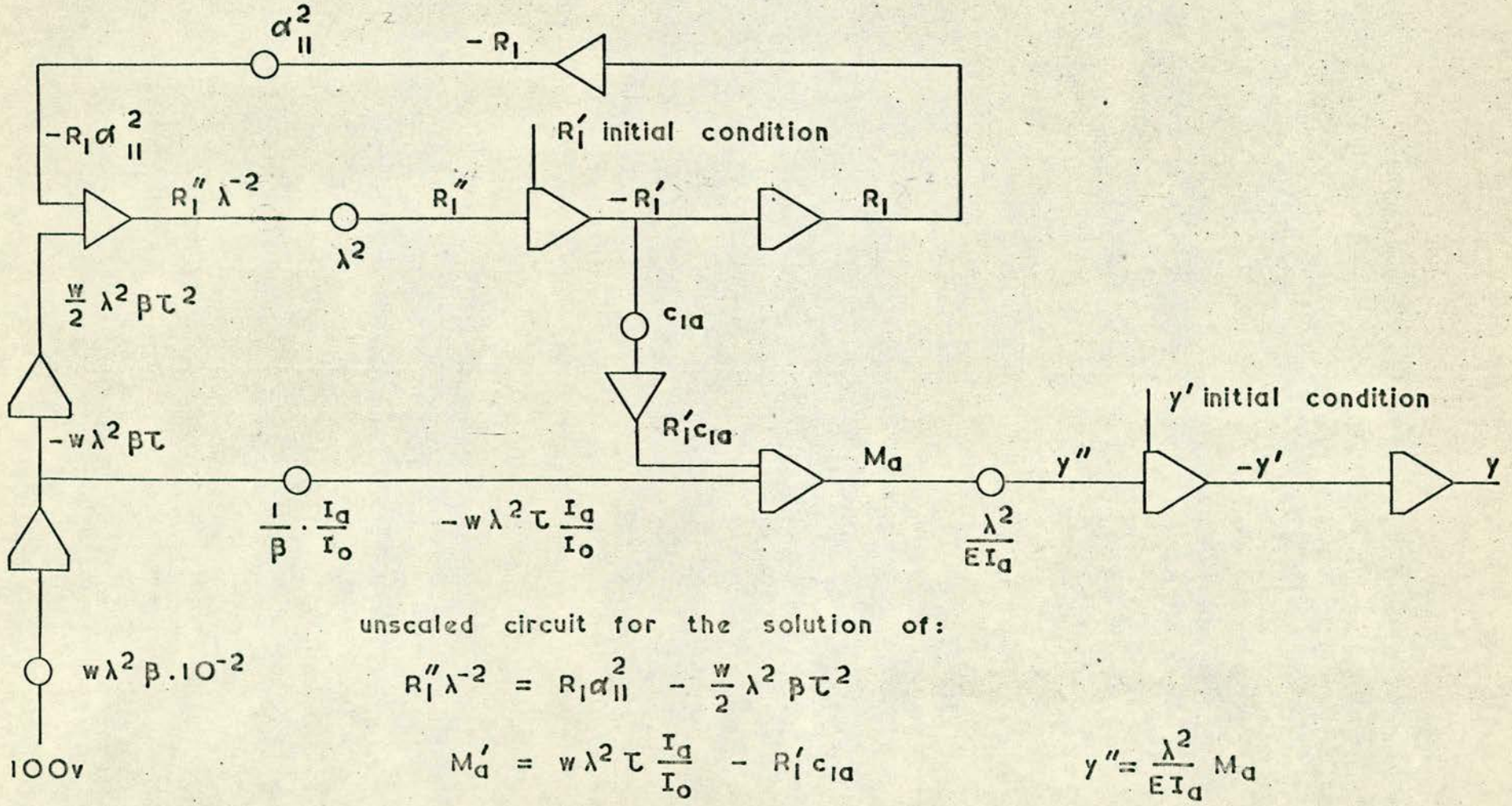

unscaled circuit for the solution of:

$$R_1''\lambda^{-2} = R_1\alpha_{11}^2 - \frac{w}{2}\lambda^2\beta\tau^2$$

$$M_a' = w\lambda^2\tau\frac{I_a}{I_o} - R_1'c_{1a} \qquad y'' = \frac{\lambda^2}{EI_a}M_a$$

FIG. 5.3 GENERAL TWO WALL CIRCUIT

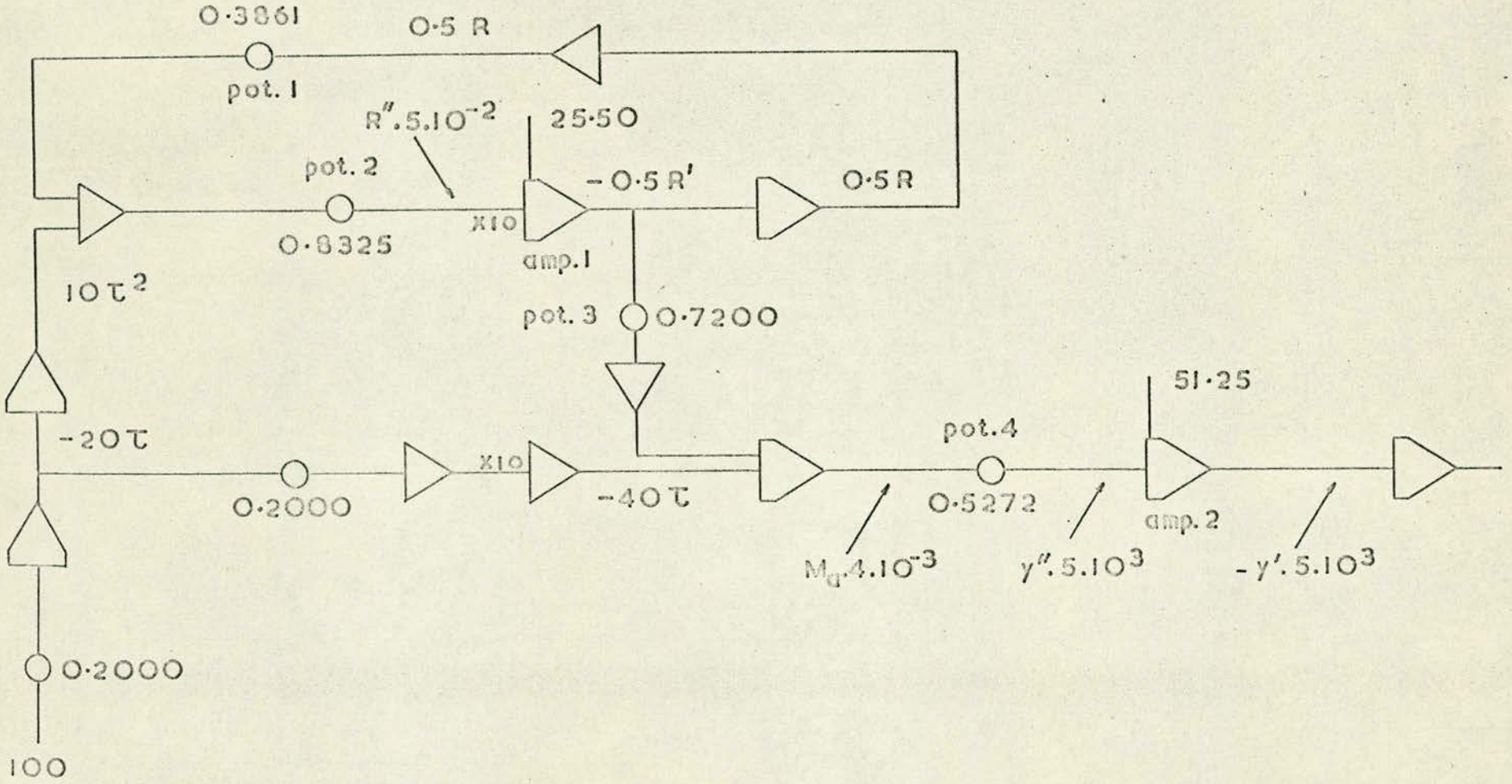

FIG. 5.4 CIRCUIT FOR CONCRETE STRUCTURE A1

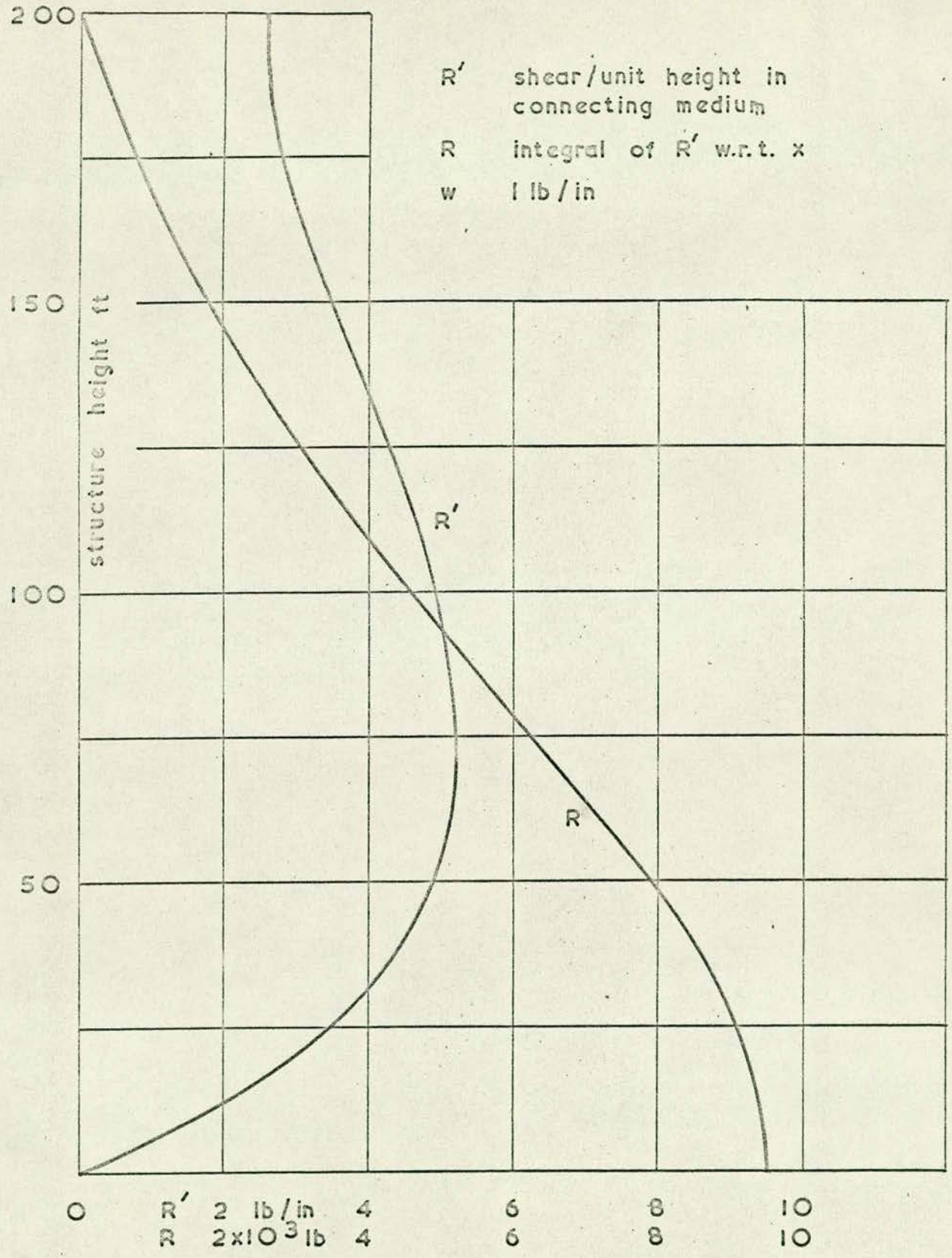

FIG. 5.5 SHEAR IN MEDIUM FOR CONCRETE STRUCTURE A I

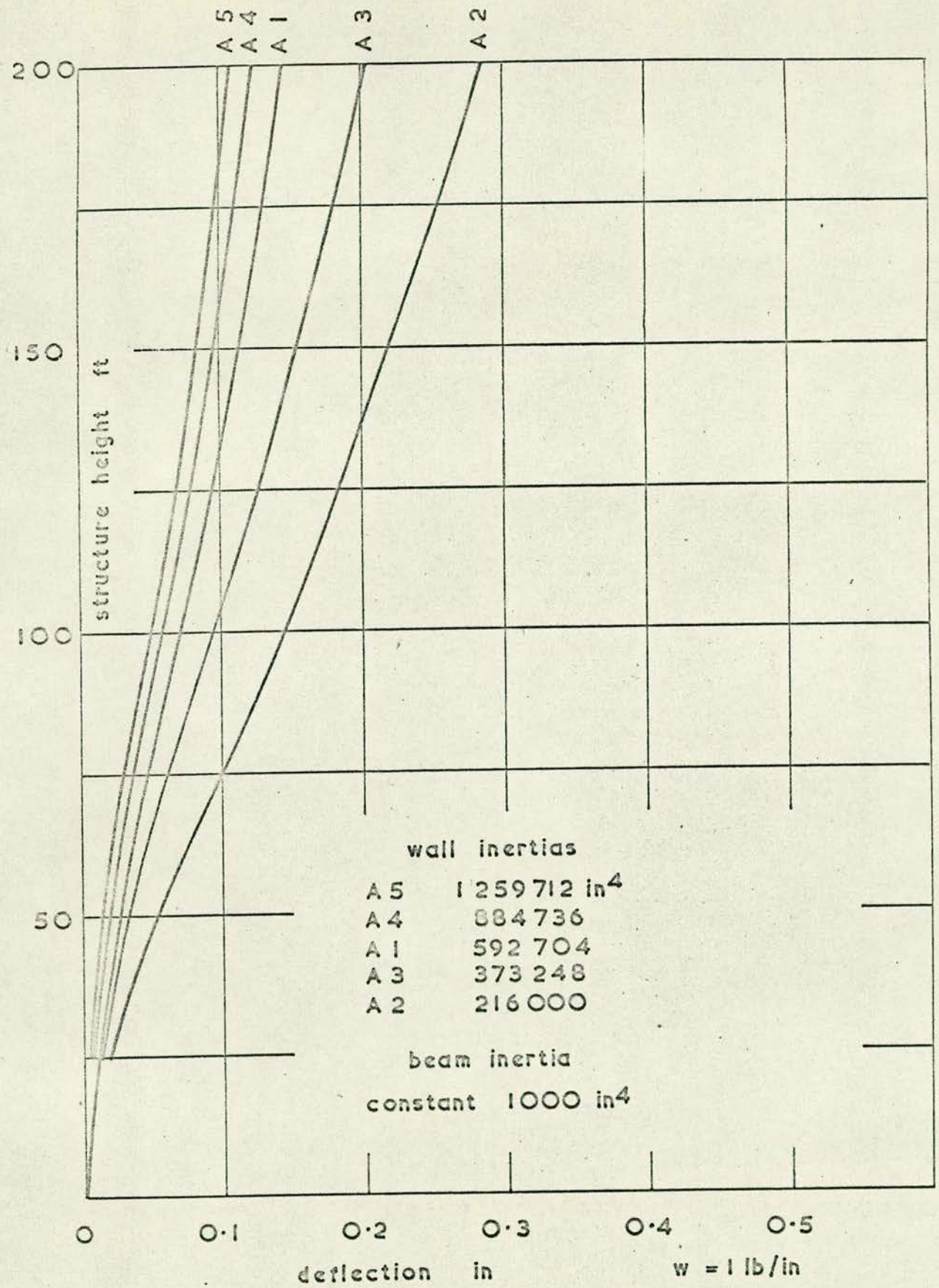

FIG. 5.6 DEFLECTIONS FOR VARYING WALL INERTIAS

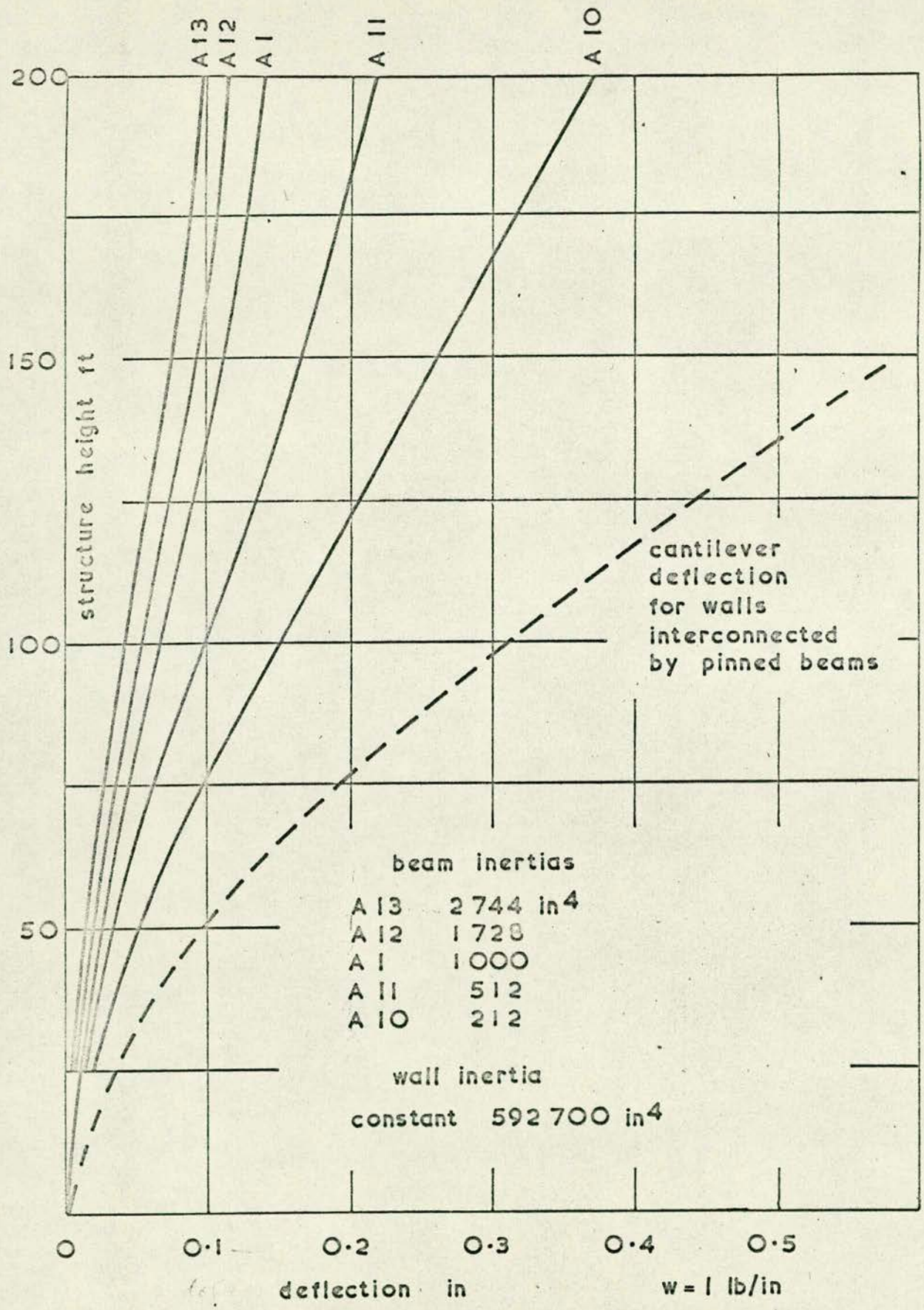

FIG. 5.7 DEFLECTIONS FOR VARYING BEAM INERTIAS

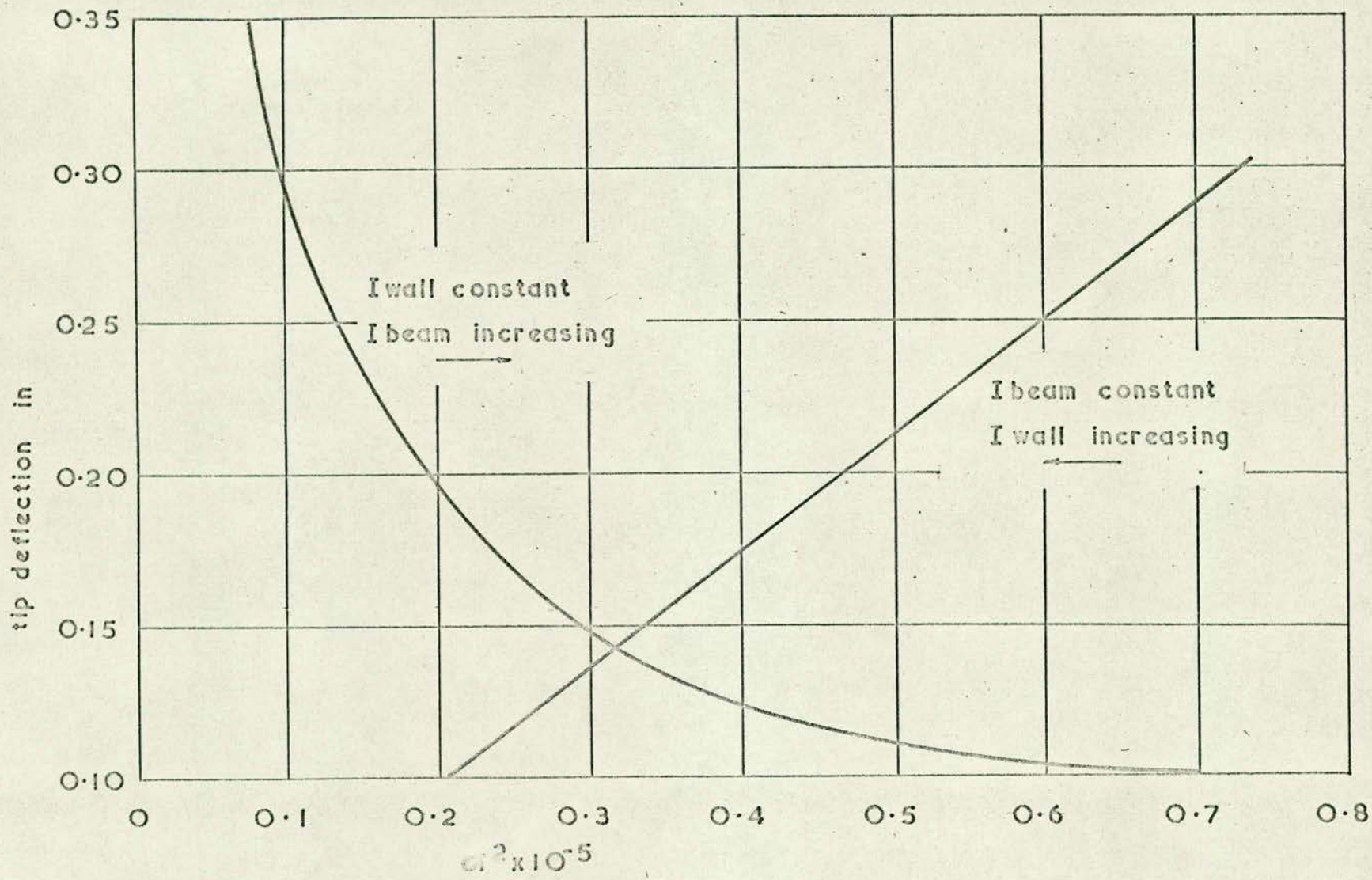

FIG. 5.8 COMPARATIVE STIFFNESSES OF CONCRETE STRUCTURES A

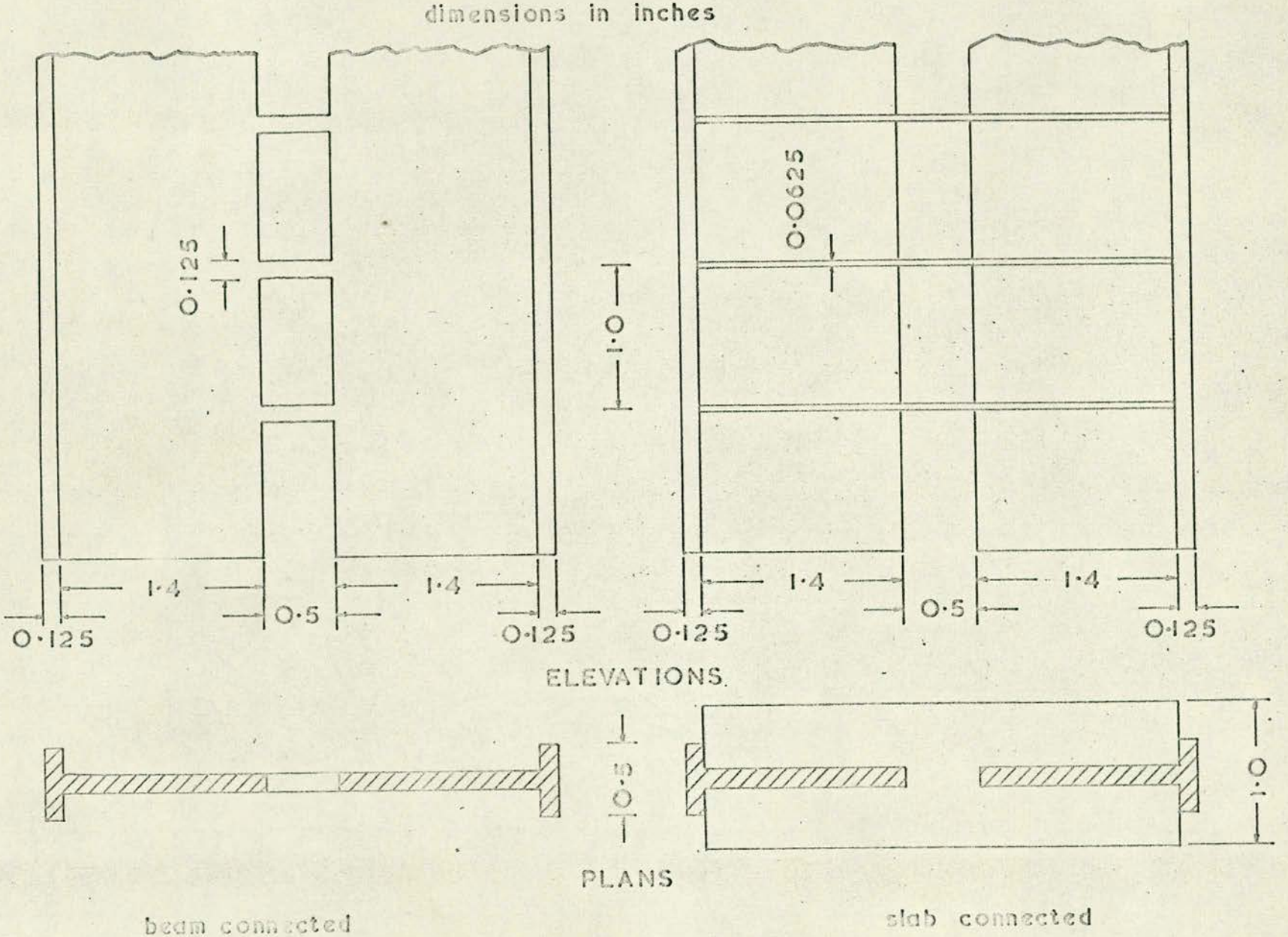

FIG. 5.9 DIMENSIONS OF TWO WALL PERSPEX MODELS

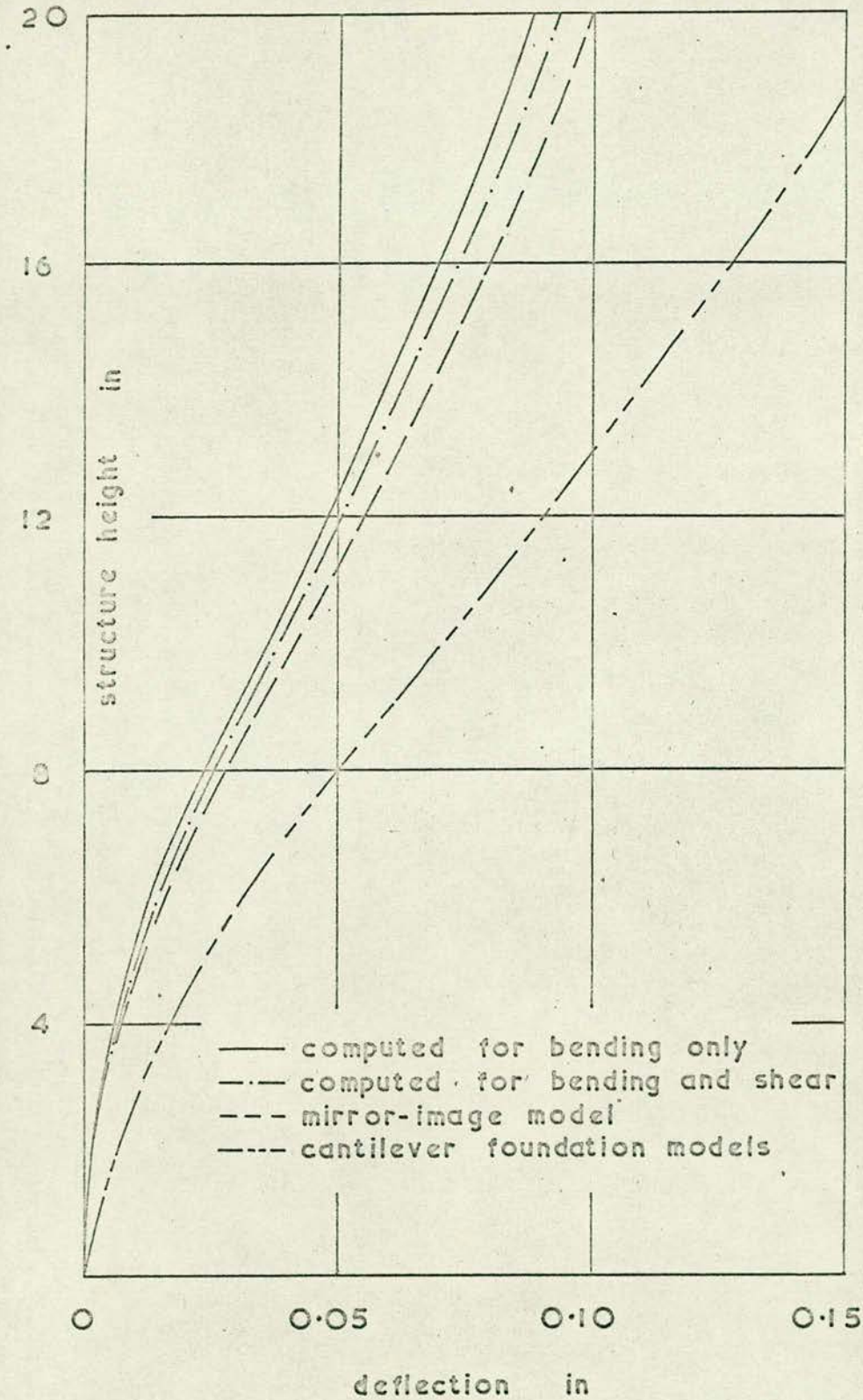

FIG. 5.10 DEFLECTION OF TWO WALL PERSPEX MODELS

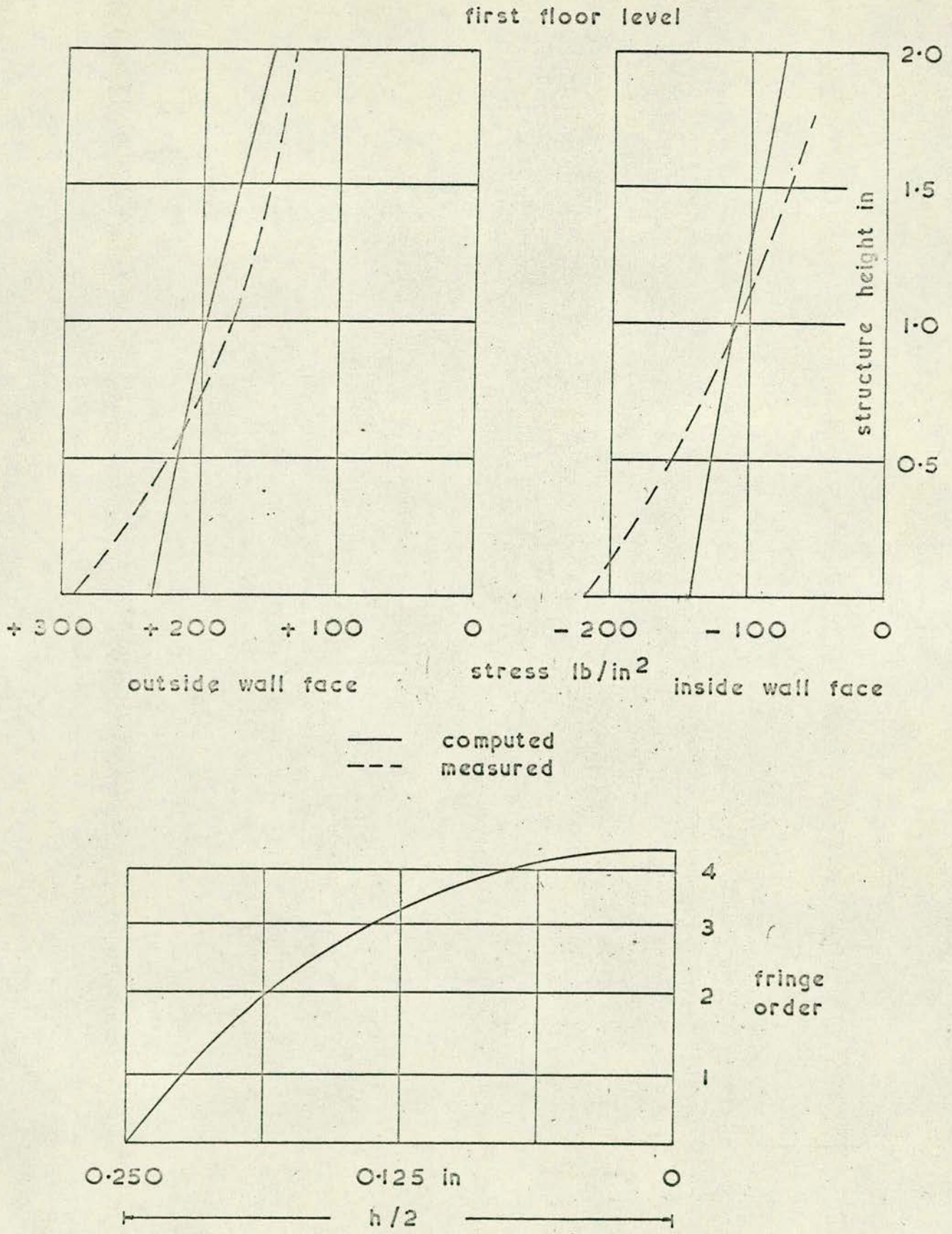

FIG. 5.11 STRESSES FROM TWO WALL ARALDITE MODEL

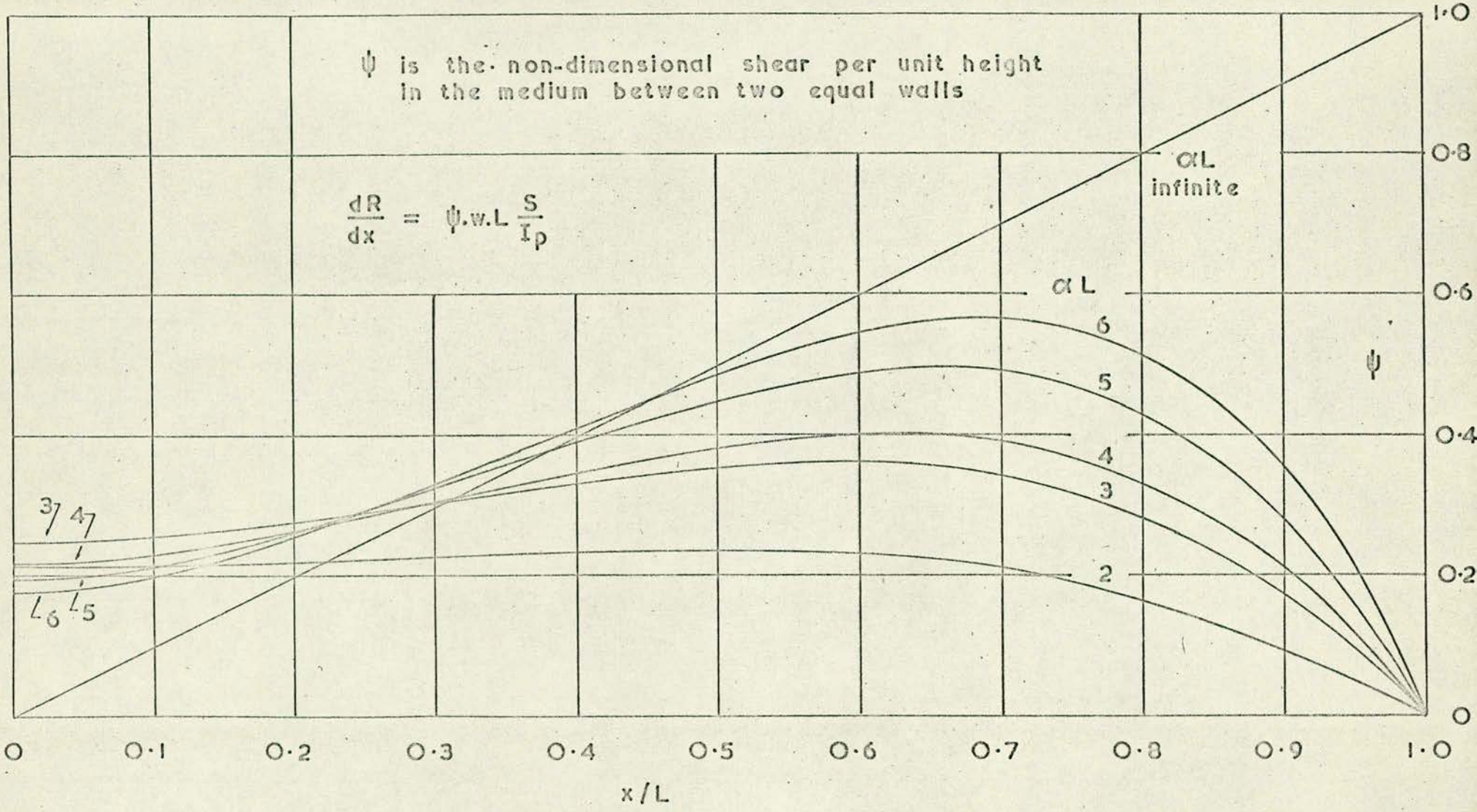

FIG. 5.12 SHEAR FUNCTIONS FOR TWO EQUAL WALLS

ϕ is the non-dimensional integral shear
in the medium between two equal walls

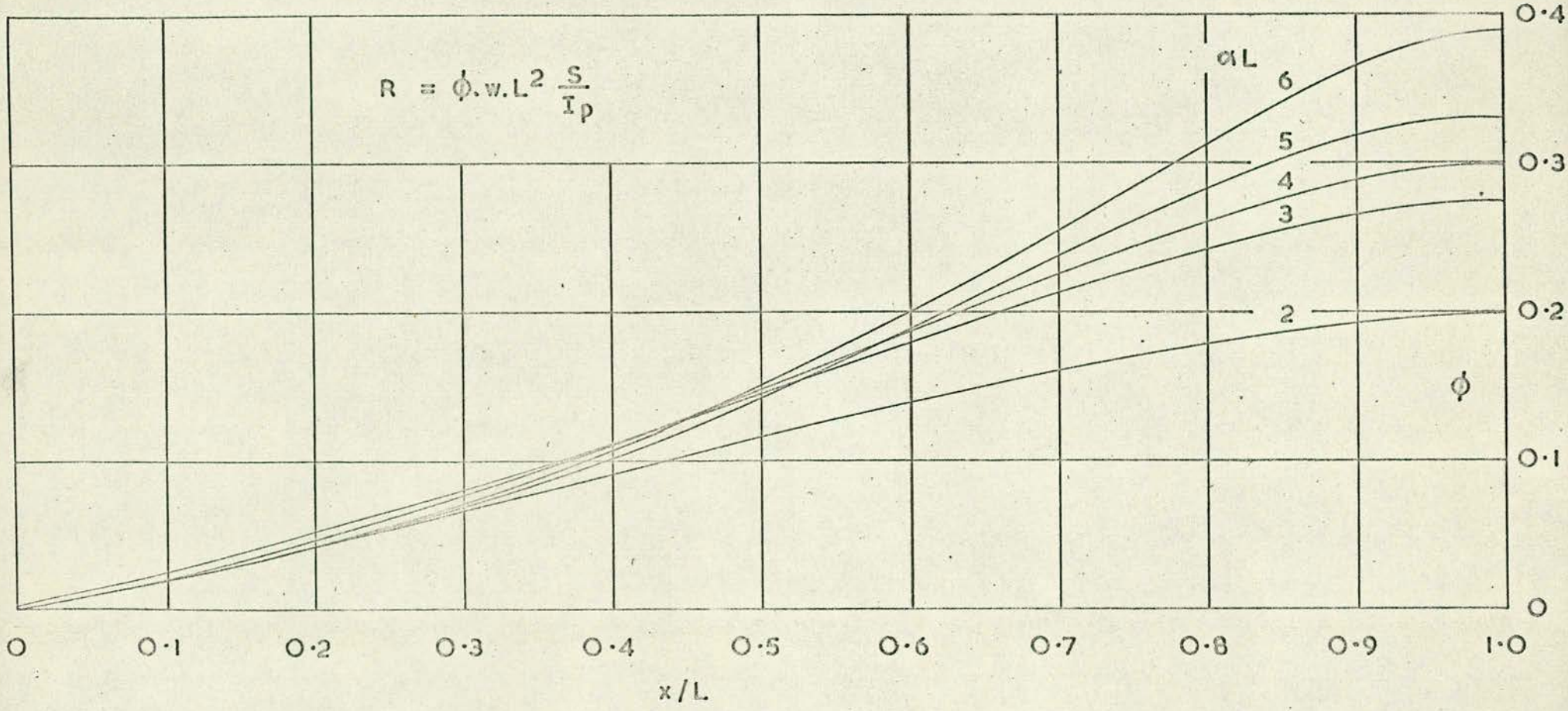

FIG. 5.13 INTEGRAL SHEAR FUNCTIONS FOR TWO EQUAL WALLS

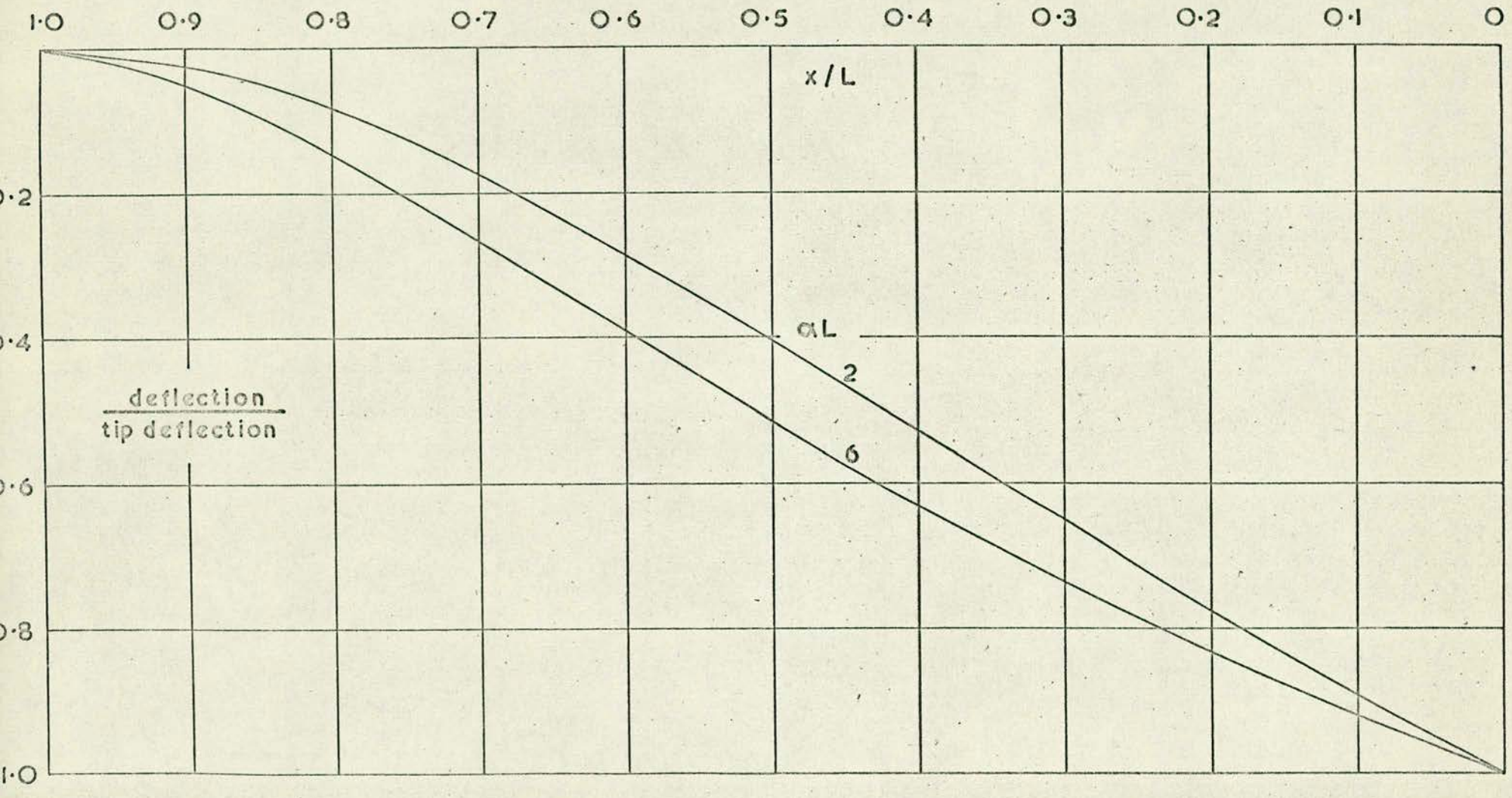

FIG. 5.14 DEFLECTION PROFILES FOR TWO EQUAL WALLS

6. EXPERIMENTS ON TWO WALL MODELS

6.1 Description of models

A number of two wall models were built and tested to determine the behaviour that might be expected in a multi-storey shear wall structure, and to provide checks on the analogue solutions. These were:

1. Twenty storey Perspex structures all having the same wall dimensions but with;
   a) a cantilever foundation, and walls interconnected with slabs,
   b) a cantilever foundation, and walls interconnected with beams of the same moment of inertia as the slabs in (a),
   c) a "mirror-image" foundation (forty storey model with central support), and with walls interconnected with beams as in (b),
2. An eight storey Araldite model with a cantilever foundation and beam interconnections.

All models were subject to dead load tests in the lateral direction, those in group 1 being measured for strains and overall deflection, while the group 2 model was investigated by photo-elasticity. The dimensions were in an approximate 40:1 scale although the structures did not refer to specific prototypes. Plans and elevations are shown in Fig. 5.9.

6.2 Construction of Perspex models

As a model material Perspex has the advantages of cheapness, workability, and low modulus of elasticity allowing readily measurable stresses and deflections. The construction details are simple but

they merit a brief review although the topic has been dealt with by various Authors[44, 45, 46, 47].

Because of its high co-efficient of thermal expansion Perspex is difficult to machine within fine tolerances; but dimensions can be kept to ± 0.005in under normal temperature conditions. The manufactured sheets are by no means constant in thickness and pieces were selected from stock, with the aid of micrometer readings, so that the thickness did not vary by more than ± 0.002in.

Rough cutting was done with a bandsaw having twelve teeth per inch and running at 5,000 ft/min . The edges of thin sheets were finished in a high speed vertical router with a negative rake cutter, steel or alloy templates being stuck to the Perspex with double sided adhesive tape. Thick sectionswere machined in a mill fitted with a spiral toothed cutter. The following specification was suggested by I.C.I. [48].

pitch	0.3
clearance	10°
back clearance	30°
rake	12°
cutting speed	500 ft/min

From the range of I.C.I. cements Tensol no. 7 was chosen for fabricating purposes. This cold-setting cement has gap filling properties and acts as a weld, its ultimate strength approaching that of the parent material. Joints were lightly abraded, degreased, and masked with P.V.C. tape before the operation. After the initial cure of about one hour, the masking was removed but the parts were not subjected to any load for a further twenty four hours.

Each wall was made from a single strip with a flange cemented to the outer edge for stability. Those with cantilever bases had their beams or slabs cemented between the walls and a $\frac{3}{4}$ in thick Perspex foundation slab cemented to the bottom of the walls. The walls and beams of the mirror-image model were cut from a single sheet and the flanges were subsequently cemented in place.

6.3 Strain and deflection measurements

The measured parameters on the Perspex models were strain and deflection. Strains were measured with Saunders-Roe electrical resistance gauges and two sizes were used; $\frac{1}{4}$ in square and $\frac{1}{8}$ in square. They are made from etched foil mounted on epoxy resin backings and Phillips quick hardening strain gauge cement PR9244/04 was used to fix them to Perspex. To get a good bond the usual preliminaries of surface abrading and degreasing were observed (49, 50, 51, 52, 53).

The automatic strain recording equipment to which the gauges were connected is described fully by the author elsewhere(54) and in Appendix C. The energising supply was 3 volts D.C. and with an amplifier gain of 1,000 the sensitivity was better than one micro-strain with negligible drift. The machine could scan up to 100 channels sequentially, results being printed out on paper tape at the rate of one per second.

Deflection measurements were made during the early experiments with Baty dial gauges having a sensitivity of 0.001in, but mechanical backlash, and the force of the internal springs, led to inaccuracies when working with small models. Boulton Paul inductive transducers were therefore used for subsequent work and proved much superior.

Each transducer, type F55, had two parts, a needle which could be attached to the specimen or model either directly or with small clamps, and a pair of co-axial coils which were held on an independent support. The coils were energised by an oscillator (5 volt, 1 KC/s) so that relative movement of the needle within them caused a change of inductance. This signal was demodulated and displayed on a direct reading meter, type C51, in terms of displacement. Sensitivity was proportional to the chosen range of the transducer and for the present experiments was 0.0001in. An ideal set up would have a demodulating and display circuit for each transducer. This however was not possible so a junction panel was made to accept twelve inputs and connect them by three way switching to a common instrument. Since every transducer has a unique gauge factor and zero setting it was necessary to take preliminary readings from the calibrated balancing potentiometers before any test. These values were reset after loading, as each gauge was read, so that the meter indicated the correct deflection.

The absence of physical contact between the transducer components meant that mountings could be simple and small magnetic clamps for the coils were adequate as well as easy to adjust. No trouble was experienced with the electronic systems; readings were stable, accurate, and consistent.

6.4 Tests on Perspex models

The models were always mounted horizontally so that dead weights could be hung from nylon cords at each panel point to simulate wind forces. The foundation slabs were bolted through angle section stiffeners to a $\frac{3}{4}$ in thick steel plate which was then bolted to a

heavy cast iron block. This arrangement was tested for foundation rotation with transducers and although the detected movements were small it was not wholly satisfactory for deflection tests (Chapter 5). A steel beam was independently fixed to the heavy base as a mounting for the transducer clamps. One face was machined so that the magnets could be positioned at any point along its length. Details of typical set ups are shown in Figs. 6.1, and 6.2.

Perspex displays considerable creep [55, 56] and special loading techniques are required. One possibility is to apply point loads through U-shaped Perspex brackets so that the creep is balanced and can hence be ignored. Alternatively, measurements can be made after a set time. If the time is short, say one minute, an instantaneous modulus of elasticity is relevant and this may be found with reference to test specimens. But when a number of loads must be put on and a number of readings taken the procedure is inaccurate since the operations cannot be instantaneous.

An on-off load cycle was therefore adopted with a period of one hour. A model was set up and left for an hour to assume its natural profile. Zero strain and deflection readings were then taken and a unit load increment was applied at each full panel point. The top point was given half a unit. After half an hour effective creep in the Perspex was complete[57, 58] so a further set of readings was taken and the loads were removed. The model was then left for half an hour and a second set of zero measurements were made. These could differ slightly from the initial set, because of electronic drift in equipment or incomplete recovery of the Perspex, so their mean was taken as true zero. A second load increment was

then applied and the procedure was repeated a sufficient number of times to get mean strains and deflections plotted linearly against load. Despite the material not being ideally elastic it is very nearly so for stresses up to 1,000 lb/in ^{2} and this limit was not exceeded. Tests on simple beams carried out in the above manner confirmed the I.C.I. value for the elastic modulus of Perspex as 0.42×10^6 lb/in^2.

A number of experiments had been done with the cantilever models before it was found that although measured stresses were in agreement with computed ones, deflections were not. A mirror-image model was therefore built. This consisted of two symmetrical pairs of twenty storey walls constructed as a continuous forty storey structure. Under test it was lightly clamped between two steel pins bearing on the flanges at the centre point so that a vertical restraint was applied. This is shown in Figs. 6.3 and 6.4. The pins were only $\frac{1}{8}$ in diameter but the system was quite stable and there was no tendency for it to rock.

Transducers were mounted on both sides of the support and the model was loaded symmetrically. Bending moments and axial forces in the walls were therefore balanced at the centre and mean deflection readings from both sides gave the answer that would be obtained from a cantilever with an ideally rigid foundation.

The model was used for displacement tests only and the imperfect nature of the previous foundations was convincingly demonstrated. Deflections from the mirror-image case were almost half those from the cantilever cases with the same dimensions.

6.5 Construction of Araldite model

Data from one photo-elastic model has been included but several specimens were tested and a manufacturing technique was developed. The material was Araldite MY753 with the following properties at 80° C (59).

material fringe value	1.35 lb/in^2/in
modulus of elasticity	1,900 lb/in^2

It is not advisable to cast thick sections of the resin because of its exothermic reaction and the maximum size of sheet was chosen as 24" x 6" x $\frac{1}{4}$" thick. The moulds were made by pre-coating two strips of plate glass with a silicon release agent (Releasil 14) and clamping them together. Lengths of $\frac{1}{4}$ in square mild steel were used as spacers round three edges. Joints between the steel and the glass were sealed with Plasticene and the mould was levelled in a vertical position with the large open end uppermost.

To fill this mould needed 600 gm of resin MY753 and 60 gm of hardener HY951. The components were weighed out and thoroughly mixed with an electric paddle. The container was allowed to stand for fifteen minutes, so that entrained air could escape, before the mixture was poured slowly into the mould. After twenty four hours the glass plates were removed with the aid of gentle leverage and the sheet of Araldite was laid flat for a few days to complete the cure.

The surfaces were always good and very flat but the edges were normally found to be stressed and $\frac{1}{2}$ in had to be cut off all round. Small bubbles tended to be trapped but their presence could be minimised by pre-heating the resin to 30°C. A complete solution is

to cure the mix in a vacuum chamber.

To construct a model a $\frac{1}{4}$ in thick sheet was cut roughly to the total width of the walls plus the openings and a $\frac{3}{4}$ in thick foundation block was cast round the bottom edge. Four lengths of threaded rod were put in as reinforcing at right angles to the walls. This overcame their tendency to pull out of the base during the heating cycle. The complete model was then machined, holes being cut in the sheet to represent the openings between each floor. The usual machining and polishing precautions were taken with the models [60, 61], the final 0.001in cuts being made with a very sharp tool in a high speed vertical router.

6.6 Tests on Araldite model

Because of its size (16 in long) the model could not be tested in a normal polariscope frame so the frozen stress method was adopted. A Sharples oven controlled by a Cambridge Instruments clock was used for the experiments. The temperature cycle was governed by a cam which gave:

room temperature to 80°C, linear rise	3 hours
80°C holding	2 hours
80°C to room temperature, non-linear fall	4 hours

Since the usual material fringe value is much reduced when loading is applied at 80°C some calibration tests were carried out with discs. Once the value had been found the model was simulated by analogue compuation to establish the load which could be put on to give a reasonable number of fringes without producing excessive deflections;

a necessary compromise for frozen stress work.

Preliminary tests had indicated that the compression wall of a plane model was liable to buckle as the plastic softened, so with the foundation bolted so a steel support in the oven the walls were propped to restrict distortion to the plane of loading. A calibration disc of 1.25 inches diameter was loaded in pure compression and put in the oven at the same time. Loads of 0.4 lb per panel point were hung on the model and these gave 8th order fringes at the base of the walls and a tip deflection of 0.75 inches.

The patterns were examined in a Sharples bench polariscope, the polariser and analyser being at 90° apart, with the quarter wave plates at 45°, to give a crossed circular set up. The background was hence dark and full fringes could be observed. Diffused white light was used to establish the fringe orders in terms of their colour magnitudes, and a monochromatic sodium light source was used for detailed studies. Photographs were taken with an Edixa reflex camera fitted with a 2 mm extension collar. The best pictures were given at an aperture setting of f11 and an exposure time of 3.5 seconds using panchromatic film.

The fringe order at the centre of the disc was n = 4.5 with a test load of 3.9 lb, so the material fringe value for shear stress was:

$$f = \frac{1}{n} \cdot \frac{4P}{\pi d} = 0.885 \text{ lb/in}^2/\text{in}$$

where f is the material fringe value for shear,

n is the fringe order at the centre of the disc,

P is the applied load,

d is the diameter of the disc.

For a $\frac{1}{4}$ in thick section the model fringe value was:

$4f = 3.740 \text{ lb/in}^2$

A first order fringe therefore shows a shear stress contour of 3.740 lb/in^2 and a difference in principal stress contour of 7.480 lb/in^2.

Some photographs are reproduced in Figs. 6.5, 6.6, 6.7, and 6.8, and it may be seen that there are sufficient fringes to determine the stresses in all of the connecting beams but only the stresses in the walls for the first storey. At the central points of beam inflection there are pure shear stresses and these were plotted in the typical parabolic pattern shown in Fig. 5.11.

The shear forces could therefore be established and compared with the values given by computation (Table 5.10). Boundary stresses in the walls are found directly from the fringe orders since there are no normal forces at the free edges. Complete analysis would require relaxation or some other technique to find the sum of the principal stresses but this was not done, nor were the stress concentrations examined at the beam wall junctions. A comparison between experimental and computed wall stresses is given in Fig. 5.11.

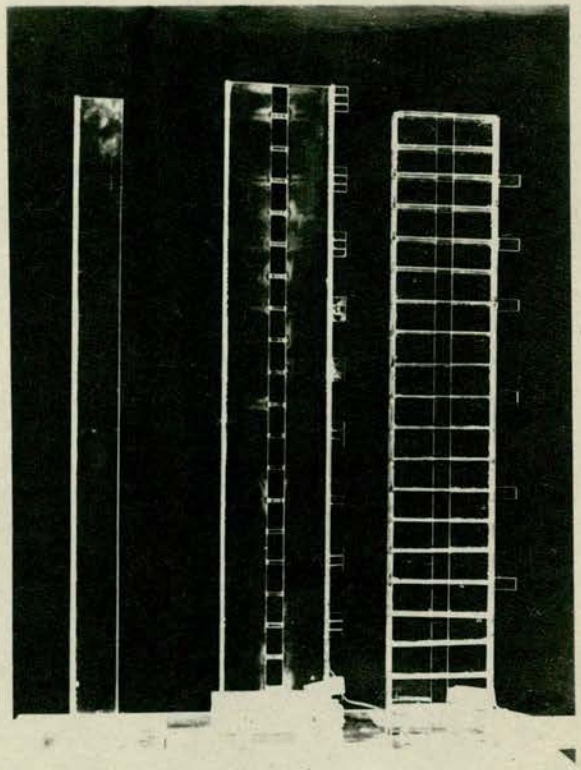

FIG. 6.1
Cantilever models showing from left to right; a single wall, beam connected walls, slab connected walls.

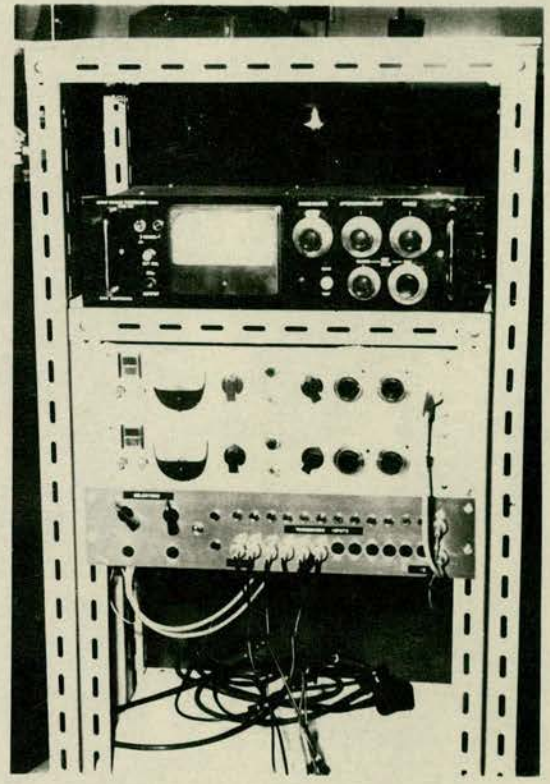

FIG. 6.2
Deflection measuring equipment showing the Bolton Paul transducer meter, two Honeywell carrier amplifiers, and the gauge distribution panel.

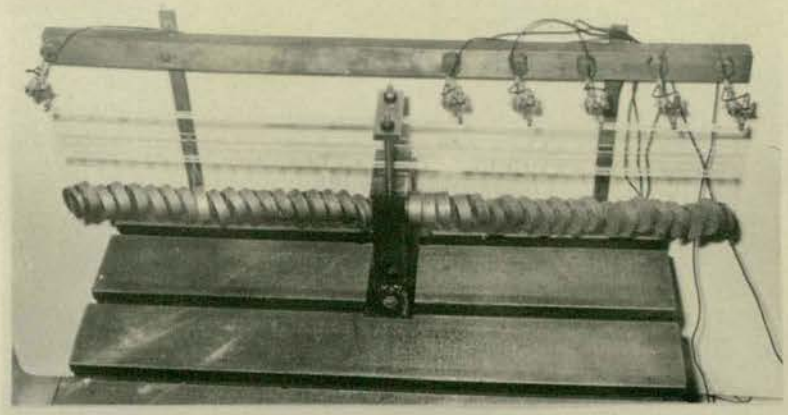

FIG. 6.3 General view of mirror-image model.

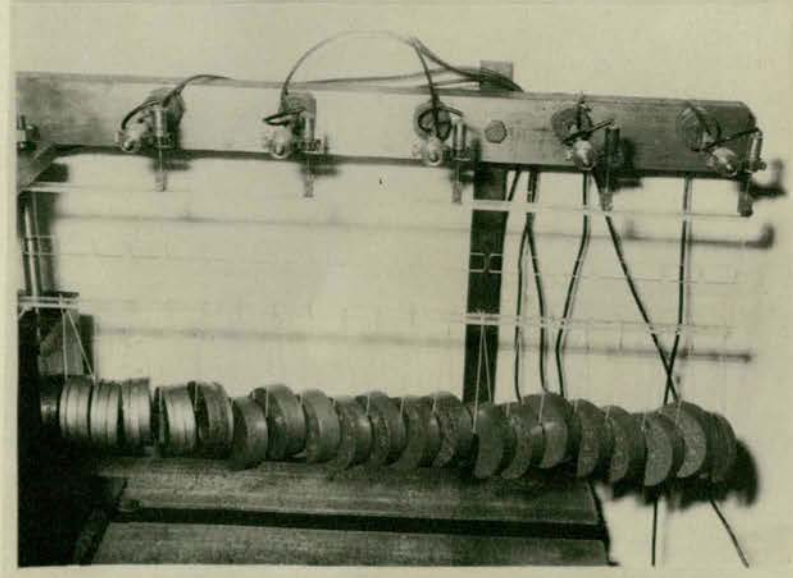

FIG. 6.4 Deflection measurements on mirror-image model.

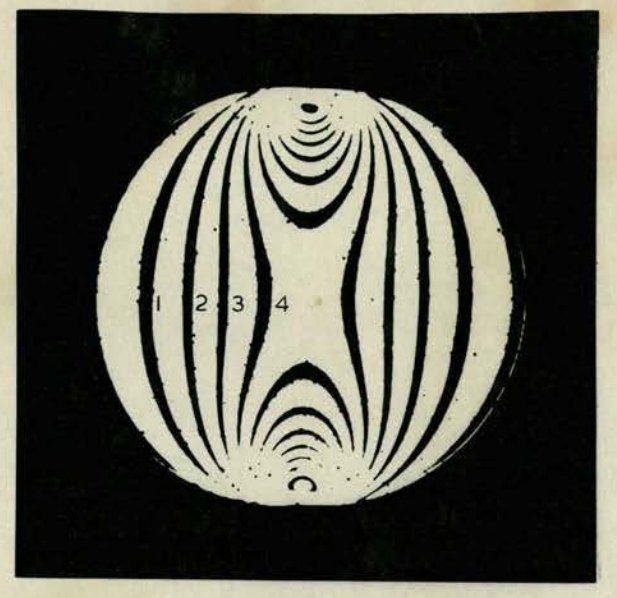

FIG. 6.5
Calibration disc from
frozen-stress experiments.

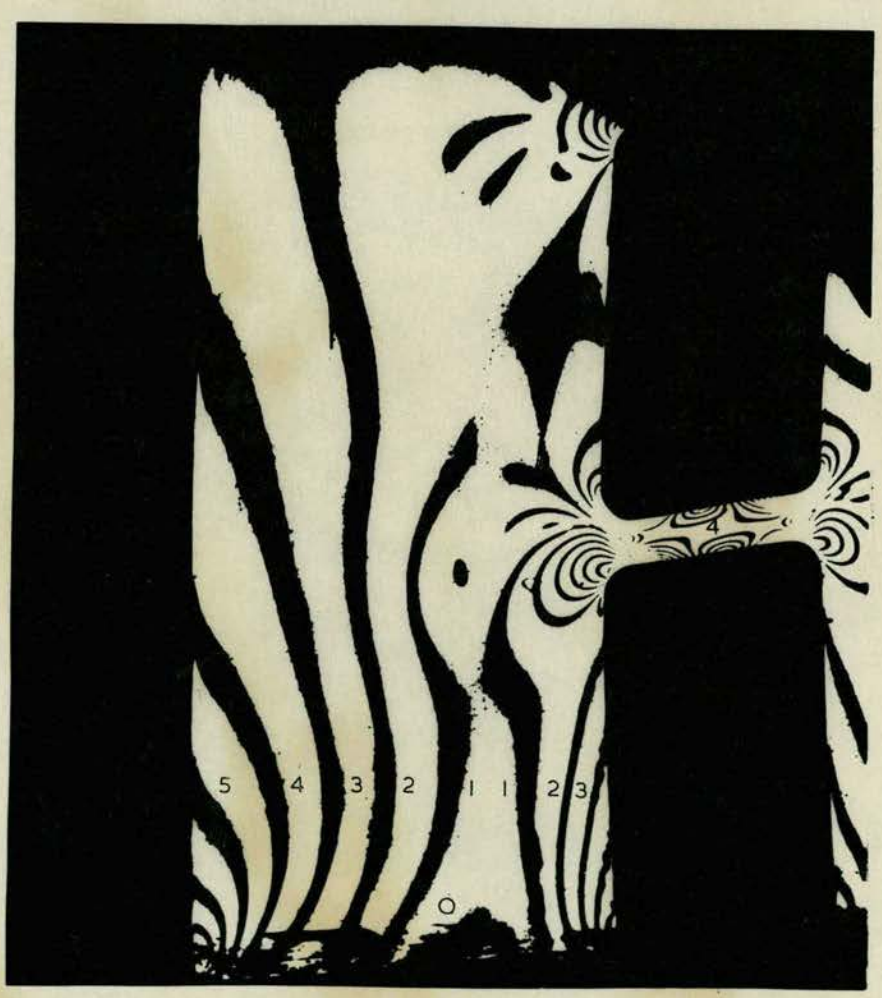

FIG. 6.6 Stress patterns on one wall of the Araldite model.

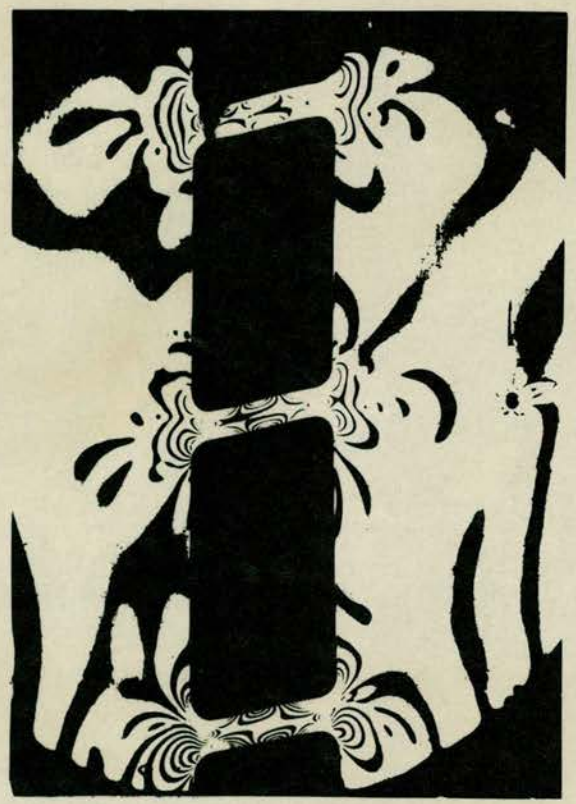

FIG. 6.7 Stress patterns in beams on the first three floors.

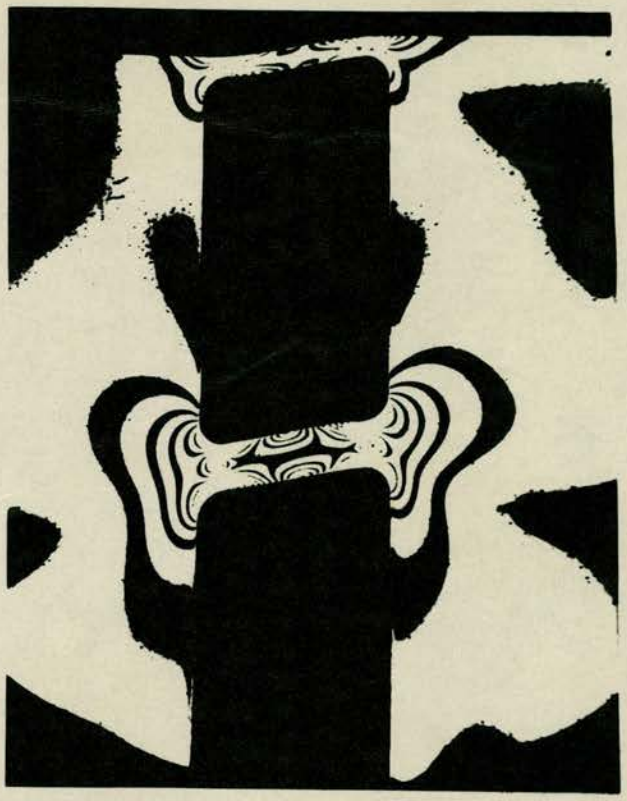

FIG. 6.8 Stress patterns in beams on the top two floors.

7. EXPERIMENTAL WORK ON A COMPLEX STRUCTURE

7.1 Essex University residence towers

As Consulting Engineers for the new University of Essex at Colchester, Messrs Harris and Sutherland designed a number of residence blocks. These are fourteen storeys high and are constructed from load-bearing brickwork. Such structures are a recent innovation in Great Britain and at present there are a number of uncertainties about their behaviour. Principal among these is the effective lateral stiffness.

The floor plan of blocks 1 and 2 is typical. It is repeated on each storey and consists of external double leaf walls and several rather irregular internal wall complexes. As well as taking vertical loads these walls must resist all lateral forces. The forces are transmitted to the walls by continuous reinforced concrete floor slabs which are perforated by holes for lift-shafts, staircases and service ducts. The walls are $4\frac{1}{2}$", 9" or $13\frac{1}{2}$" thick, depending on their position, and are in Stretcher, English, or Quetta bond.

The overall behaviour is therefore difficult to assess. The work of the Structural Ceramics Research Unit has brought insight into the properties of brickwork panels and model brick structures. Model shear wall assemblies with one to three storeys have been investigated but little is available at a practical level on the structural nature of complicated wall units and interconnecting slabs.

Accordingly, a Perspex model of the central core of the building was made. Measurements were taken of strains and deflection with the preliminary aim of establishing the effective moments of inertia and the stress distributions in the walls.

The experimental deflection profiles were analysed by the following methods.

1. Calculations by elementary theory assuming ideal cantilever action and considering bending only.
2. The above method modified for the effects of shear.
3. Basic function analysis.

Since this work was carried out before the continuum theory was fully developed the results were used directly to check the original designs. At a later stage the model was expressed in terms of an equivalent structure and simulated by analogue computation.

The plan arrangement of two subsequent blocks, 3 and 4, was changed somewhat from the configuration of blocks 1 and 2 and the design of these was checked by computation only.

7.2 Preliminary design

Tentative designs were based on simplifications regarding the structural behaviour. It was first assumed that the wall to wall joints in any of the wall units (Fig. 7.1) would be rigid. Any unit could therefore be considered as a cantilever beam with appropriate webs and flanges. The cantilevers would be fixed at the base and extend the full height of the structure. Because of their relative flexibility (compared with the wall units) it was thought that the slabs would act as pin ended struts. Although the units are separated by the slabs at each floor it was fair to assume that their self weight would give vertical continuity to the walls.

The building would thus act as a series of pure cantilevers. Consider the core, shown in Fig. 7.2, loaded perpendicularly to the X-X axis. Its effective moment of inertia would be the sum of the

moments of inertia of the eight wall units about their own centroids.

$$I_{e(xx)} = I_{1x} + I_{2x} + \ldots\ldots + I_{8x} \qquad (7.1)$$

where I_{1x} is the moment of inertia of unit 1 about its centroid, parallel to the X-X axis. The dimensions and inertias of the model wall units are given in Table 8.1.

It is known that with pin connected slabs (section 3.1) the wall units resist the total external moment M_o in proportion to their moments of inertia.

$$\frac{M_{1x}}{I_{1x}} = \frac{M_{2x}}{I_{2x}} = \ldots\ldots\ldots\ldots = \frac{M_{8x}}{I_{8x}} \qquad (7.2)$$

and

$$\frac{M_{ox}}{I_{e(xx)}} = \sum_{n=1}^{8} \frac{M_{nx}}{I_{nx}} \qquad (7.3)$$

Wall stresses would be due to bending only and the maximum stress in any unit could be found from the simple expression:

$$\sigma = \frac{M_{ox}}{I_{e(xx)}} \cdot \bar{y} \qquad (7.4)$$

where $\bar{y}$ is measured from the centroid to the extreme fibre of the unit concerned (Fig. 7.1 and Table 8.1).

To calculate deflection the structure would be thought of as a cantilever with a moment of inertia $I_{e(xx)}$. For loading perpendicular to the Y-Y axis an equivalent moment of inertia may be found in the same way.

To sum up, such an analysis relies on the following assumptions.

1. Each wall unit acts as a full height cantilever beam and the

stress distribution is that pertaining in such a section under the action of bending.

2. There is no co-action between the various units - the slabs act as pin jointed beams. The rigid nature of the wall to slab junctions and the stiffness of the slabs are ignored.

It was to test these arguments that a model was made of the central core.

7.3 Tests on Perspex model

The plan arrangement of the wall complexes in the core is shown in Fig. 7.2 A geometric scale of 1:48 produced a model whose storey height was two inches compared with eight feet in the prototype.

The sizes of the internal brick walls were scaled directly in this ratio and the inner leaf only of the external walls was considered as load bearing. Since the floors are of reinforced concrete the geometric scale does not apply and the Swiss Code of Practice (NORM113) ratio:

$$\frac{E \text{ concrete}}{E \text{ brickwork}} = 2$$

was used to calculated the model floor depth. Table 7.1 shows how standard Perspex sheets provided most of the required thicknesses.

Table 7.1

Scaled dimensions

construction material	prototype dimension (in)	scaled dimension (in)	Perspex thickness (in)
brickwork	4.5	0.0938	0.0938
brickwork	9.0	0.1875	0.1875
brickwork	13.5	0.2313	0.2500
R.C.	4.0	0.1666	0.1563

The relationships between a structural model and its prototype depend fundamentally on the elastic moduli of the elements, the geometric scale factor and the nature of the loading. All behaviour is assumed to be linear to permit the laws of superposition. Ideally the Poissons' ratios of both model and prototype should be equal; but in cases where bending and axial stresses predominate, a dimensional analysis demonstrates that it is permissible to waive this rule.

Brickwork is only approximately elastic, but the results from an elastic model will give quantitative data relative to the influence of the geometric configurations of the wall complexes, and qualitative information on the magnitudes of expected stresses and deflections.

The self weight of the building may cause effects which cannot be estimated by superposition but the involved techniques for simulating body forces were not used. Any errors due to this were neglected.

The usual theory of models[62, 63] gives the following scale factors for point loads:

$$\begin{aligned} y &= s\, y_m \\ F &= s^2 \cdot \frac{E}{E_m} \cdot F_m \\ M &= s^3 \frac{E}{E_m} \cdot M_m \\ \sigma &= \frac{E}{E_m} \sigma_m \end{aligned} \qquad (7.5)$$

The subscript "m" refers to the model and s is the geometric scale factor.

1:S = 1:48

Construction of the model differed slightly from the method given in Chapter 6. The storeys were made separately in a jig and each assembly was put in a milling machine so that the tops of the walls could be cut level. The upper storeys were then cemented together, and the first storey was cemented to a $\frac{1}{2}$ in thick Perspex base slab.

The model was initially built to seven storeys but the performance was unsatisfactory because of its rigid nature and an inadequate foundation. It was therefore extended to fourteen storeys and the foundation was made considerably stiffer. Details of the mounting and the experimental set up can be seen in Figs. 7.4, 7.5, 7.6 and 7.7.

Deflections were measured with variable inductance transducers fitted above the centres of the slabs. Strains were found with electrical resistance gauges. Forty three sets were distributed at representative points on the walls, the majority being positioned as shown in Fig. 7.3 just above the first floor. A row of gauges was also put on a vertical axis of one of the walls in unit 3 to give a relationship between stress and structure height.

The gauges measured bending and axial strains. Torsional effects were thought to be negligible for uniform loading because deflection tests showed that the shear centre of the building was very near its geometric centre.

Four series of experiments were carried out. Each of them involved loading one side of the model as shown in Fig. 7.3. During the E1 and E2 series the structure was loaded on the longer sides and weights were hung from four points on each slab. For tests E3 and E4 the structure was

turned through 90° and weights were hung from two points on each slab. The on-off load cycle method was used to avoid creep errors. Four load increments were applied in each test, the maximum being 8lb per floor giving a total moment at the foundation of 15681b in. No foundation movements were detected but, as will be explained later, there was possibly some distortion.

7.4 Elementary analysis of deflection curves

The simplest way of estimating equivalent inertias was to assume pure cantilever action. The deflected form of a cantilever under a uniformly distributed load of 1 lb/in is given by:

$$y = \frac{1}{EI_e}\left(\frac{x^4}{24} - \frac{L^3x}{6} + \frac{L^4}{8}\right) + \frac{\chi}{2A^*G}\left(L^2 - x^2\right) \qquad (7.6)$$

where A* is the effective web area .

The first term is bending deflection and the second is an approximate shear correction but the complex shapes of the wall units preclude knowing accurately the values of A*. In each direction A* was estimated as the sum of the areas of those walls which were parallel to the loading and thus acted as webs.

Any pair of co-ordinates from the experimental curves could be fed into equation 7.6 if their form were that of a simple cantilever. But it may be seen from Fig. 7.8 that both curves exhibit a point of inflection. It hence becomes necessary to fit simple deflections to the measured ones and this was achieved by using the co-ordinates of the points of inflection. Such a substitution will over-estimate the rigidity below these points and under-estimate it above them.

The point of inflection for loading perpendicular to the X-X axis was measured at x = 10in, and for loading perpendicular to the Y-Y axis at x = 12in. Corresponding values of y were put in equation 7.6 to find equivalent inertias on the basis of bending only and bending with shear. The results are given in Table 7.3.

7.5 Basic function analysis of deflection curves

The basic function method was adopted from work on the analysis of grid frameworks by Hendry and Jaeger[64]. They show that a beam with any type of end conditions, loaded along its length in any manner, may be analysed by basic functions. These functions consider bending effects only. A given load may be divided into an infinite number of basic functions, each basic function having the property of producing a deflection of the same shape as itself. The equation satisfied by all basic functions is:

$$\frac{d^4 F(x)}{dx^4} = K.F_{\cdot}(x) \qquad (7.7)$$

where K is a constant, and

$F(x)$ is a basic function.

If $K = \theta^4$ the functions for a cantilever are of the form:

$$F(x) = A(\cosh \theta x - \cos \theta x) - (\sinh \theta x - \sin \theta x) \qquad (7.8)$$

When interest is centred on deflections the first basic provides a good approximation and tends to eliminate the need for separate calculations on shear distortion.

The first basic for a cantilever is:

$$F_1(x) = 1.362\,(\cosh \theta_1 x - \cos \theta_1 x) - (\sinh \theta_1 x - \sin \theta_1 x) \quad (7.9)$$

where $\theta_1 = \frac{0.597\,\Pi}{L}$

If the load profile on the cantilever is written as:

$$w(x) = w_1 . F_1(x) + w_2 F_2(x) + \ldots\ldots\ldots \quad (7.10)$$

it may be shown that

$$w_n = \frac{\int_0^L w(x) . F_n(x) . dx}{A_n^2 \; L} \quad (7.11)$$

For a uniformly distributed load w:

$$w_1 = \frac{w}{A_1^2 . L} \int_0^L F_1(x) . dx \quad (7.12)$$

Substituting in equation 7.12 from equation 7.9.

$$w_1 = \frac{wL}{1.857 \times L \times 0.597\,\Pi} \left[1.362\,(\sinh \theta_1 x + \sin \theta_1 x) - \cosh \theta_1 x + \cos \theta_1 x \right]_{x=0}^{x=L}$$

and substituting for θ_1:

$w_1 = 0.575\ w.$

In terms of the first basic only:

$$w(x) = 0.575\ w . F_1(x) \quad (7.13)$$

Substituting for $F_1(x)$ in equation 7.13 from equation 7.7:

$$w(x) = 0.575\ w \frac{1}{\theta_1^4} \frac{d^4 F(x)}{dx^4} \quad (7.14)$$

The general deflection equation for a beam is:

$$\frac{d^4}{dx^4} \left(\frac{y(x)}{} \right) = w(x) / EI_e \qquad (7.15)$$

and substituting in equation 7.15 from equation 7.14 and integrating:

$$y(x) = \frac{w}{EI_e} \left(\frac{0.575\ F_1(x)}{\theta_1^4} \right)$$

This expression can also be written as:

$$y(x) = \frac{wL^4}{\Pi^4 EI_e} \left(\frac{0.575\ F_1(x)}{(0.597)^4} \right) \qquad (7.16)$$

The required function y(x) is the first basic deflection function of an experimental curve. This must be found in terms of $F_1(x)$ and substituted into equation 7.16. The only unknown will be I_e.

Let an experimental curve be denoted y(x).

$$y(x) = y_1\ F_1(x) + y_2\ F_2(x) + \ldots\ldots\ldots \qquad (7.17)$$

Therefore:

$$y_1 = \frac{\int_0^L y(x)\ F_1(x).\ dx}{A_1^2\ L} \qquad (7.18)$$

(It may be noted that equation 7.18 has the same form as equation 7.11)

An approximate integration may be carried out numerically as follows. Divide the length of the beam L into N equal intervals; take the ordinates of y(x) and $F_1(x)$ at the mid-point of each interval and find their product.

Then:

$$\int_0^L y(x).\ F_1(x)\ dx. \doteq \frac{L}{N} \sum_{N=1}^{N} \text{ordinate } y(x)_N \text{ x ordinate } F_1(x)_N \qquad (7.19)$$

Loading perpendicular to X-X axis

Deflections are taken from Fig. 7.8 and $F_1(x)$ is obtained from Fig. 7.9. Table 7.1 gives the necessary data for the curves divided into seven intervals.

Table 7.1

First basic for loading perpendicular to X-X

$\frac{x}{L}$	$1/14$	$3/14$	$5/14$	$7/14$	$9/14$	$11/14$	$13/14$
$y(x)_3 \times 10^3$	0.15	0.80	1.80	3.00	3.80	4.50	4.90
$F_1(x)$	0.06	0.20	0.49	0.90	1.35	1.90	2.48
$y(x) \cdot F_1(x) \times 10^4$	0.90	1.60	8.82	27.00	51.30	85.50	121.52

by addition: $\sum_{1}^{7} y(x) \cdot F_1(x) = 0.029439$

and from equation 7.19:

$$\int_0^L y(x)\ F_1(x)\ .\ dx = \frac{28}{7} \times 0.029439 = 0.1178 \text{ in}^2$$

From equation 7.18:

$$y_1 = \frac{0.1178}{1.857 \times 28} = 0.002265 \text{ in}$$

therefore $y(x) = 0.002265\ F_1(x)$

By substituting in equation 7.16 for y(x), w (1 lb/in) and E (0.42×10^6 lb/in^2) the equivalent inertia, $I_{e(xx)}$ is found (Table 7.3).

Loading perpendicular to Y-Y axis

Table 7.2 gives similar data for the other experimental curve where

loading is perpendicular to Y-Y.

Table 7.2

First basic for loading perpendicular to Y-Y axis

$\frac{x}{L}$	$1/14$	$3/14$	$5/14$	$7/14$	$9/14$	$11/14$	$13/14$
$y(x)_3$ x 10^3	0.35	1.30	2.80	4.80	7.50	9.80	11.70
$F_1(x)$	0.06	0.20	0.49	0.90	1.35	1.90	2.48
$y(x).\ F_1(x)$ x 10^4	0.21	2.60	13.72	43.20	101.25	186.20	290.16

From Table 7.2, $y(x) = 0.004900\ F_1(x)$ and $I_{e(yy)}$ is obtained by substitution (Table 7.3).

7.6 Equivalent moments of inertia

The inertias calculated on the assumption of independent cantilever units are compared in Table 7.3 with results from the analysis of the experimental deflection curves.

Table 7.3

Equivalent moments of inertia

Method	$I_{e(xx)}$ (in^4)	$I_{e(yy)}$ (in^4)
1. Calculations from experimental curves by elementary theory considering bending only	29.20	12.33
2. The above method modified for shear distortion	34.05	13.70
3. Basic function analysis	30.00	13.87
4. Preliminary design	9.75	14.39

A review of Table 7.3 shows that for loading perpendicular to the Y-Y axis the experimental inertias are in good agreement with the theoretical value. This is to be expected because there is little scope for composite action. Most of the walls acting as webs run the full width of the units.

The experimental inertias about X-X are roughly three times as large as the theoretical value. The actual sizes vary with the method used, but they illustrate convincingly that the original assumptions are too conversative and that there is co-action between the walls and the floor slabs.

7.7 Stress distributions

The results from the strain gauges were converted to average stresses on the walls, and the resultant stress distributions at the second floor level are shown in Figs. 7.10 and 7.11. Stresses were assumed to vary linearly between the points where measurements were taken (Fig. 7.3).

From the stress patterns the moments on the wall units were calculated and they are compared in Table 7.4 with the externally applied moment to provide an equilibrium check.

Table 7.4

Total moment at 1st floor level

(w = 1 lb/in: section at x = 25.625 in)

test	applied moment (lb in)	measured moment (lb in)
load perpendicular to X-X axis	329	353
load perpendicular to Y-Y axis	329	337

Consddering first the E1 and E2 series of tests with loading perpendicular to the Y-Y axis the following points may be noted from Fig. 7.10.

1. The "I" type elements at either end of the building act in the expected manner: the neutral axes coincide with the centres of the walls.
2. The four angle sections have neutral axes which are near the free ends of their webs and not, as would occur with normal cantilever bending, at the centroids close to their flanges. This effect is due to the floor slabs, which span between corresponding pairs of angles, acting as beams and introducing bending moments and axial forces at the wall-slab joints.
3. The two internal wall complexes behave as units with neutral axes approximately coinciding with their centroids, thus showing that the webs are sufficiently rigid to carry the necessary shear between the flanges. It is interesting to note that there are stress increases at the free ends of some flanges and decreases at others.

From the E3 and E4 series of experiments the stress distribution for loading perpendicular to the X-X axis was plotted in Fig.7.11. The pattern here is significantly different from anything predicted by simple theory. There is a large degree of composite action. Again, considering the wall complexes in turn the following points arise.

1. The neutral axes of the end "I" beams lie outside the elements and the stress is of the same nature over the whole of each element. This indicates a large axial force component and a re-distribution

of bending moments; both are caused by interaction of walls and slabs. The stress increases at the free ends of the long flanges are due to their proximity to the corners of the angle units.

2. There is also evidence of composite action in the behaviour of the angle sections. Their neutral axes are near the free ends of their webs. The short floor span between the angles and the "I" beams makes the units act with a fair degree of continuity.

3. The stresses on the internal wall units show predominately bending action with neutral axes near their centroids.

These stress distributions on the core correspond to the type which might be expected in a plane row of shear walls so it was decided to attempt a theoretical analysis of the model loaded perpendicular to the X-X axis.

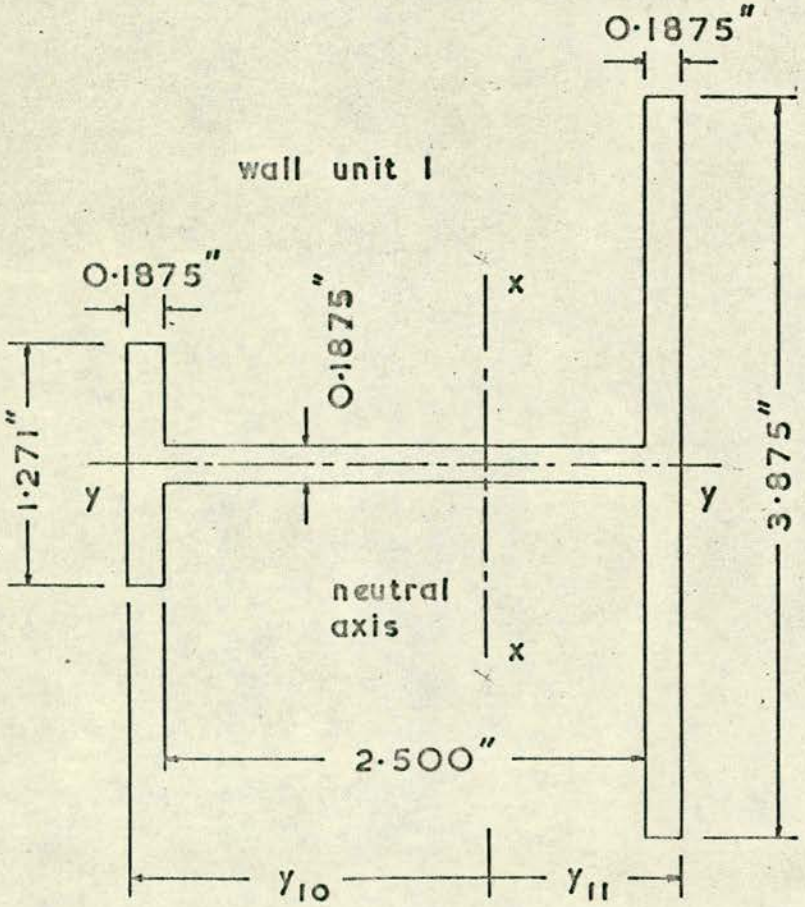

moments of inertia

I_{xx} 1·8656 in^4

I_{yy} 0·9426 in^4

distances from neutral x-x axis to extreme fibres

y_{10} 1·8949 in

y_{11} 0·9801 in

FIG. 7.1 TYPICAL WALL UNIT

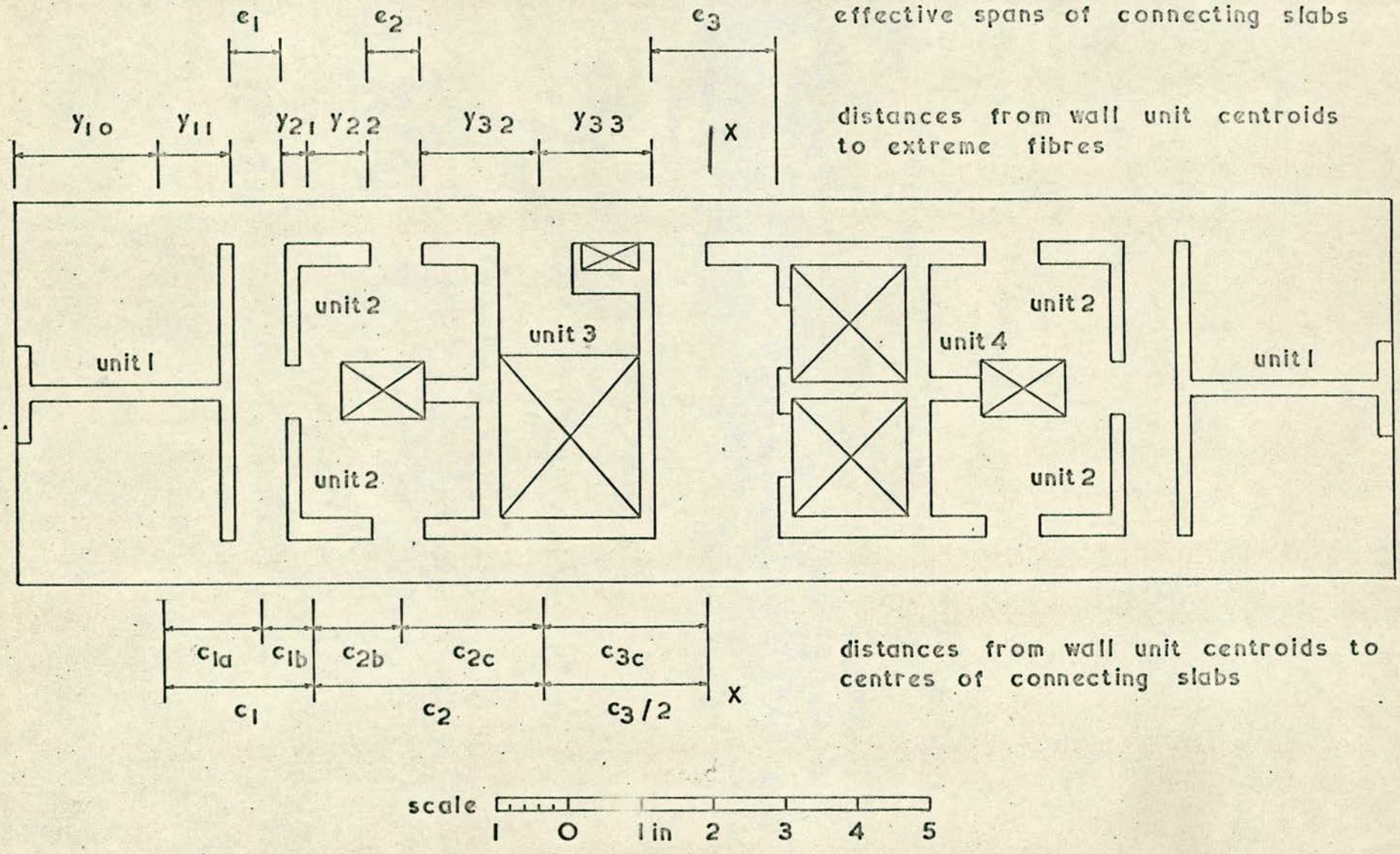

FIG. 7.2 PLAN OF ESSEX BLOCK I MODEL

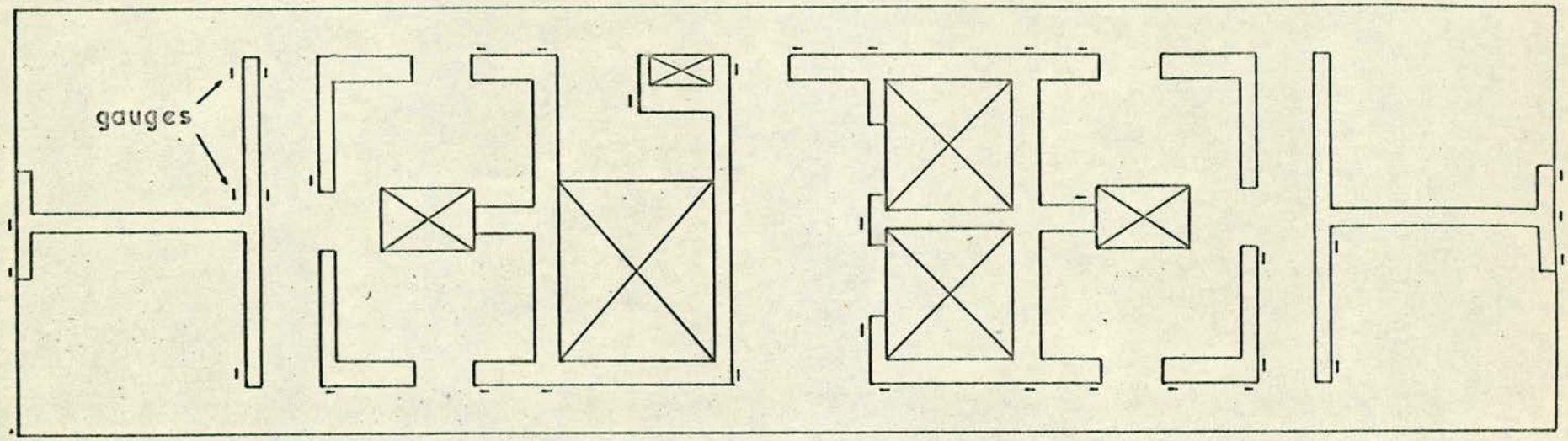

strain gauge positions on 2nd floor
gauges mounted 5/16in above slab

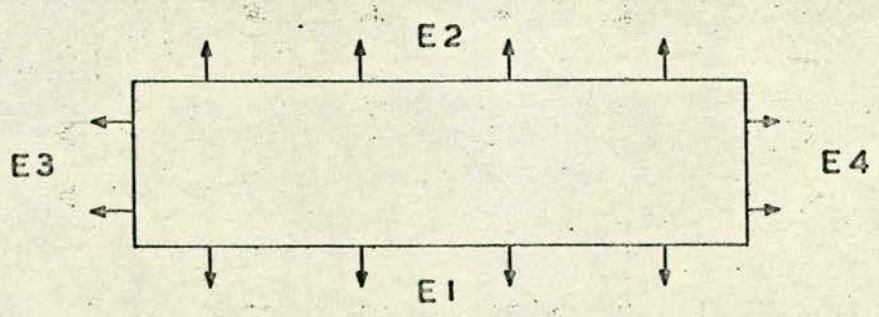

directions and positions of loads

FIG. 7.3 GAUGE POSITIONS ON MODEL

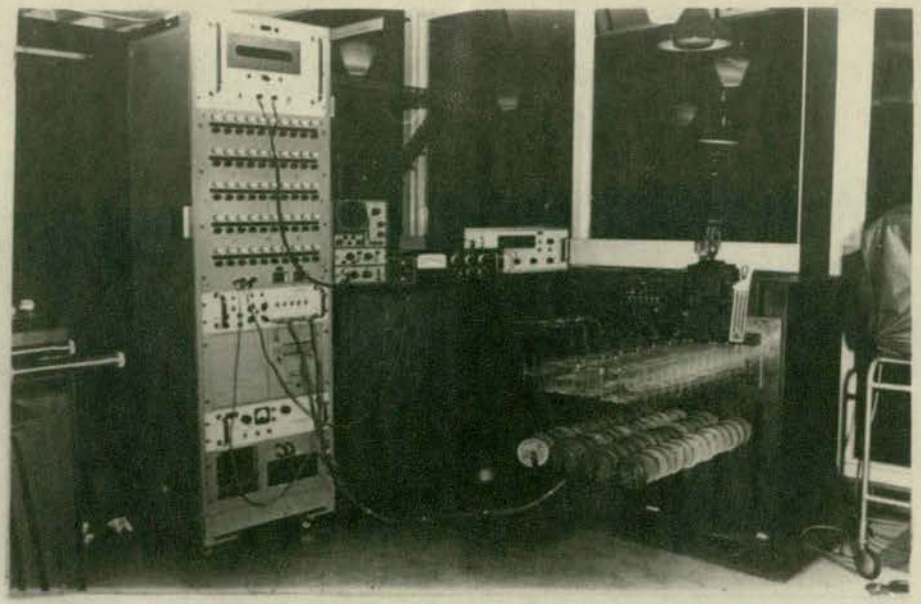

FIG. 7.4 Experimental set up for test E2 showing from left to right, the data logger, oscilloscope, deflection transducer meter, digital voltmeter. The model and its foundation are in the foreground on the right.

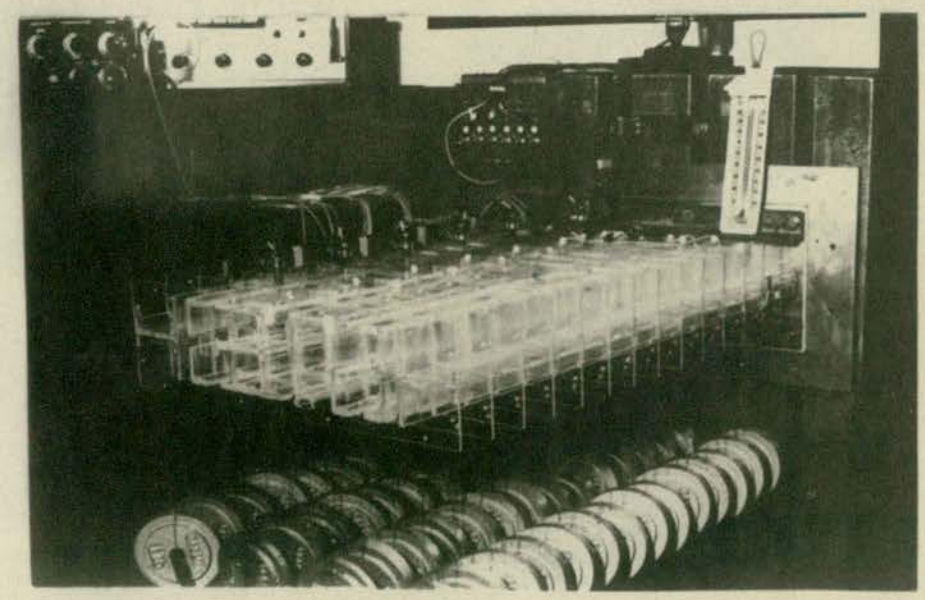

FIG. 7.5 A close-up of the model in the E2 position.

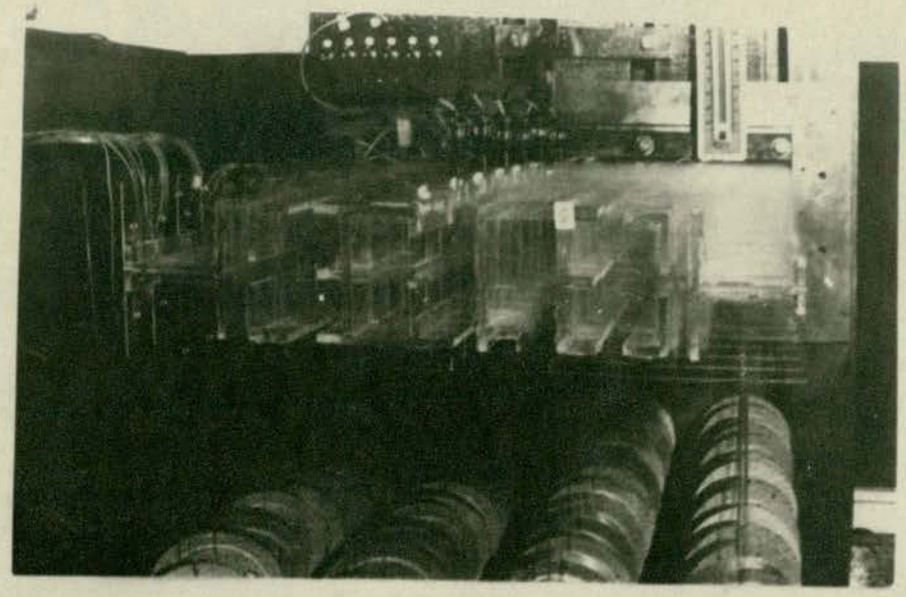

FIG. 7.6 An end view of the model showing the wall units.

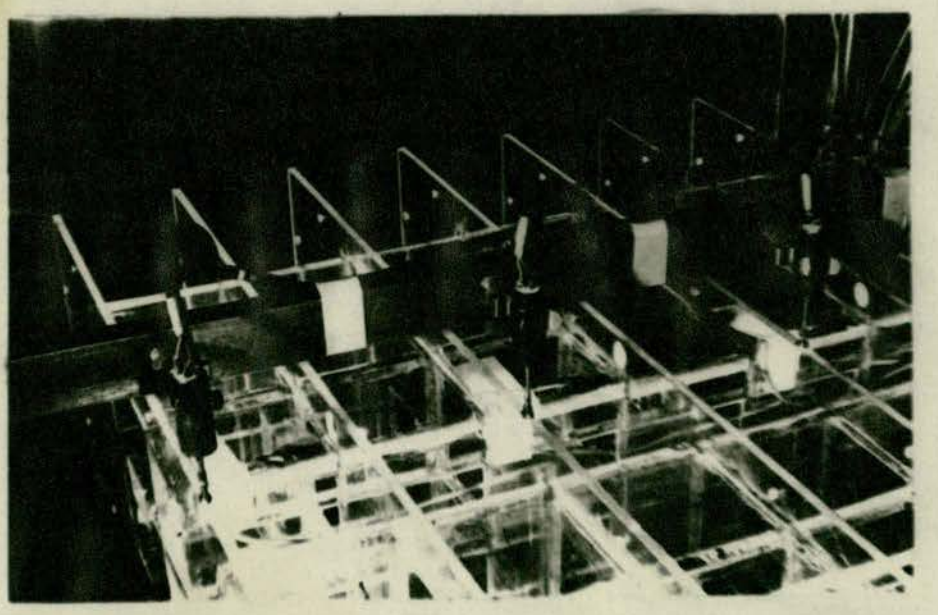

FIG. 7.7 A close-up showing deflection transducers and strain gauges.

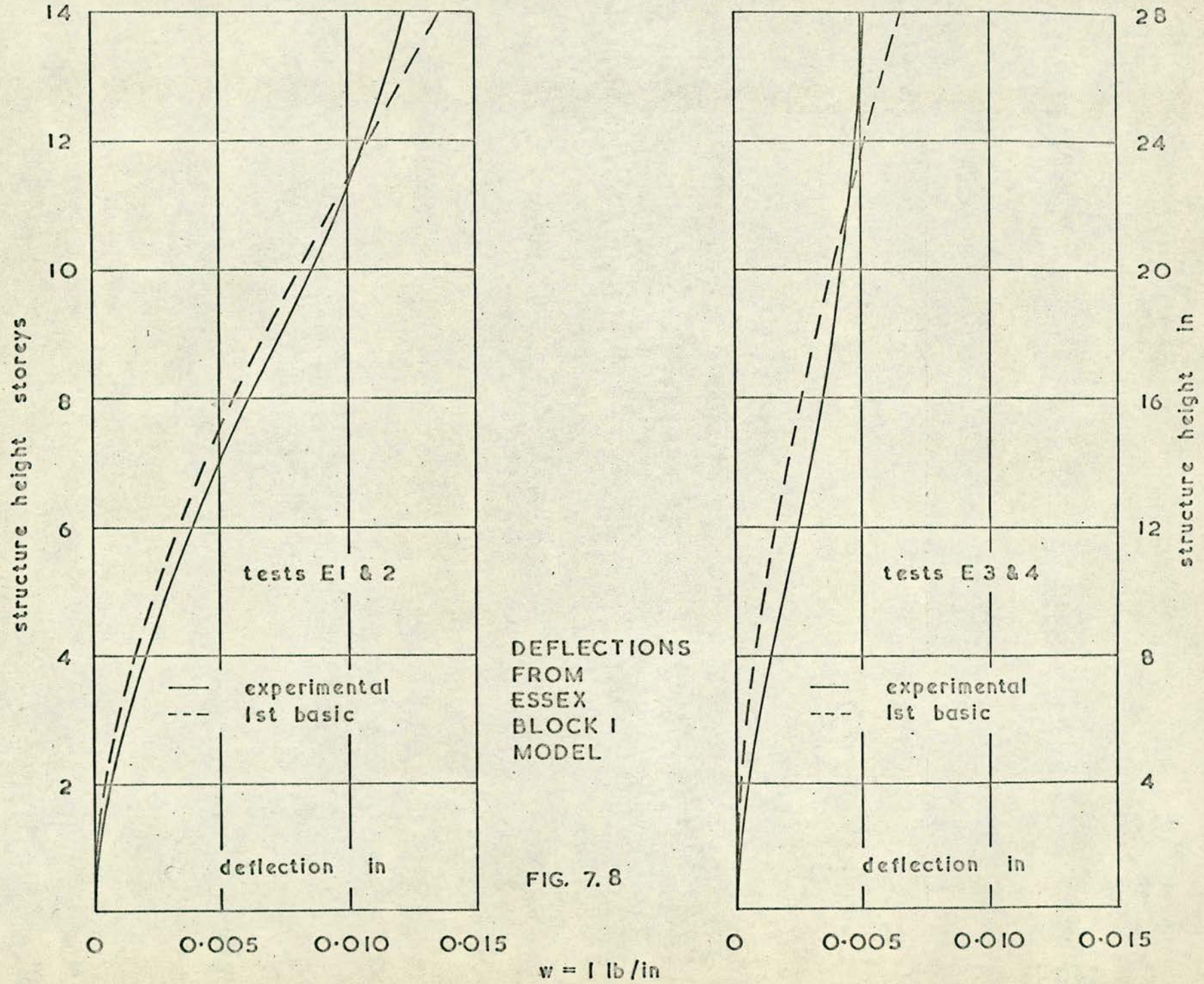

DEFLECTIONS FROM ESSEX BLOCK I MODEL

FIG. 7.8

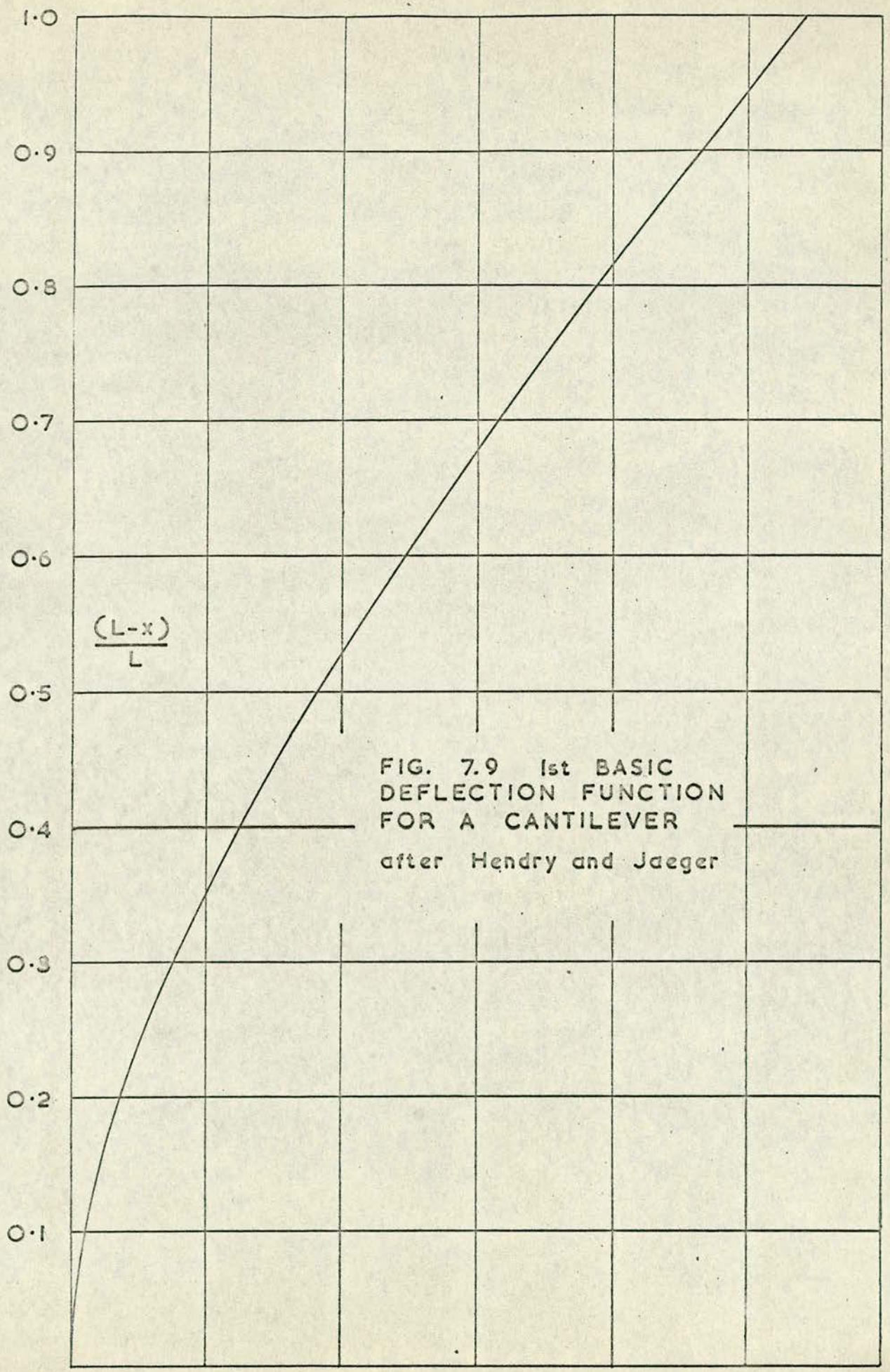

FIG. 7.9 1st BASIC DEFLECTION FUNCTION FOR A CANTILEVER

after Hendry and Jaeger

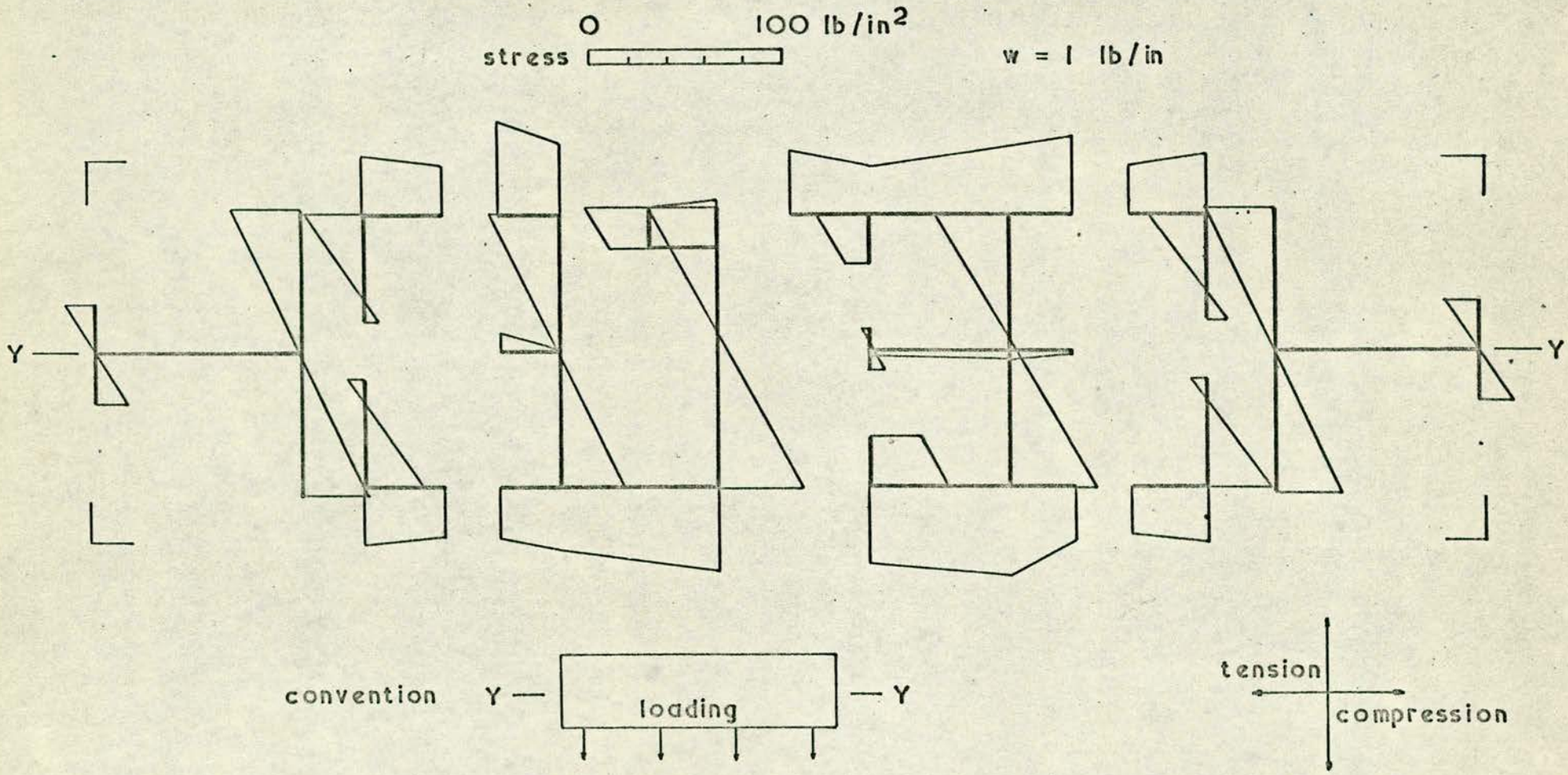

FIG. 7.10 STRESS DISTRIBUTION ON MODEL WITH LOAD PERPENDICULAR TO Y-Y

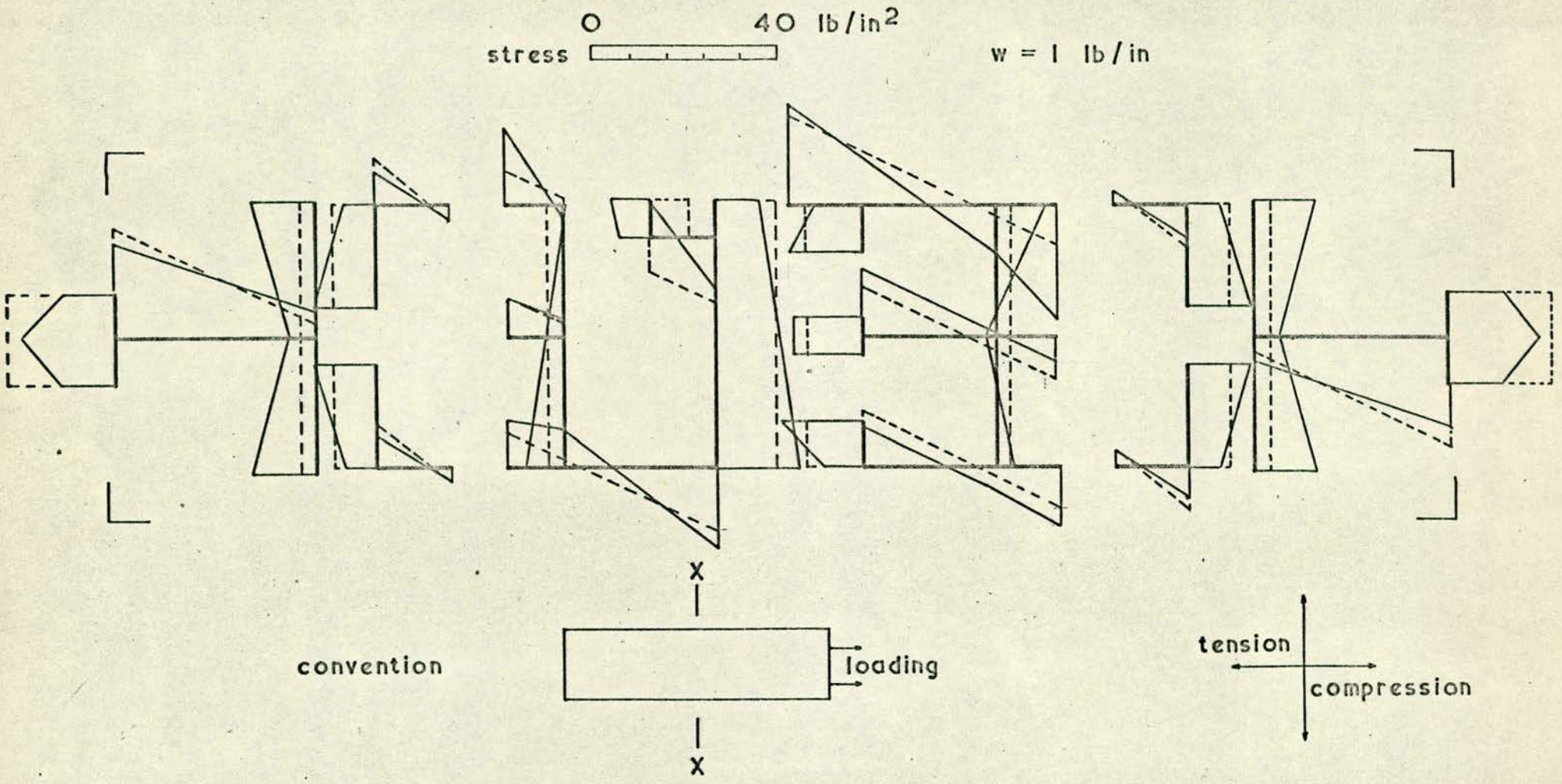

FIG. 7.11 STRESS DISTRIBUTION ON MODEL WITH LOAD PERPENDICULAR TO X-X

8. ANALOGUE SOLUTIONS FOR COMPLEX STRUCTURES

8.1 Equations for Essex blocks 1 and 2

The analogue computer methods having been developed and tested on simple models, it was possible to extend the techniques to deal with more complicated systems. The first example was taken as the central core of Essex University block 1 loaded parallel to the longitudinal axis (Chapter 7). The plan layout is complex but it could be taken as approximately symmetrical about the X-X axis. With this simplification the number of redundants was reduced and a mathematical model was set up which could be simulated on the size of computer available.

The general equations (Chapter 3) are in terms of a plane array of walls so that the wall units belonging to the real structure had to be expressed in terms of a row of hypothetical walls, each of which had an appropriate area, moment of inertia, and centroid. The equivalents for the end "I" units had the same properties as the real ones, while a single wall was used to replace each pair of angles. Mean areas and inertias of the two central units were taken as approximate values for the two symmetrical central walls in the equivalent structure. This equivalent system, shown in Fig. 8.1, thus has six plane walls, instead of the actual eight wall units, interconnected by five sets of slabs.

Suitable dimensions of the connecting elements were more difficult to assess because of the presence of holes and uncertainties about the effective widths and spans of the floor slabs. Without a considerable programme of experimental work on the stress distribution in such slabs

these uncertainties cannot be resolved. It was estimated however that the minimum effective slab width would be the length of the model wall unit flanges, and the spans would be the shortest distance between the ends of the connected units. An exception was made for the span of the central connecting medium which was assumed to be the clear distance between the web ends of the units; the projecting web on unit 4 was ignored. These assumptions may be clarified by reference the Figs. 7.2 and 8.1 which show the real and equivalent structures. Dimensions are given in Tables 8.1 and 8.2.

The next step was to establish the mathematical model which represented the substitute structure. The shear connection equations for a system with five connecting media are obtained from equations 3.13:

$$
\begin{aligned}
R_1'' &= R_1 \alpha_{11}^2 + R_2 \alpha_{12}^2 + \ldots\ldots + R_5 \alpha_{51}^2 - M_o \beta_1 \\
R_2'' &= R_1 \alpha_{11}^2 + R_2 \alpha_{22}^2 + \ldots\ldots + R_5 \alpha_{52}^2 - M_o \beta_2 \\
&\ldots\ldots\ldots\ldots\ldots\ldots \\
R_5'' &= R_1 \alpha_{15}^2 + R_2 \alpha_{52}^2 + \ldots\ldots + R_5 \alpha_{55}^2 - M_o \beta_5
\end{aligned}
\qquad (8.1)
$$

Since the structure has been taken as symmetrical there will be symmetry of the variables, so that $R_1 = R_5$ and $R_2 = R_4$. The number of dependent functions is now reduced from five to three. The α^2 and β constants are derived from geometric data and elastic constants and if symmetry is taken into account it can be shown that:

$$
\begin{aligned}
\alpha_{11}^2 &= \alpha_{55}^2 & \alpha_{12}^2 &= \alpha_{54}^2 & \alpha_{13}^2 &= \alpha_{53}^2 \\
\alpha_{21}^2 &= \alpha_{45}^2 & \alpha_{22}^2 &= \alpha_{44}^2 & \alpha_{23}^2 &= \alpha_{43}^2
\end{aligned}
$$

$$\alpha^2_{31} = \alpha^2_{35} \qquad \alpha^2_{32} = \alpha^2_{34}$$
$$\alpha^2_{41} = \alpha^2_{25} \qquad \alpha^2_{42} = \alpha^2_{24}$$
$$\alpha^2_{51} = \alpha^2_{15} \qquad \alpha^2_{52} = \alpha^2_{14} \qquad (8.2)$$

Equations 8.1 can therefore be reduced by making use of the modified constants given in equations 8.2.

$$R''_1 = R_1 (\alpha^2_{11} + \alpha^2_{51}) + R_2 (\alpha^2_{21} + \alpha^2_{41}) + R_3 \alpha^2_{31} - M_o \beta_1$$
$$R''_2 = R_1 (\alpha^2_{12} + \alpha^2_{52}) + R_2 (\alpha^2_{22} + \alpha^2_{42}) + R_3 \alpha^2_{32} - M_o \beta_2 \qquad (8.3)$$
$$R''_3 = 2 R_1 \alpha^2_{13} + 2R_2 \alpha^2_{23} + R_3 \alpha^2_{33} - M_o \beta_3$$

Equations 8.3 now represent a simple array of six walls with five media in terms of an array of three walls with three media. The third medium is connected to the third wall in the normal manner but its vertical line of inflection is supplied with restraints which simulate the other half of the structure.

Moments on the walls must be evaluated with the aid of the $M_{t'}$ functions and by applying the conditions of symmetry, these functions can be inferred from equations 3.10 as:

$$M_{t';1} = - \frac{2R_1}{I_o} \left(c_{1a} (I_b + I_c) - c_{1b} I_a \right) + \frac{2R_2}{I_o} c_2 I_a + \frac{2R_3}{I_o} c_{3c} I_a$$
$$M_{t';2} = - \frac{2R_1}{I_o} c_1 I_c - \frac{2R_2}{I_o} \left(c_{2b} I_c - c_{2c} (I_a + I_b) \right) + \frac{2R_3}{I_o} c_{3c} (I_a + I_b)$$
$$M_{t';3} = 0$$

equations (8.4)

The moment equations are quite straight forward.

$$M_a = M_{oa} - R_1 c_{1a} - M_{t',1}$$

$$M_b = M_{ob} - R_1 c_{1b} - R_2 c_{2b} + M_{t',1} - M_{t',2} \qquad (8.5)$$

$$M_c = M_{oc} - R_2 c_{2c} - R_3 c_{3c} + M_{t',2} - M_{t',3}$$

By substitution from equations 8.4 equations 8.5 become:

$$M_a = \frac{I_a}{I_o} (M_o - 2 R_1 c_1 - 2R_2 c_2 - R_3 c_3)$$

$$M_b = \frac{I_b}{I_o} (M_o - 2 R_1 c_1 - 2R_2 c_2 - R_3 c_3) \qquad (8.6)$$

$$M_c = \frac{I_c}{I_o} (M_o - 2 R_1 c_1 - 2R_2 c_2 - R_3 c_3)$$

Equations 8.6 satisfy the original assumption that the wall moments are in proportion to the wall inertias. The constants in equations 8.3 are found from equations 3.14 to be:

$$(\alpha^2_{11} + \alpha^2_{51}) = \frac{K_1}{E_w I_o} (\frac{I_o}{A_a} + \frac{I_o}{A_b} + 2c_1^2)$$

$$(\alpha^2_{21} + \alpha^2_{41}) = \frac{K_1}{E_w I_o} (- \frac{I_o}{A_b} + 2 c_1 c_2)$$

$$\alpha^2_{31} = \frac{K_1}{E_w I_o} 2 c_1 c_{3c}$$

$$(\alpha^2_{12} + \alpha^2_{52}) = (\alpha^2_{21} + \alpha^2_{41})$$

$$(\alpha^2_{22} + \alpha^2_{42}) = \frac{K_2}{E_w I_o} (\frac{I_o}{A_b} + \frac{I_o}{A_c} + 2 c_2^2) \qquad (8.7)$$

$$\alpha^2_{32} = \frac{K_2}{E_w I_o} (- \frac{I_o}{A_c} + 2 c_2 c_{3c})$$

$$\alpha^2_{13} = \frac{K_3}{K_1} \alpha^2_{13}$$

$$\alpha^2_{23} = \frac{K_3}{K_2} \alpha^2_{32}$$

$$\alpha_{33}^2 = \frac{K_3}{E_w I_o}\left(\frac{2I_o}{A_c} + 2c_3^2\right)$$

$$\beta_1 = \frac{K_1}{E_w I_o} c_1$$

$$\beta_2 = \frac{K_2}{E_w I_o} c_2$$

$$\beta_3 = \frac{K_2}{E_w I_o} c_3$$

where $I_o = 2(I_a + I_b + I_c)$

With the elastic moduli for Perspex as:

$E = 0.42 \times 10^6 \text{lb/in}^2$

$G = 0.17 \times 10^6 \text{lb/in}^2$

The constants can be evaluated from the data in Tables 8.2 and 8.3.

Table 8.1

Properties of model wall units about X-X axis (Fig. 7.2)

wall unit	length (in)	distances from centroid to extreme fibre (in)	area (in^2)	moment of inertia (in^4)
1	2.8750	$y_{1,0}$ 1.8949 $y_{1,1}$ 0.9810	1.4339	1.8656
2	1.1145	$y_{2,1}$ 0.3371 $y_{2,2}$ 0.7774	0.5307	0.0580
3	3.0625	$y_{3,2}$ 1.5964 $y_{3,3}$ 1.4661	2.9736	3.0726
4	(a) 3.719 (b) 2.781	$y_{4,3}$ 2.2180 $y_{4,3}$ 1.2800 $y_{4,2}$ 1.5010	3.2272	2.7085

N.B. Unit 4 (a) includes outstanding portion of web whereas unit 4 (b) neglects this.

Table 8.2

Properties of equivalent wall units about X-X axis (Fig. 8.1)

model wall unit	equivalent wall	distance from centroid to extreme fibre (in)	distance from centroid to centre of connecting medium (in)	area (in^2)	moment of inertia (in^4)
1	A	y_{Ao} 1.895 y_{A1} 0.980	c_{1a} 1.319	1.434	1.866
two of 2	B	y_{B1} 0.337 y_{B2} 0.777	c_{1b} 0.675 c_{2b} 1.116	1.061	0.116
mean of 3 and 4	C	y_{C2} 1.439 y_{C3} 1.483	c_{2c} 1.777 c_{3c} 2.298	3.101	2.891

Table 8.3

Properties of connecting slabs

medium	walls connected	span e (in)	storey height d (in)	width t (in)	thickness h (in)	moment of inertia I_h (in^4)
1	A and B	0.675	2.000	3.875	0.1563	1.226×10^{-3}
2	B and C	0.675	2.000	3.875	0.1563	1.226×10^{-3}
3	C and C	1.630	2.000	3.875	0.1563	1.226×10^{-3}

The total height was L = 28in so a convenient time scale was $x = 10\tau$ to give a computation time of 2.8 seconds. To scale the variables to suitable voltage levels the applied load was simulated as w = 0.4 lb/in.

The scaled equations from 8.3, 8.5 and 8.6 are therefore:

$$R_1'' = 0.8346\,(6.000\,R_1 + 0.5890\,R_2 + 2.300\,R_3 - 10\,\tau^2)$$

$$R_2'' = 1.211\,(0.4050\,R_1 + 5.024\,R_2 + 1.750\,R_3 - 10\,\tau^2)$$

$$R_3'' = 0.1556\,(1.994\,R_1 + 2.210\,R_2 + 2.982\,R_3 - 10\,\tau^2)$$

$$2M_a' = 20\tau \times 0.7660 - 1.472\,R_1' - 2.220\,R_2' - 1.760\,R_3'$$

$$100M_b' = 20\tau \times 2.380 - 4.750\,R_1' - 6.880\,R_2' - 5.470\,R_3'$$

$$2M_c' = 20\tau \times 1.186 - 2.360\,R_1' - 3.350\,R_2' - 2.726\,R_3'$$

$$y'' \times 10^5 = 20\,M_a \times 0.6380$$
$$= 100\,M_b \times 0.2052$$
$$= 20M_c \times 0.4120$$

equations (8.8)

8.2 Analogue solutions for blocks 1 and 2

To solve for all functions in equations 8.8 the analogue circuit needed twenty-five integrators, fifteen summers and thirty-three potentiometers. This is shown in Figs. 8.2a and 8.2b. A separate circuit was set up for each of the three bending moment functions, but since these circuits are identical, with the exception of potentiometer settings, only one was strictly necessary. These

settings could have been changed to find moments and deflection for one wall at a time. It was, however, pointed out in Section 4.4 that the use of separate circuits provides a check on the solution process.

During computation it was found that the final R' conditions were sensitive to changes of $\pm$ 0.02 volts in the initial conditions so the "balancing" operation had to be carried out with care. The trial and error phase was completed with both manual and automatic methods but the latter was much the faster and a solution was found, starting with zero initial conditions, in about one minute.

The force and moment functions for the equivalent structure are plotted in Figs. 8.3 and 8.4. The static equilibrium equation is:

$$M_o = 2(M_a + M_b + M_c) + 2R_1 (c_1 + c_2) + 2R_2(c_2 + c_3) + R_3c_3$$

and at the foundation level the error between the left and right hand sides of this equation was only 1%. A further check showed that the computed wall moments were in proportion to the wall inertias.

To find the stresses on the second floor walls, at the level of the strain gauges, the equivalent system was reconverted to the real one. At this height the equivalent forces for a load of w = 1 lb/in were:

axial force in wall A	R_1 = 17.0 lb
axial force in wall B	$(R_2 - R_1)$ = 6.5 lb
axial force in wall C	$(R_3 - R_2)$ = -12.5 lb
moment on wall A	M_a = 15.6 lb in
moment on wall B	M_b = 1.2 lb in
moment on wall C	M_c = 24.0 lb in

The stresses on wall unit 1 were obtained directly from R_1 and M_a. Each of the number 2 units has half the area and inertia of wall B so the axial force $(R_2 - R_1)$ and the moment (M_b) were divided by two to get the corresponding values for the model units. The axial forces on the two central walls C were summed to give $2(R_3 - R_2)$ and this was divided between units 3 and 4 in proportion to their areas. The moments on C were summed, $(2\ M_c)$, and divided between units 3 and 4 in proportion to their inertias.

The converted stresses on the model are shown in Fig. 7.11 together with the experimental results. It may be noted that the distributions on the outer "I" and angle units compare well. Stresses on the internal units are not so coincident but this is to be expected. Obviously it is impossible to represent their complex shapes accurately in terms of simple equivalent walls. Even so the agreement is fair and the correct orders of stress are reproduced at almost all points.

The deflection profiles as found by experiment and theory are given in Fig. 8.5. These differ in two respects; the magnitudes of the measured one are larger, and its form exhibits a more marked point of inflection than the computed curve. If the shapes were exactly similar the discrepancy could be explained by body rotation. To obtain a best fit the method of least squarea was used and it was found that this could account for a body rotation of 6.25×10^{-5} radians. Rotation could have been eliminated by constructing the model in a mirror-image form but the desirability of this was not appreciated

until a theoretical solution had been found. Even with a corrective rotation the profiles are not coincident and this must be due to the approximations which were made in formulating equations for the equivalent structure.

In addition there is the problem of evaluating shear distortions with accuracy. The shape factors of the units are largely unknown and shear distortion compatability between the units cannot be reconciled with the original assumptions since the I/A ratios are not the same for each unit. An estimate was made by calculating the distortion of an equivalent rectangular section with the same area as the webs of the units. This increased the computed deflection, based on bending alone, by 18%.

8.3 Equations for Essex blocks 3 and 4

The form of construction for blocks 3 and 4 was the same as for 1 and 2 but the layout was altered. For loading parallel to the X-X axis the stiffness was much the same as before and results from the original model indicated that design could proceed confidently. In the Y-Y direction, however, a number of walls had been removed and the structural stiffness was reduced. The complete plan has a number of irregular wall units but there are two main sections each of which can be represented as three equivalent walls interconnected by slabs. One of these is shown in Figs. 8.6 and 8.7.

It was decided that if the two sections could be designed to take all of the lateral load the complete structure would be more than adequately stiff. The sections differ slightly in plan but only one will be

considered here.

The outer wall units 1 and 3, and 2 and 4, were combined to form equivalent walls A and C, while the central unit 5 was reduced to an equivalent wall B. Some of the units have long unsupported flanges and effective lengths were taken for calculating purposes.

Stress function solutions are available [65, 66] for wide flange T- and L- beams on continuous simple supports and there are empirical formulae in C.P.114(1957) for concrete beams. Strain gauge readings from the model of blocks 1 and 2 indicated that these recommendations might be conservative for the height to width ratio of the wall units considered here so the Code of Practice values were increased as shown in Table 8.4.

Table 8.4

Effective flange widths

source	T - beam	L - beam
Timoshenko, Sechler	$0.363\ d + t_w$	
C.P.114	$0.33\ d + t_w$	$0.17\ d + t_w$
C.P.114	$12\ t_f + t_w$	$4\ t_f + t_w$
values adopted	$14\ t_f + t_w$	$7\ t_f + t_w$

where d is the storey height,

t_w is the web thickness,

t_f is the flange thickness.

The equivalent outer walls (A and C) are each composed from two parallel wall units with different properties. Areas and inertias of

the equivalent walls were taken as the sum of the values of the real units and an equivalent centroid was calculated from the moments of area of the units. Effective slab widths were assumed to be the distances between the webs of the outer pairs of units.

Geometric data for the real and substitute systems is given in Tables 8.5, 8.6 and 8.7.

Table 8.5

Properties of wall units about X-X axis (Fig. 8.6)

wall unit	length (in)	distances from centroid to extreme fibres (in)		area (in^2)	moment of inertia (in^4)
1	145.1	$y_{1,0}$	87.9	1855	4.604×10^6
		$y_{1,1}$	57.2		
2	140.6	$y_{2,0}$	84.2	1837	4.469×10^6
		$y_{2,2}$	56.4		
3	145.5	$y_{3,0}$	67.5	2168	5.575×10^6
		$y_{3,1}$	78.0		
4	145.1	$y_{4,0}$	68.1	1321	2.535×10^6
		$y_{4,2}$	77.0		
5	135.0	$y_{5,1}$	62.8	5565	14.401×10^6
		$y_{5,2}$	72.2		

Table 8.6

Properties of equivalent wall units about X-X axis (Fig. 8.7)

wall unit	equivalent wall	distance from centroid to extreme fibre (in)	distance from centroid to centre of connecting medium (in)	area (in^2)	moment of inertia (in^4)
1 and 3	A	$y_{A,0}$ 76.9 $y_{A,1}$ 68.4	c_{1a} 84.9	4023	10.179×10^6
5	B	$y_{B,1}$ 62.2 $y_{B,2}$ 72.2	c_{1b} 88.7 c_{2b} 79.3	5565	14.401×10^6
2 and 4	C	$y_{C,2}$ 65.1 $y_{C,0}$ 77.8	c_{2c} 81.6	3158	7.004×10^6

Table 8.7

Properties of connecting slabs

medium	walls connected	span e (in)	storey height d (in)	width t (in)	thickness h (in)	moment of inertia I_h (in^4)
1	A and B	33	96	153	4	816
2	B and C	33	96	153	4	816

The equivalent structure in this case is a simple three wall array and no modification of the equations is necessary. Constants were evaluated initially on the basis of:

$\frac{E \text{ brickwork}}{E \text{ concrete}} = 0.5$

with E concrete $= 2 \times 10^6$ lb/in^2

and ν concrete $= 0.2$

For a height of 1350in the computation time was scaled to 13.5 seconds (integrator gains of 1) and computable equations for a simulated load of w = 0.1 lb/in are given below:

$$R_1'' = 0.3013\,(0.5\,R_1 \times 0.5020 + 0.5\,R_2 \times 0.2568 - 0.5\,\tau^2)$$

$$R_2'' = 0.2792\,(0.5\,R_1 \times 0.2770 + 0.5\,R_2 \times 0.5154 - 0.5\,\tau^2)$$

$$M_a' \times 10^{-2} = 5\tau \times 0.6486 - R_1' \times 0.5631 - R_2' \times 0.5219$$

$$M_b' \times 10^{-2} = 5\tau \times 0.9050 - R_1' \times 0.7855 - R_2' \times 0.7281$$

$$M_c' \times 10^{-2} = 5\tau \times 0.4464 - R_1' \times 0.3874 - R_2' \times 0.3591$$

$$0.5y'' \times 10^{-7} = M_a \times 10^{-2} \times 0.4912$$

$$= M_b \times 10^{-2} \times 0.3521$$

$$= M_c \times 10^{-2} \times 0.7146$$

equations (8.9)

8.4 Analogue solution for blocks 3 and 4

Equations 8.9 were solved with an analagous, but simplified, version of the circuit used for equations 8.8. The same procedure was used as before the find forces in the structure from the computed results: for a load of w = 1 lb/in.

axial force in wall A	R_1	$= 17.16 \times 10^2$ lb
axial force in wall B	$(R_2 - R_1)$	$= 2.24 \times 10^2$ lb
axial force in wall C	R_2	$= -14.92 \times 10^2$ lb

moment on wall A	M_a	$= 12.60 \times 10^4$ lb in
moment on wall B	M_b	$= 19.20 \times 10^4$ lb in
moment on wall C	M_c	$= 8.68 \times 10^4$ lb in

The moments on walls A, B and C were distributed among the wall units in proportion to their moments of inertia.

$M_1 = \frac{I_1}{I_1 + I_3}$	M_a	$=$	5.70×10^4 lb in
$M_2 = \frac{I_2}{I_2 + I_4}$	M_c	$=$	5.54×10^4 lb in
$M_3 = \frac{I_3}{I_1 + I_3}$	M_a	$=$	6.90×10^4 lb in
$M_4 = \frac{I_4}{I_2 + I_4}$	M_c	$=$	3.14×10^4 lb in
$M_5 = M_b$		$=$	19.20×10^4 lb in

Bending and direct stresses were evaluated in the walls at foundation level and they are as shown in Fig. 8.9.

It was assumed that this section would carry half of the lateral load resulting from a wind pressure of 20 lb/in^2 on the face of the building (C.P.3 Chapter V, Exposure C) to give a line load of w = 63 lb/in on the equivalent structure. When the results from Fig. 8.9 are extrapolated the maximum tensile stress in the brickwork is found to be 95 lb/in^2. Dead load stresses were calculated as 93 lb/in^2 so there was a possibility of very small net tensile

stress under the worst loading conditions.

One feature of the analysis which was open to speculation was the ratio chosen between the elastic moduli of brickwork and reinforced concrete. Further computations were therefore carried out to investigate the importance of this assumption.

8.5 Influence of elastic moduli

Stress distribution is unaffected by actual values of the elastic moduli for brickwork and reinforced concrete. It is however, influenced by their ratio; a ratio which is largely unknown at present. If $E_{concrete} : E_{brickwork}$ has the limiting value of zero, the slabs may be considered to act as pinned connections and the walls will behave as a series of cantilevers. If $E_{concrete} : E_{brickwork}$ is 2,700 the stiffness of the slabs would be such as to give the effect of solid interconnections, and the whole building would act as a single isotropic cantilever. Between these extremes the possible ratios depend on the properties of the concrete slabs, the type of brick, and a number of factors related to brickwork bond and mortar strength. The problem is further complicated by lower brickwork strengths higher up the structure and the non-linear nature of the stress-strain curves for brickwork. As the stress increases the elastic modulus becomes larger.

Equations 8.9 were therefore modified for $E_{concrete} : E_{brickwork}$ ratios of 1, and 4. As the ratio increases the stresses decreased in a non-linear manner. Graphs are shown in Fig. 8.9 of this effect and it may be seen that if the 1:1 ratio is exceeded there are comparatively small stress reductions.

The maximum stress always occurs at the outer end of unit 1 and the changes at this point are summarised in Table 8.8.

Table 8.8

Stress at outer end of unit 1 ($w = 63$ lb/in^2)

ratio $\frac{E_{concrete}}{E_{brickwork}}$	resultant stress (lb/in^2)
0	161
1	103
2	95
4	85

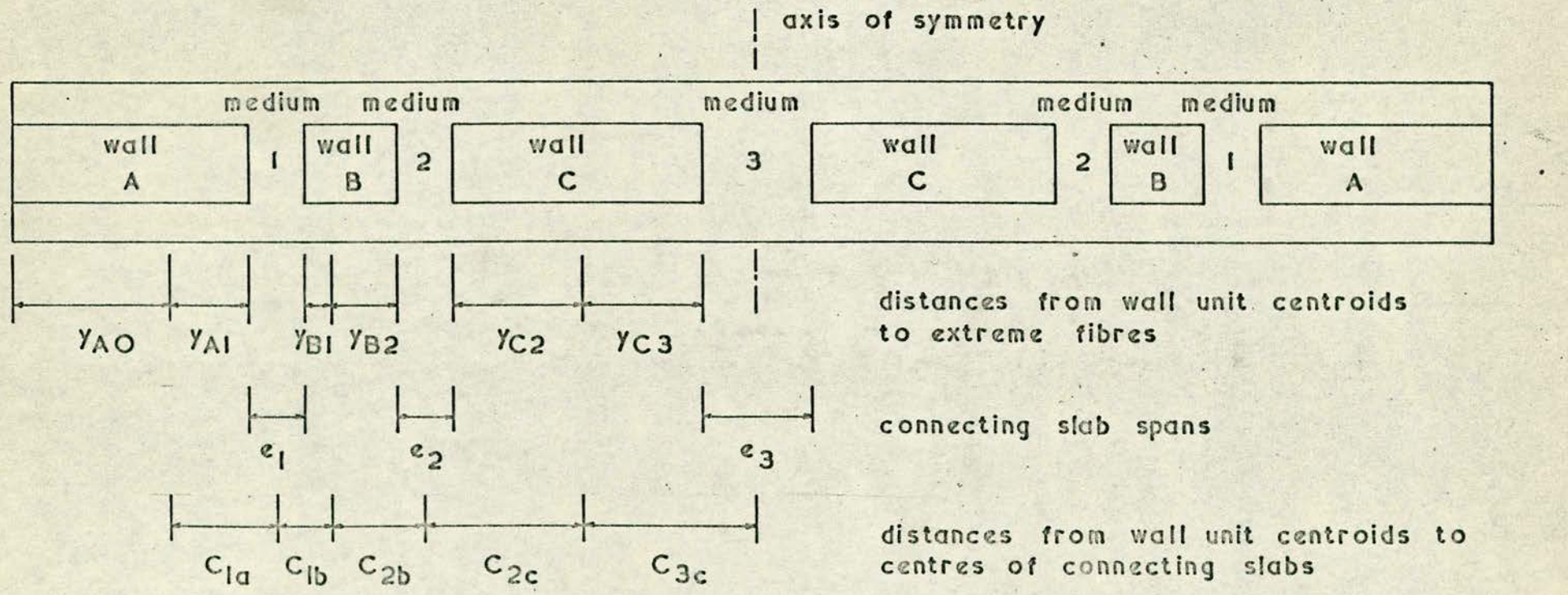

FIG. 8.1 PLAN OF EQUIVALENT STRUCTURE FOR ESSEX BLOCK I MODEL

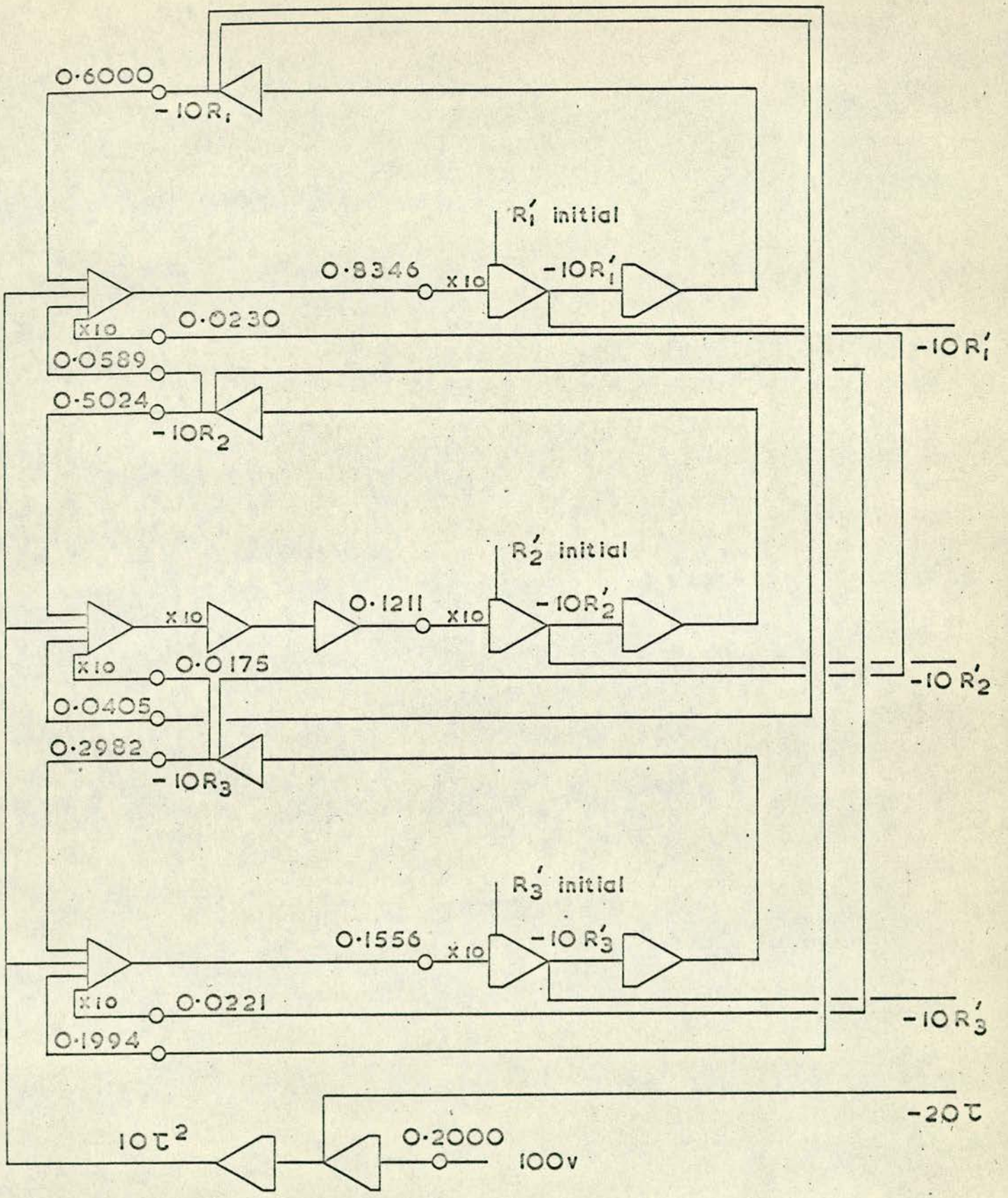

interconnected loops for the simultaneous solution of R_1 R_2 R_3

FIG. 8.2a CIRCUIT FOR ESSEX BLOCK I MODEL

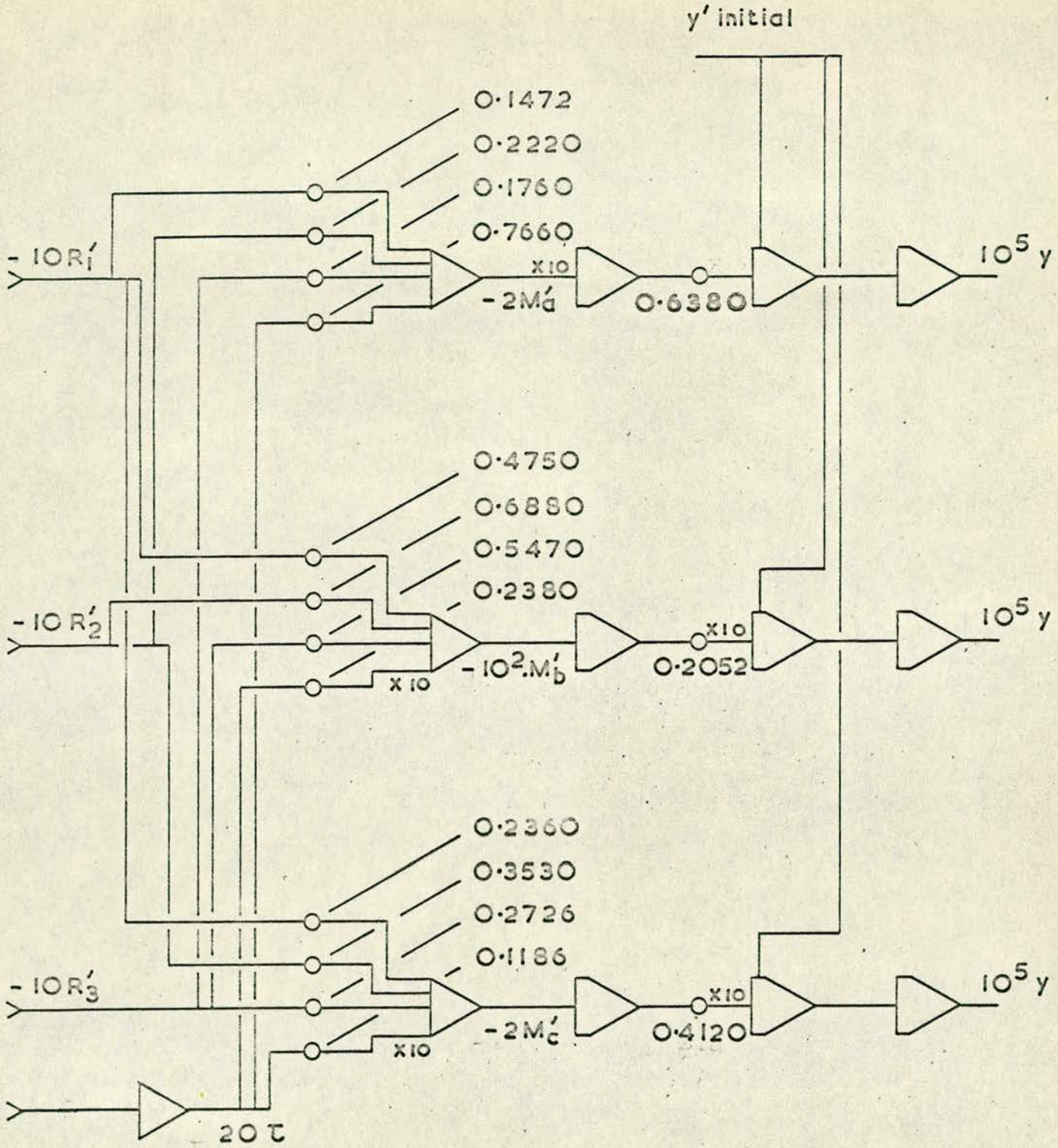

circuits for the solution of $M_a M_b M_c$ and y

FIG. 8.2b CIRCUIT FOR ESSEX BLOCK 1 MODEL

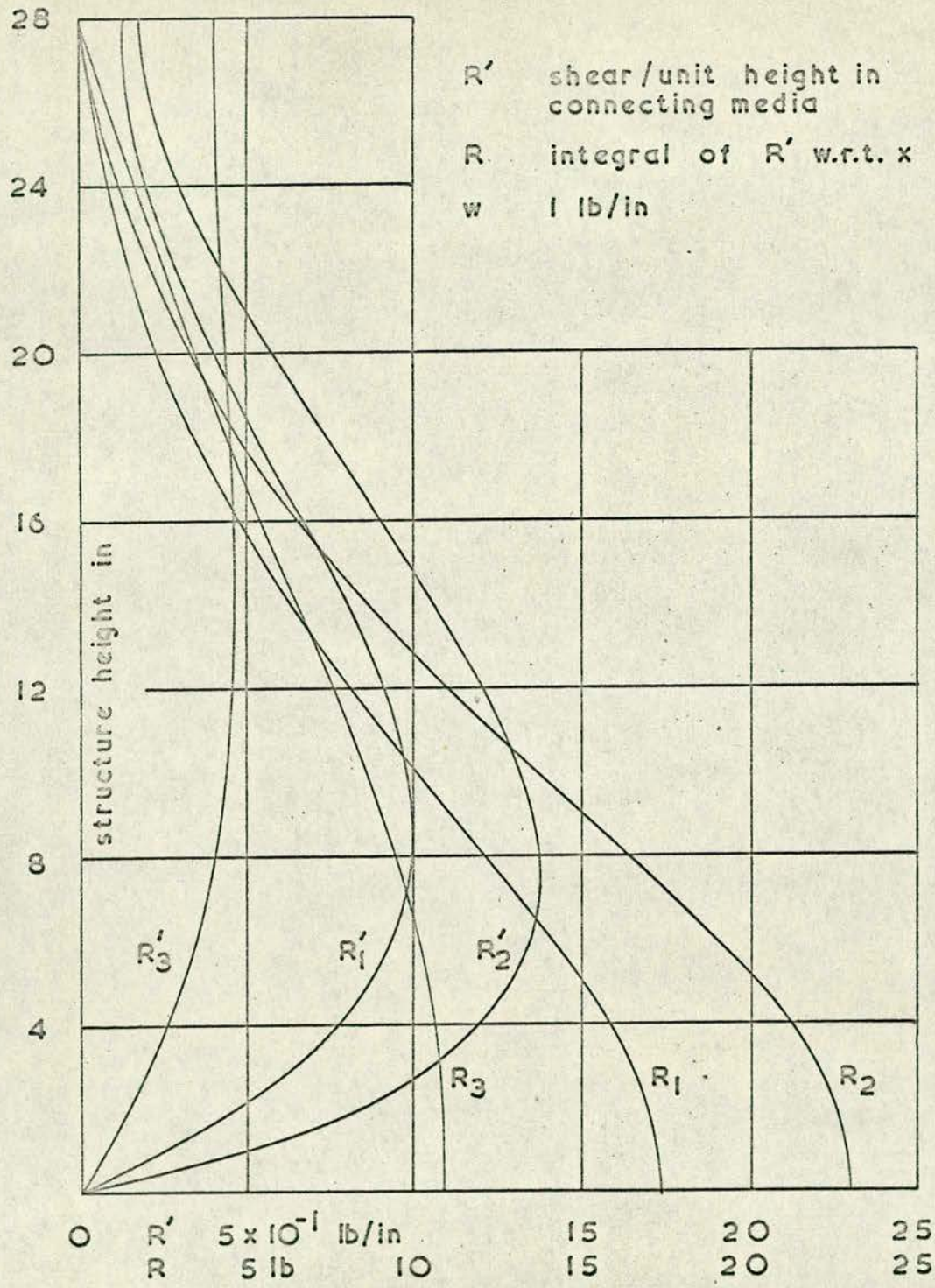

FIG. 8.3 SHEAR IN MEDIA FOR ESSEX BLOCK I MODEL

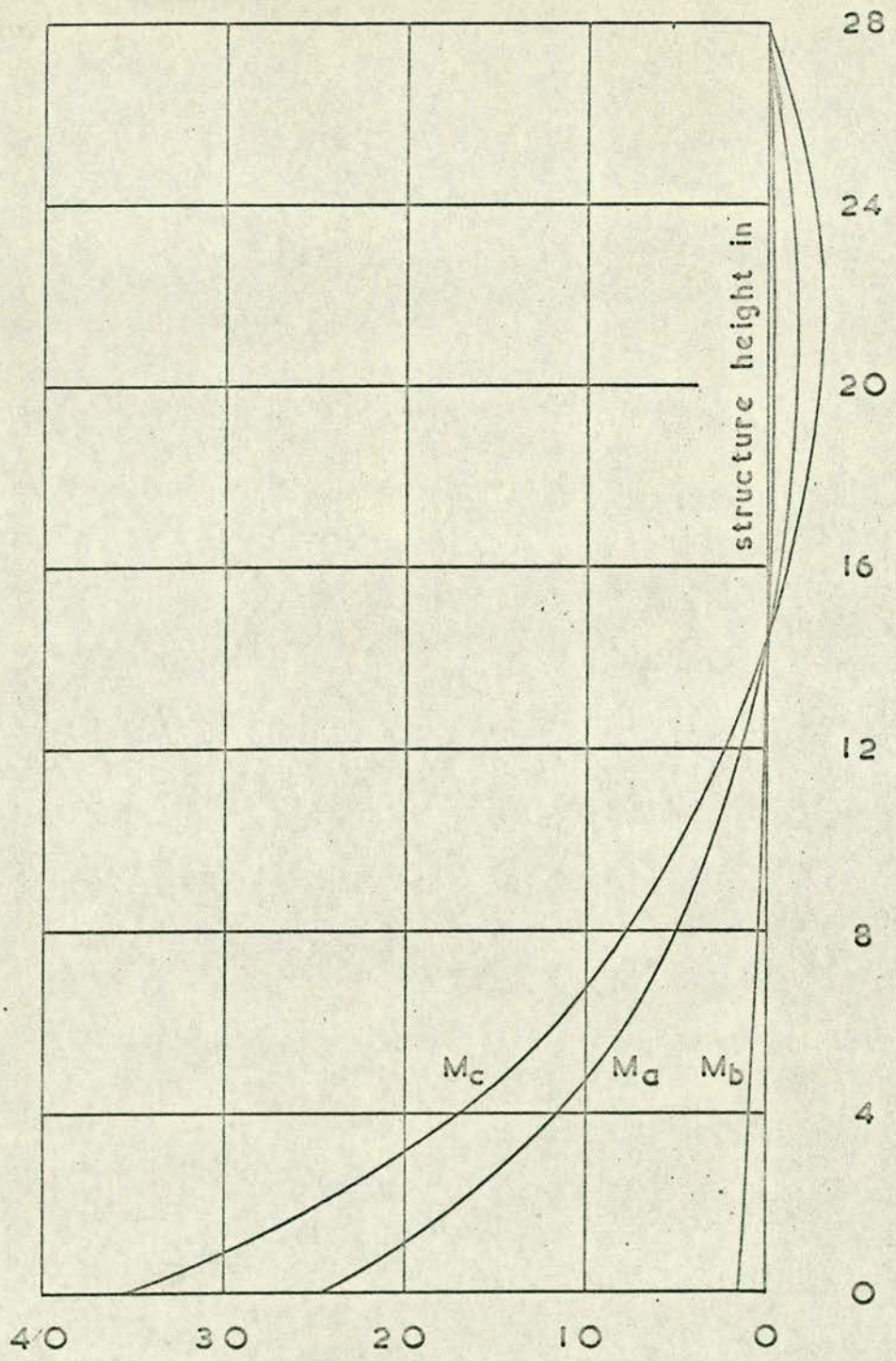

FIG. 8.4 WALL MOMENTS FOR ESSEX BLOCK I MODEL

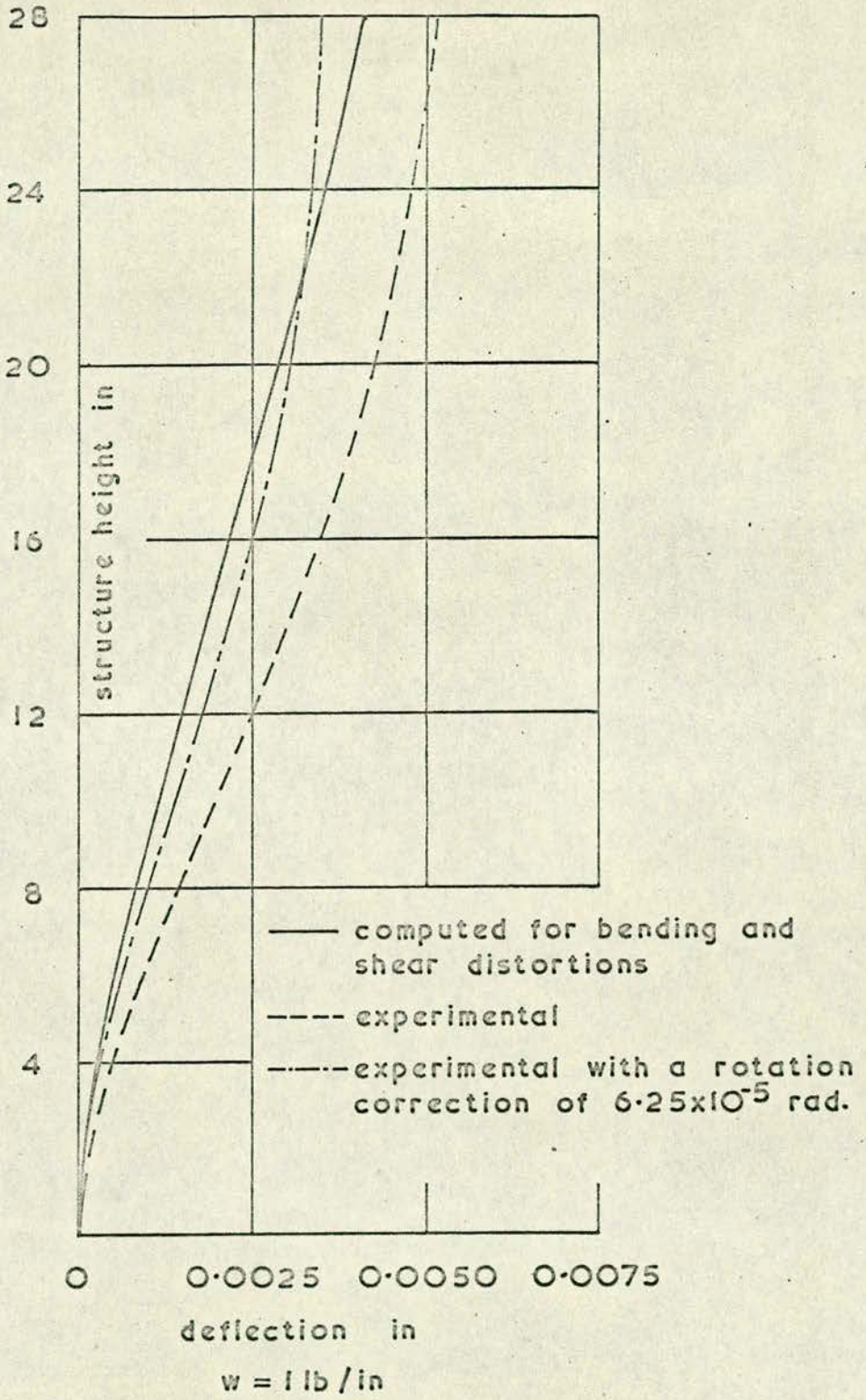

FIG. 8.5 DEFLECTIONS FOR ESSEX BLOCK 1 MODEL

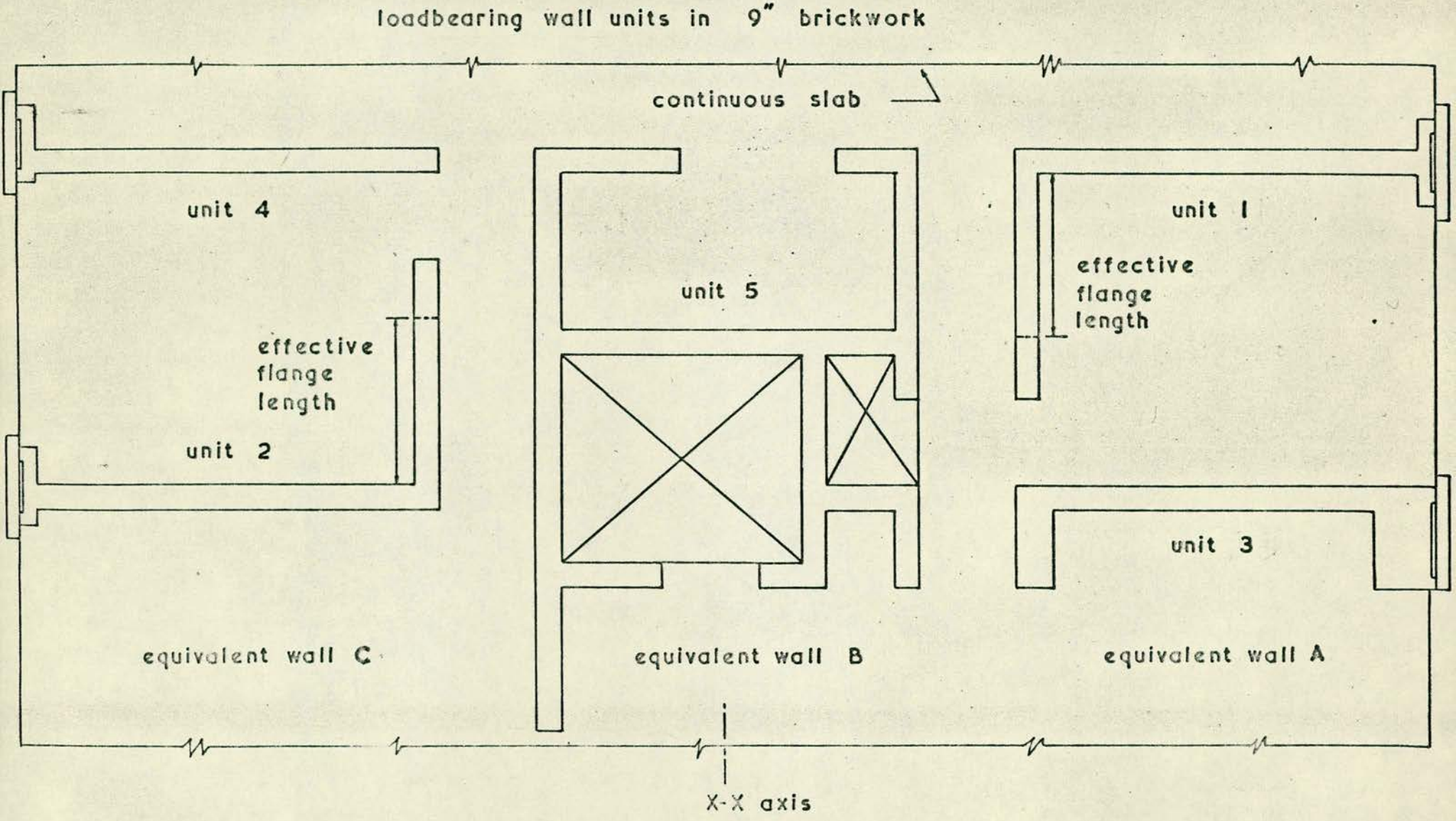

FIG. 8.6 SECTION FROM ESSEX BLOCK 3

y_{AO} etc. distances from wall unit centroids to extreme fibres

e_1 etc. connecting slab spans

C_{1a} etc. distances from unit centroids to centres of slabs

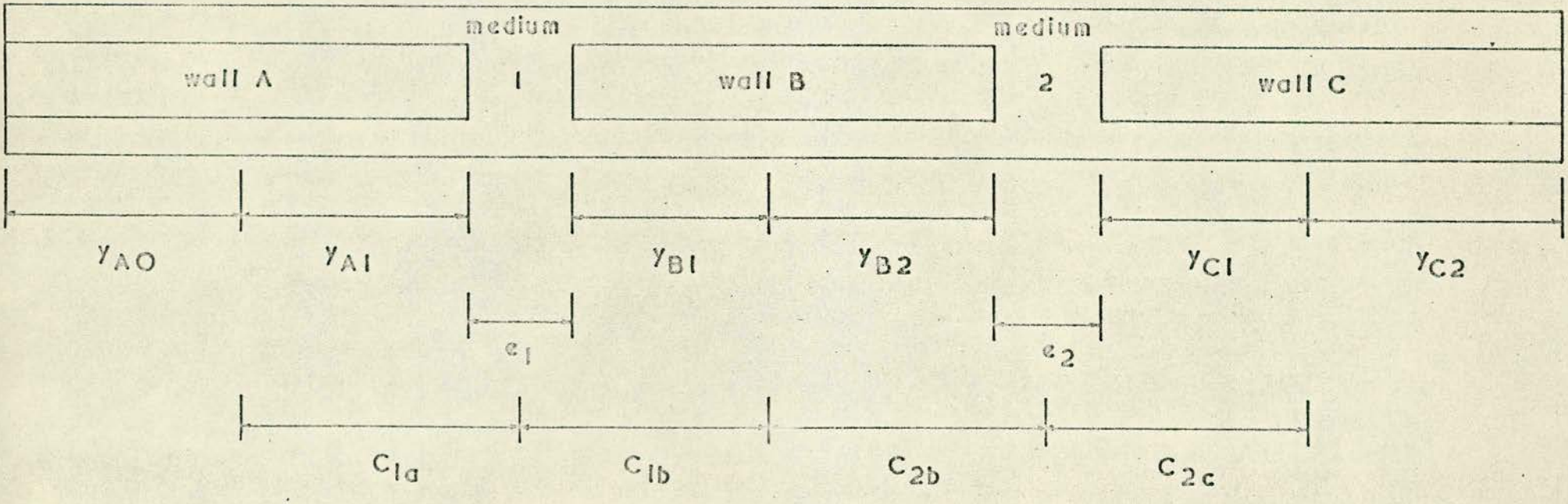

FIG. 8.7 PLAN OF EQUIVALENT STRUCTURE FOR ESSEX BLOCK 3

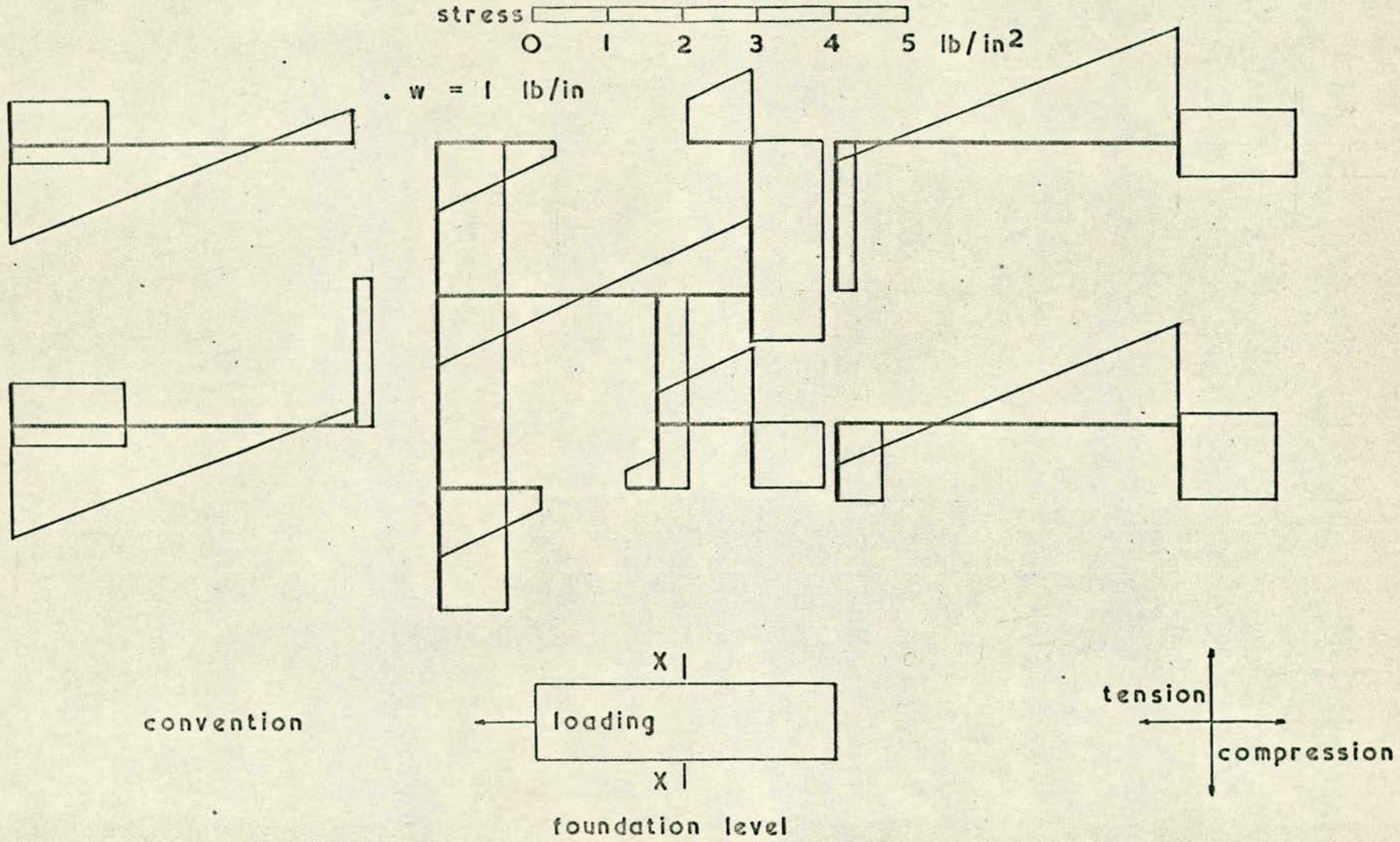

FIG. 8.8 STRESS DISTRIBUTION ON ESSEX BLOCK 3 SECTION

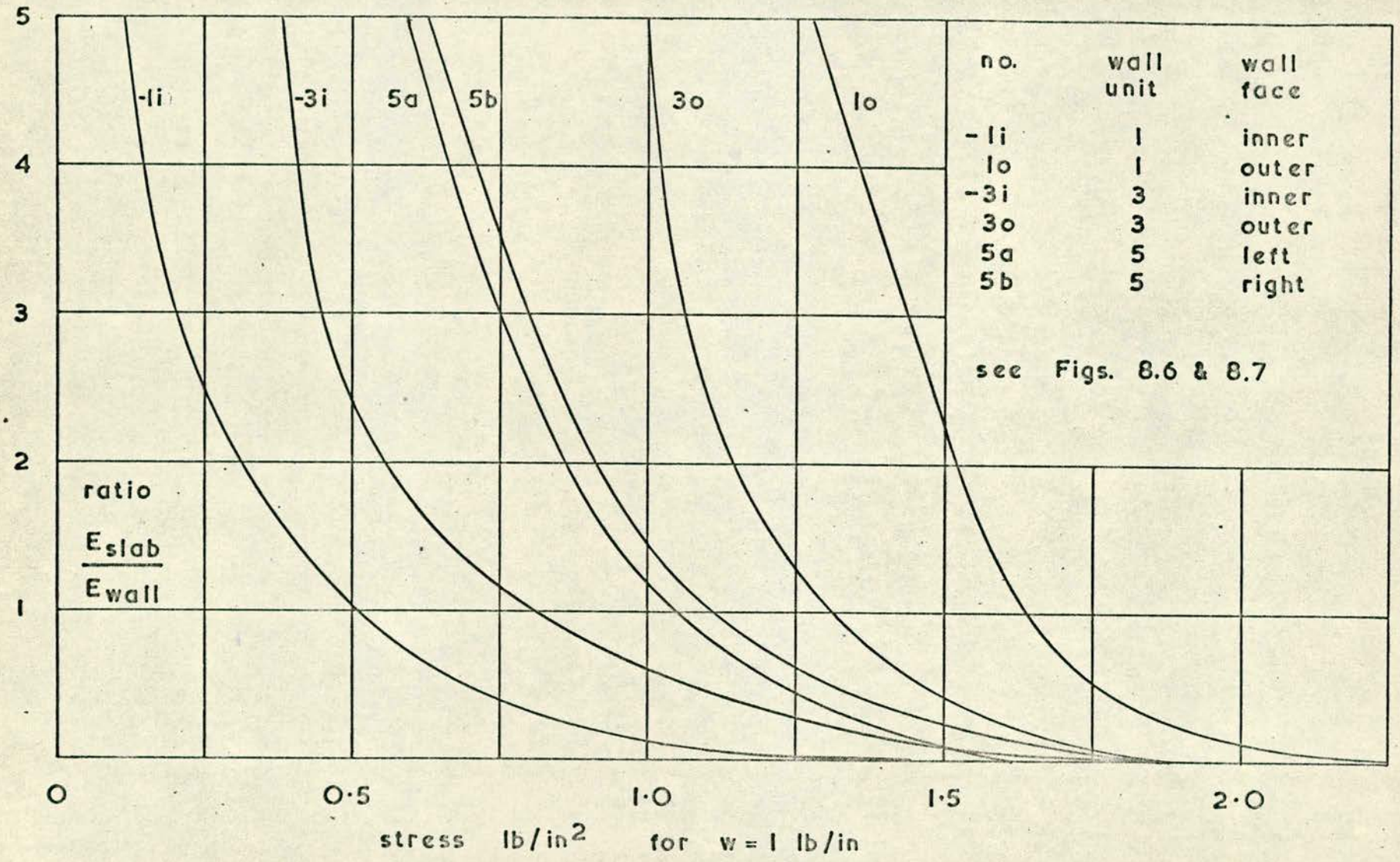

FIG. 8.9 WALL STRESSES PLOTTED AGAINST ELASTIC RATIO

9, CONCLUSIONS

9.1 Summary

It has been shown that the structural behaviour of a plane array of interconnected walls or wall units, under lateral load, can be approximated by the behaviour of an equivalent system. The equivalent system is ideally elastic, with a rigid foundation, and the interconnecting beams are replaced with continuous media which are rigidly fixed to the walls.

A general mathematical model has been devised to represent the equivalent system in terms of differential equations. These equations may be solved by analogue computation and computed results compare favourably with results from model tests.

9.2 Analogue computation

Since the equations conforming to the behaviour of the equivalent system contain only one independent variable, structure height, they can be set up on a general purpose analogue computer. The equations have mixed boundary values, not all of which are known, thus particular solutions cannot be obtained directly. Trial and error is the most satisfactory method for finding the unknown conditions and a technique was developed to make use of automatic iteration circuits. With these circuits the computer could converge on the unique solution in a few seconds. The number of plane interconnected walls which could be simulated was limited to six (five redundant functions) by the size of the computer, but the walls could be of any height. If sufficient computing equipment were available the method could be extended to deal with walls whose stiffness varied with height. The computer output

included all internal forces as continuous functions and static checks showed that the equilibrium between internal and external forces was always within 3%.

9.3 Two wall models

Stresses measured at discrete points on the outer flanges of simple two wall Perspex models agreed within 5% of computed values. Boundary stresses measured by photo-elasticity on a two wall model compared favourably with computed values at mid-storey heights, but there were discrepancies in the vicinity of the wall-beam junctions. These discrepancies were to be expected since the complex nature of stresses around a joint (either wall to foundation or beam to wall) cannot be represented by linear stress distribution functions. The importance of the stress concentrations was not considered in the present work.

Measured deflection profiles from Perspex models with cantilever foundations were 74% larger than the computed profiles and this differencewas due to foundation rotation. It is thought the rotation was caused by elastic deformations of the holding-down bolts. Satisfactory experimental results were only achieved when a mirror-image model was tested and in this case measured deflections were 7% larger than the computed deflections. However the equivalent structures simulated by computation are stiffer than real structures because in practice the beams are not rigidly fixed to the walls at the wall edges. Although the beams are far more flexible than the walls the point of fixity must be some distance inside the walls, thus the equivalent span of the beams is slightly greater than the clear distance between the walls.

To determine the equivalent span must be the subject of further research. The results achieved, however, are sufficiently accurate for design work and the non-dimensional charts given in Chapter 5 enable any pair of symmetric walls to be analysed directly.

9.4 Residence blocks

The prototype Essex University blocks are constructed from load-bearing brickwork wall units and reinforced concrete floors whereas the model was built from an elastic material (Perspex) with all joints rigidly cemented. The model represented an ideal structure and the behaviour of the model only approximated to the behaviour of the prototypes. However the tests provided information on the distribution of force and stress in multi-wall systems. It is apparent that each wall unit acts as a beam with webs and flanges, and together with the floor slabs, the units form a composite system to resist lateral load forces. The experimental results from loading applied perpendicularly to the X-X axis of the model indicated that the wall units were analogous to a row of plane interconnected walls. The neutral axes were not at the centroids of the units but were displaced towards the centre of the structure: an effect which was due to axial forces transmitted by the floor slabs. Couples from the axial forces on corresponding units at either end of the structure served to reduce the net moments on the walls. Measured stresses on the walls were therefore considerably smaller than stresses calculated on the basis of individually cantilevered walls (the original design assumption). Further evidence of composite behaviour was provided by the point of inflection on the experimental deflection profile. A point of

inflection at about two-thirds of the structure height above the base is typical of interconnected shear wall assemblies, and it indicates the position at which the net bending moments on the walls are zero. Below the point of inflection the net wall moments are positive and above it the moments are negative, the external moment being regarded as positive. Analysis of the deflection curves by simple cantilever theory and by basic functions showed that the equivalent moment of inertia of the structure, about the X-X axis, was three times as large as the sum of the individual wall unit inertias.

To provide a theoretical solution the model was expressed in terms of an equivalent structure in which the floor slabs were replaced by continuous media. The properties of the wall units were defined as their areas, their inertias and the positions of their centroids. This substitute system was simulated by analogue computation to obtain internal forces and moments on the wall units. When linear stress variations were assumed on the walls the results accorded well with experimental data. The computed deflection profile was smaller than the measured profile but in the light of experience gained with simple models this discrepancy could be due, in part, to foundation rotation of the model.

A typical section from a further tower block was analysed theoretically and the mathematical model was modified to simulate the effects of various ratios between the moduli of elasticity of the floors and walls. It was originally assumed that the elastic modulus of the floors (reinforced concrete) was twice that of the walls (brickwork) and computations showed the net stresses in the walls would not be significantly altered if the ratio were one, (8% stress increase) or four (10% stress decrease).

9.5 Final conclusions

In practice many engineers design the wall units in tall frameless blocks, particularly those built from load-bearing brickwork, as individually acting cantilevers. To make such an assumption is to underestimate the rigidity of these structures and to overestimate the stresses in the walls. The method developed in this Thesis for plane arrays of interconnected walls can be applied to complex systems if the properties of the wall units and floor slabs are known. Even if conservative assumptions are made about the effective stiffness of the components (walls and slabs) the analysis will lead to worthwhile stress reductions.

The continuum methods have not previously been extended to complex systems because of solution difficulties. It was found, however, that an analogue computer was ideal for simulating the behaviour of the necessary equations and accurate solutions could rapidly be found. Furthermore the degree of complexity of the equations does not affect the manner of computation. It is concluded that the technique of analogue computation is the best currently available for analysing tall interconnected systems of walls by continuum methods.

ACKNOWLEDGEMENTS

The author wishes to thank Professor A.W. Hendry for his continued help and encouragement throughout this work, and especially for providing the opportunity to work on the design projects connected with the Essex University residence blocks and with the foundations required in the vicinity of the Mersey tunnel. Valuable discussions were held with Dr. I.F. Christie on analogue computation and Dr. S.R. Davies on experimental techniques. Thanks are due to Messrs Harris and Sutherland, Consulting Engineers, for details of the Essex University residence blocks and for their financial support of the model tests.

The experimental work on the Essex University model was described in a paper presented for the Institution of Civil Engineers Medal competition, 1965. Analogue computation methods are contained in a paper presented to the Symposium on Tall Buildings to be held at the University of Southampton in April 1966. The proceedings are to be published by Pergamon Press. Techniques of repetitive analogue compution for boundary value problems are included in a joint discussion by the author and Dr. I.F. Christie published in the Proceedings of the American Society of Civil Engineers, Journal of the Engineering Mechanics Division (EM6) December 1965.

Appendix C is reproduced from a paper by the author in Research and Development for Industry No.41, June-July 1965. The contents of Appendix E have been taken from reports presented to Messrs Bingham Blades and Partners, Consulting Structural Engineers.

Finally the author would like to express his appreciation for the assistance given by the workshop personnel, in particular . Mr. R.S. Elder and Mr. C. Cope, and thank Miss N. Hamilton for typing and duplicating this Thesis and Miss P. Anderson for photographic work.

REFERENCES

1. Pippard, A.J.S., Studies in Elastic Structures, Arnold, London, 1952.

2. Chitty, L., On the cantilever composed of a number of parallel cross beams interconnected by cross bars, Phil. Mag., 7, (38), 1947.

3. Eriksson, O., Analysis of wind bracing walls in multi-storey housing, Ingenioren International Edition, 5, (4), 1960.

4. Beck, H., Contribution to the analysis of coupled shear walls, J. Am. Concr. Inst., 5, (59), 1962.

5. Rosman, R., Photo-elastic investigation of a horizontally loaded cross-wall of a multi-storey block, Der Bauingenieur, 37, (12), 1962.

6. Rosman, R., An approximate method of analysis of walls of multi-storey buildings, Civ. Engng publ. Wks Rev., 59, (690), 1964.

7. Arcan, M., Calculation procedure for wall skins with a row of openings. Photo-elastic examination, Bautechnik, 41, (3), 1964.

8. Coull, A., Private Communication, University of Southampton, Southampton, England.

9. Kani, G., Analysis of multi-storey frames, Ungar, New York, 1956.

10. Livesley, R.K., Matrix methods of structural analysis, Pergamon Press, London, 1964.

11. Brotton, D.M., The application of digital computers to structural engineering problems, Spon, London, 1962.

12. Zbirokowski-Koscia, K., Estimating wind stresses in cross-walls with large openings, Civ. Engng publ. Wks Rev., 53, (624), 1958.

13. Green, N.B., Bracing walls for multi-storey building, J.Am. Concr. Inst., 59, (3), 1952.

14. Clark, L.G., Deflection of laminated beams, Trans. Am. Soc. civ Engrs, 119, 1954.

15. Deschapelles, B., Beam analogy for the solution of vierendeel trusses, Proc. Am. Soc. civ Engrs, 88, (ST 5), 1962.

16. Frishmann, W.W., Prabbhu, S.S., and Toppler, J.F., Multi-storey frames and interconnected shear walls subjected to lateral loads, Concr. constr. Engng., 58, (6 and 7), 1963.

17. Rosenblueth, E., and Holtz, I., Elastic analysis of shear walls in tall buildings, J. Am. Concr. Inst., 31, (12), 1960.

18. Cardan, B., Concrete shear walls combined with rigid frames in multi-storey buildings subject to lateral loads, Proc. Am. Concr. Inst., 58, (3), 1961.

19. Khan, F.R., and Sbarounis, J.A., Interaction of shear walls and frames, Proc. Am. Soc. civ Engrs, 90, (ST 3 Part 1), 1964.

20. Bandel, H., Frames combined with shear trusses under lateral loads, Proc. Am. Soc. civ Engrs, 88, (ST 6), 1962.

21. Clough, R.W., Wilson, E.L., and King, I.P., Large capacity multi-storey frame analysis programme, Proc. Am. Soc. civ Engrs, 89, (ST 4), 1962.

22. Tezcan, S.S., Moment equations for computer analysis of frames, Ibid.

23. McLeod, I.A., Private Communication, Department of Civil Engineering, University of Glasgow, Glasgow, Scotland.

24. Benjamin, J.R., and Williams, H.A., The behaviour of one storey brick shear walls, Proc. Am. Soc. civ Engrs, 84, (ST 4), 1958.

25. Benjamin, J.R., and Williams, H.A., Behaviour of one storey reinforced concrete shear walls containing openings, J.Am. Concr. Inst., 30, (5), 1958.

26. Benjamin, J.R., and Williams, H.A., Behaviour of reinforced concrete shear walls, Trans. Am. Soc. civ Engrs, 124, 1959.

27. Benjamin, J.R., and Williams, H.A., Reinforced concrete shear wall assemblies, Proc. Am. Soc. civ Engrs, 86, (ST 8, Part 1), 1960.

28. Benjamin, J.R., Statically Indeterminate Structures, McGraw-Hill, New York, 1959.

29. Holmes, M., Steel frames with brickwork and concrete infilling, Proc. Inst. civ Engrs, 19, Paper No. 6501, 1961.

30. Holmes, M., Combined loading on infilled frames, Proc. Inst. civ Engrs, 25, Paper No. 6621, 1963.

31. Wood, R.H., Stability of tall buildings, Proc. Inst. civ Engrs, 11 Paper No. 6280, 1958.

32. Smith, B.S., Lateral stiffness of infilled frames, Proc. Am. Soc. civ Engrs, 88, (ST 6), 1962.

33. Wood, R.H., Studies in composite construction Part I. The composite action of brick panel walls supported on reinforced concrete beams. Res. Pap. natn. Bldg Stud., No. 13, 1952.

34. Wood, R.H., Studies in composite construction Part II. The interaction of floors and beams in multi-storey buildings. Res. Pap. natn. Bldg Stud., No. 22, 1955.

35. Structural Ceramics Research Unit, Reports on load-bearing brickwork, Department of Civil Engineering, University of Edinburgh, Edinburgh, Scotland.

36. Murthy, C.K., Model studies related to load-bearing brickwork, Ph.D. Thesis, University of Liverpool, 1964.

37. Sinha, B.P., Reports on load-bearing brickwork, Structural Ceramics Research Unit, Department of Civil Engineering, University of Edinburgh, Edinburgh, Scotland.

38. Amaratunga, M.M., An investigation into the linear elastic behaviour of structural walls containing openings, Ph.D. Thesis, University of Southampton, 1963.

39. Liauw, T.C., An investigation into the behaviour of frame-wall structures, Ibid.

40. Ashley, R., Introduction to Analog Computation, Wiley and Sons, New York, 1963.

41. Huskey, H.D., and Korn, G.A., Computer Handbook, McGraw-Hill, New York, 1962.

42. Jackson, A.S., Analog Computation, McGraw-Hill, New York, 1960.

43. Batchelor, W., and Cranston, W.B., Private Communication, Cement and Concrete Association, Research and Development Department, Wexham Springs, Bucks., England.

44. Sparkes, S.R., and Chapman, J.C., Model methods with particular reference to three recent applications in the fields of steel, composite and concrete construction, Struct Engr., 39, March 1961.

45. Johnson, A.E., and Homewood, R.H., Stress and deformation analysis from reduced-scale plastic-model testing, Proc. Soc. exp. Stress Analysis, XV111, (2), 1961.

46. Zender, G.W., Experimental analysis of aircraft structures by means of plastic models, Proc. Soc. exp. Stress Analysis, X1V, (1), 1956.

47. Preece, B.W., and Davies, J.D., Models for Structural Concrete, C.R. Books, London, 1964.

48. Perspex acrylic materials, booklets by Imperial Chemical Industries.

49. Dietz, A.G.H., and Campbell, W.H., Bonded wire strain gage techniques for polymethyl methacrylate plastics, Proc. Soc. exp. Stress Analysis, V, (1), 1947.

50. Eney, W.J., Discussion on above paper, Ibid.

51. Frocht, M.M., et al, The effect of gage current on strain measurement, Proc. Soc. exp. Stress Analysis, XV1, (2), 1956.

52. Durelli, A.J., et al, Introduction to the Theoretical and Experimental Analysis of Stress and Strain, McGraw-Hill, New York, 1958.

53. Strain Gauges and Strain Measuring Equipment, Philips Technical Report.

54. Soane, A.J.M., Automatic strain recording equipment, Research and Development for Industry, No. 41, 1965.

55. Cowan, H.J., The design of concrete structures with the aid of models, Indian Concr. J., October 1959.

56. Findley, N.W., and Reed, R.M., Concerning strain gage measurement of creep in plastics, Proc. Am. Soc. exp. Stress Analysis, XX, (1), 1963.

57. Hoff, E.A.W., Some mechanical properties of a commercial polymethyl methacrylate, J. appl. Chem., Lond., August 1952.

58. Charlton, T.M., Use of models for obtaining influence lines for deflection of structures with linear elasticity, Civ. Engng., Lond., 54,(634),1959.

59. Hendry, A.W., Elements of Experimental Stress Analysis, Pergamon Press, London, 1964.

60. Hendry, A.W., An Introduction to Photo-elastic Analysis, Blackie and Son, London, 1948.

61. Frocht, M.M., Photoelasticity, Vols, I and II, Wiley and Sons, New York, 1958.

62. Langhaar, H.L., Dimensional Analysis and Theory of Models, Wiley and Sons, New York, 1951.

63. Charlton, T.M., Model Analysis of Structures, Spon, London, 1954.

64. Hendry, A.W., and Jaeger, L.G., The Analysis of Grid Frameworks and Related Structures, Prentice-Hall, New Jersey, 1958.

65. Sechler, E.E., Elasticity in Engineering, Wiley and Sons, New York, 1952.

66. Timoshenko, S., Strength of Materials, Part II, Van Nostrand, New York, 1956.

Abbreviations taken from the World List of Scientific Periodicals.

APPENDIX A

PRINCIPAL NOTATION

symbol	significance
A_j	cross sectional area of wall J
b	thickness of wall
b_s	effective width of slab
c_{mi}	distance from centre line of connecting medium m to centroid of wall I
c_{mj}	distance from centre line of connecting medium m to centroid of wall J
c_m	$c_{mi} + c_{mj}$
d	storey height
e_m	span of connecting medium m
E_s, E	modulus of elasticity of connecting beams or slabs
E_w, E	modulus of elasticity of walls
F(x)	basic function
G_m	modulus of rigidity of beams or slabs
h	depth of beams or slabs
I_e	equivalent moment of inertia of structure
I_h	moment of inertia of beam or effective slab
I_j	moment of inertia of wall J
I_o	sum of moments of inertia of individual walls ($I_o = I_a + I_b + I_c + ...$)

symbol	significance
I_t	moment of inertia of total cross section about its centroid
K	shear constant (defined in text)
L	total height of structure
M_o	bending moment on structure from external lateral loading $(wx^2/2)$
M_{oj}	bending moment on wall J from external lateral loading assuming pin-connected media $(M_{oj} = M_o I_j/I_o)$
M_j	resultant bending moment on wall J
$M_{t',m}$	moment on adjacent walls from component of horizontal force in medium m
N_j	axial force in wall J $(N_j = R_n - R_m)$
Q_j	resultant shear in wall J $(= M'_j)$
R'_m	specific shear force in connecting medium m
R_m	component of axial force in adjacent walls from medium m (integral of R'_m)
S	static moment of one wall about the centroid of the whole cross-section
t_m	component of horizontal force in medium m
w	value of external U.D.L.
x	co-ordinate of height measured from the top of the structure.
y	co-ordinate of deflection measured from the deformed axis of the structure

symbol	significance
y_{jm}	distance from centroid of wall J to extreme fibre adjacent to medium m
α^2, β	constants related to the geometry of the structure
θ	basic function constant
λ	computer time scale constant
σ_b	bending stress in a wall
σ_d	direct stress in a wall
τ	computer time
ϕ	non-dimensional integral shear force in medium
χ	shear distribution constant (1.2 for a rectangular section)
ψ	non-dimensional shear force in medium
ν	Poisson's ratio

APPENDIX B

ANALOGUE SUB-CIRCUITS

The symbols representing the basic sub-circuits, for potentiometers, summers and integrators are shown in Fig. B.1. On each integrator provision is made for setting up an initial condition, and the simplest method is to feed the initial condition input with a voltage from the armature end of a potentiometer whose high end is connected to a $\pm$ 100 volts source. If the initial condition value is critical then a more sensitive circuit, with two potentiometers and two summers, should be used. This is also shown in Fig. B.1 and, since the input to one of the summers is attenuated by a factor of ten, there is in effect a coarse control and a fine control. The technique was of assistance when the R' initial conditions were being manually adjusted because the final conditions were very sensitive to small initial changes.

Before discussing the automatic iteration circuits it will be useful to consider the operational conditions of the integrators. These conditions are; Problem Check, Compute, or Hold, and they are determined by energising, in suitable combinations, three relays on each integrator. The relays (RLa, RLb and RLc) associated with a typical amplifier are shown on a circuit diagram in Fig. B.2. In the Problem Check state all the relays are energised and the amplifier acts as a summer with the initial condition as an input. The integrating capacitor can therefore become charged to the voltage applied at the initial condition input. Before going to Compute, the Hold mode must be selected. This de-energises relays a and b giving the integrator a capacative feedback. For computation all relays are de-energised so

that the main inputs are connected to the amplifier. Normally the relays on all amplifiers are operated synchronously, in the required combinations, by the main control circuits within the computer. The special sub-circuits for iteration took advantage of recent modifications to the 247 machine whereby the relays on certain pairs of amplifiers (C1, C2; D1, D2; D4, D5) could be controlled independently. The -24v supply lead to the energising coil on each of the relays had been rewired so that it could be intercepted at the patch panel. On the panel there were then two holes associated with each relay and if these holes were linked the relay was operated in the usual manner by the main controls. If the link was removed the relays could be independently energised. The arrangement is shown in Fig. B.3.

The feedback loop to affect iteration is shown in Fig. B.4 and it may be seen that there are two special sub-circuits (amplifiers 2 and 3) to apply corrections to the initial condition voltage of amplifier 1 which is in the main circuit. Amplifier 2 acts as a "sample and hold" circuit with a short time constant so that it can rapidly follow the output of amplifier 1. Amplifier 3 is controlled to act as an "integrate and hold" circuit and its output is fed to the initial condition input of amplifier 1.

The 247 machine has two timers, A and B, and in the repetitive mode the normal automatic sequence is:

Problem Check (maintained for time set on timer B)
Compute (" " " " " " A)
Problem Check (" " " " " " B)
etc.

These modes apply to all the amplifiers in the main circuit, including amplifier 1, but excluding amplifiers 2 and 3. (Fig.B.4) To control amplifier 2 so that it does not go into the Problem Check mode when timer A stops, the patch panel links for relays RLa and RLb are removed. Additional control facilities on the computer include a -24v "timer B finish signal" which gives a -24v signal while timer A is running,,but not when timer B is running. This was used to energise relay RLc on the "hold and integrate" amplifier and maintain it in the Hold state while the main circuit was computing for the time set on timer A. When timer A finished and timer B started the -24v signal was switched off automatically and relay RLc become de-energised so that amplifier 3 started integrating and continued to do so for as long as timer B ran. The gain of this circuit is determined by the potentiometer setting and the length which timer B runs.

The complete sequence is shown in Table B.1.

Table B.1

Sequence of events

stage	timer operation	amplifier mode		
		1	2	3
1	B running	P.C.	H	C
2	B stops	P.C.	H	H
3	Hold	H	H	H
4	A running	C.	C (sample)	H
5	A stops	P.C.	H	H
1	B running	P.C.	H	C
etc.				

where P.C. is Problem Check

H is Hold

C is Compute

It was desirable that the special sub-circuits could be set to have zero outputs at the start of a problem or when an overload had occured. This was done by taking connections from relays RLb on amplifiers 2 and 3 to a keyswitch. With the switch in the ON position the integrator capacitors discharged when the main circuit was in the Problem Check mode, and with the switch in the OFF position the amplifiers could operate in Hold or Compute modes only.

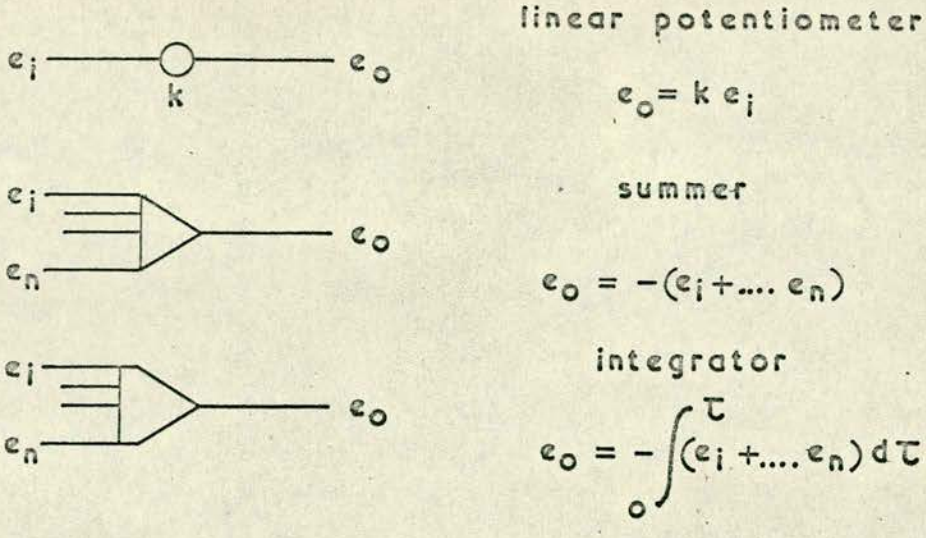

basic sub-circuit symbols

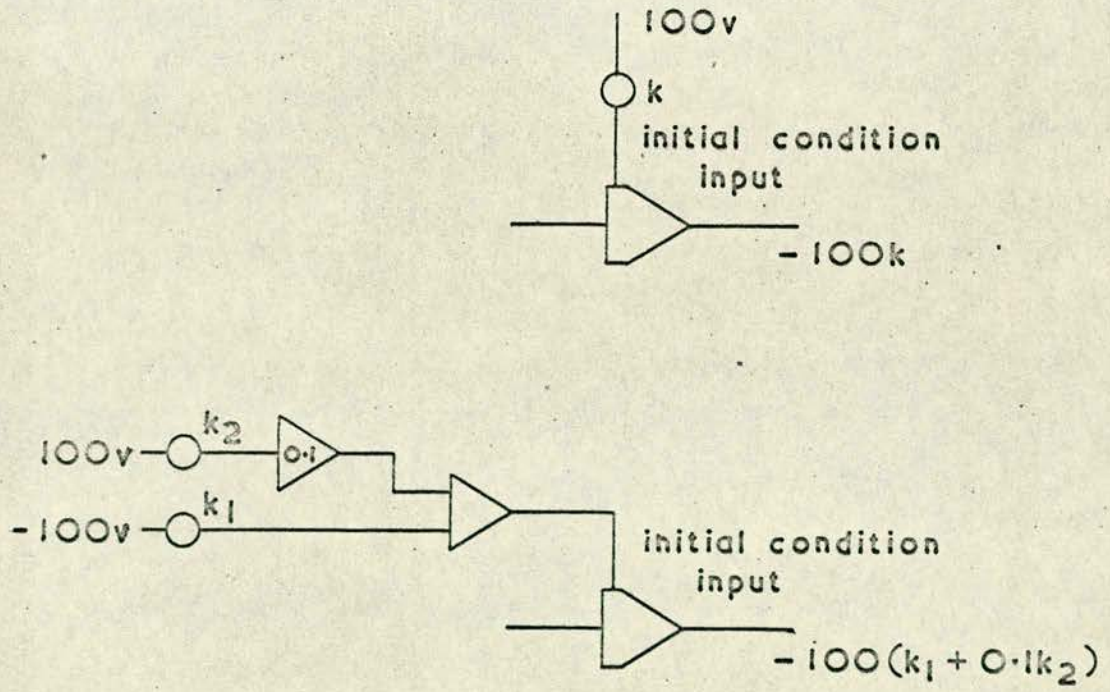

initial condition circuits

FIG. B.1 BASIC SUB-CIRCUITS

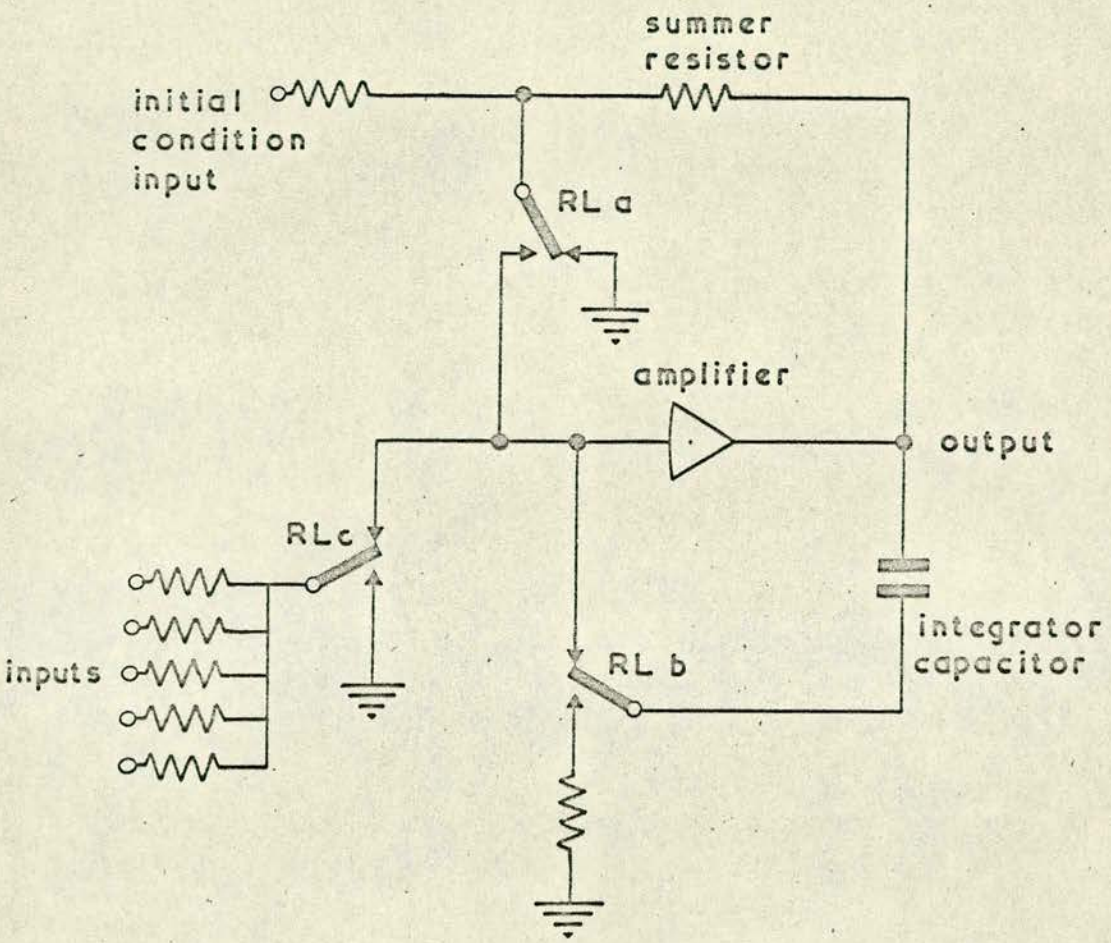

relays shown in the de-energised position

circuit from Solartron 247 manual

FIG. B.2 SIMPLIFIED SUMMER-INTEGRATOR DIAGRAM

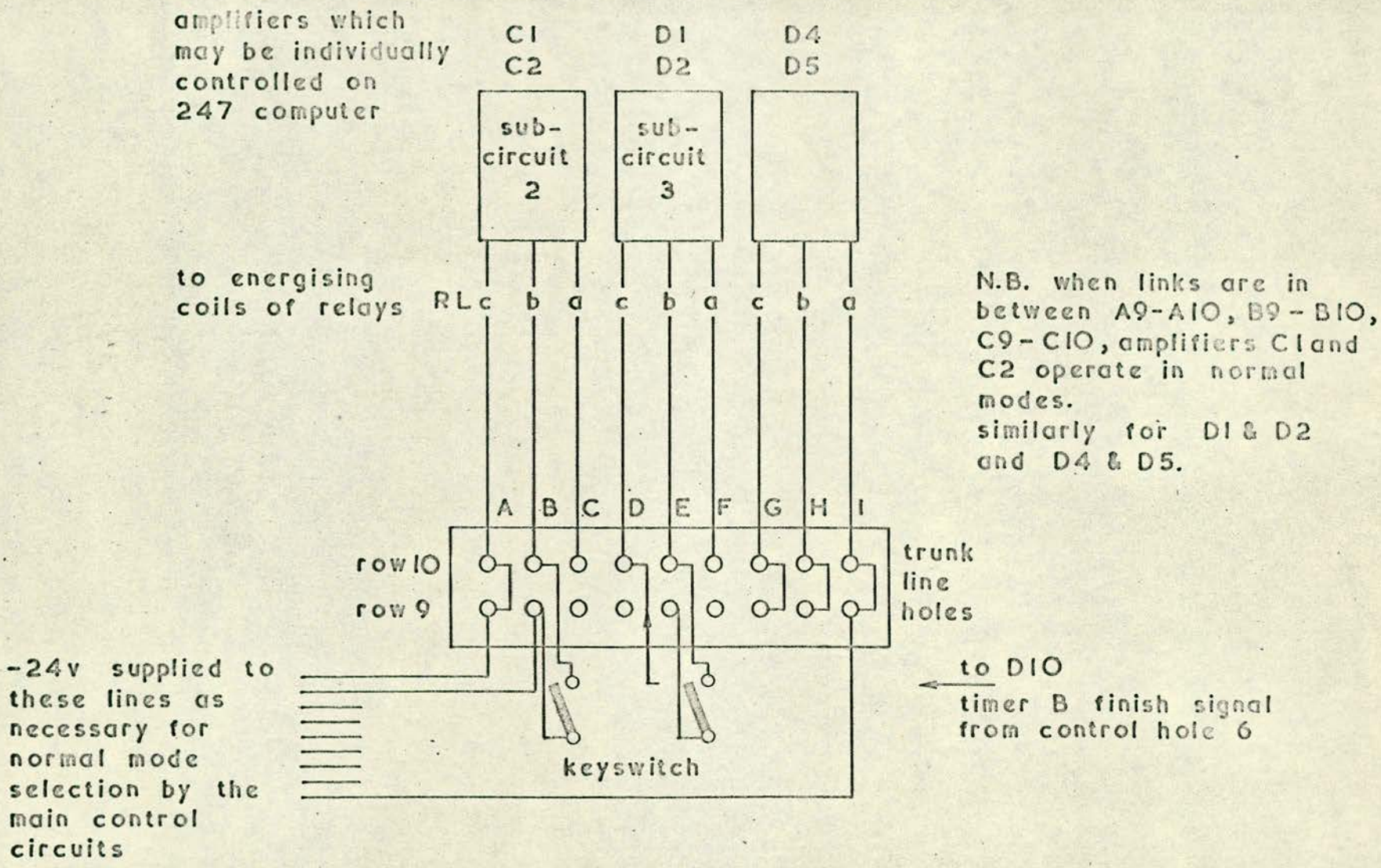

FIG. B.3 PATCH PANEL CONNECTIONS ON 247 COMPUTER

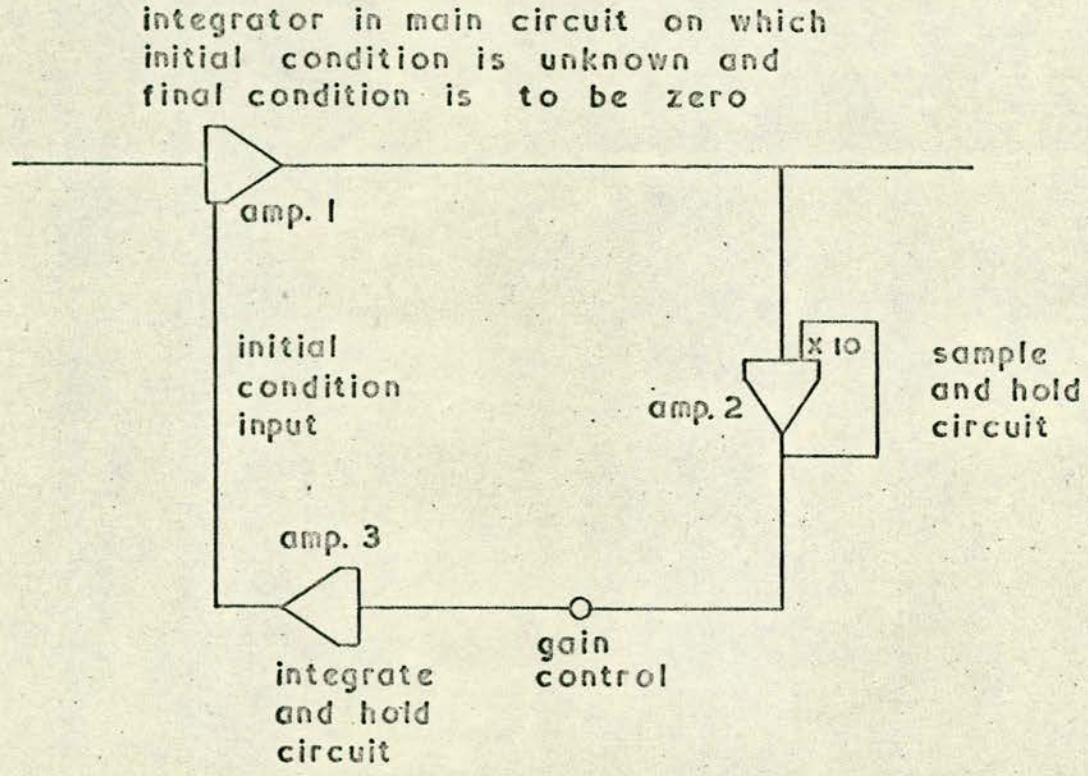

FIG. B.4 ITERATION CIRCUIT

APPENDIX C

AUTOMATIC STRAIN RECORDING EQUIPMENT

Data logging systems may be adapted to accept information from any transducer device which produces an output voltage as the analogue of some physical quantity such as force, pressure, displacement or strain. The equipment described here has basically been designed to be used in conjunction with electrical resistance strain gauges, energised by a direct current, low voltage, power supply.

The application of automatic techniques to the scanning and logging of transducer outputs has proved to be a valuable aid to the rapid collection of experimental results from structural testing. If strain gauges are cemented to a test specimen or structure, the data logging system can measure and record the strains arising from any type of static or quasi-static loading. The present system has provision for one hundred sets of strain gauges to be connected to the equipment (although additional equipment is available to increase this to one thousand) and strains are calculated from voltage readings printed out by the machine on paper tape. These readings may give the strains directly, or may have to be multiplied by a conversion factor (as described in the following section). The machine prints at the relatively low speed of one channel a second, but, even so, a hundred channels may be scanned and recorded in less than two minutes, and if it is intended to use a digital computer, or digital data plotting units, for the analysis of experimental results, then a tape punch may be incorporated into the output system instead of, or as well as, a printer.

Basic strain gauge theory

The fundamental principle of this type of strain measurement is the change in potential difference across the arms of a Wheatstone bridge as a result of changes in resistance of one or more of these arms. The arms are made up of strain gauges (either wire or foil) which are cemented to the specimens under study. The gauge resistances are altered by strains in the specimens or by environmental changes in temperature and humidity.

Since strain is the primary interest here, the gauges are wired up to form one half of a Wheatstone bridge circuit, in sets of active and compensating units; the latter units eliminate all effects other than those due to strain. The actual arrangement of elements on the specimens depends on the phenomena being investigated, whether bending, shear, torsion or direct strains. The other half of the Wheatstone bridge is a pair of matched wire-wound resistors which provide a reference for all sets of gauges.

The circuit for an active and a compensating gauge, with resistances of $R_o + \Delta R$ and R_o respectively, is shown in Figure 2: the reference resistors both have the value R_1. All the other strain gauge half-bridges being used in a given experiment are connected between C and D, as is the low-voltage power supply. The voltage measuring equipment (input impedance R_m) is connected between A and B.

Under steady conditions, the out-of-balance voltage ΔV across points A and B will be given by:

$$\Delta V = U \frac{\Delta R}{4R_o + 2\Delta R + \frac{R_o}{R_m}(4R_o + 3\Delta R)} \qquad (1)$$

where U is the power supply voltage. It may be assumed for practical purposes that:

$\Delta R \leq R_o$, $\Delta R \leq R_m$, and $R_o \leq R_m$, so that equation (1) reduces to:

$$\Delta V = U \frac{\Delta R}{4R_o} \qquad (2)$$

Considering a single gauge of resistance R_o, it may be shown that a strain e, producing a change in resistance of ΔR, is related to ΔR by the equation:

$$\Delta R = R_o k e \qquad (3)$$

where k is the gauge factor. Combining equations (2) and (3)

$$e = \frac{4\Delta V}{kU} \qquad (4)$$

If the value of U is set such that $\frac{4}{Uk} = 10^n$, where n is an integer, then the strain e is produced directly as $e = 10^n$ x (reading from voltage measuring equipment).

Similarly, for materials with linear stress-strain relationships and known elastic constants a suitable value of U may be found such that stress readings are given directly. This is, however, of limited use, for too low a value of U will give inaccurate results because of insensitivity, whilst too high a voltage may damage the gauges and may also cause unwanted heating effects in the specimen.

From equation (4) strains e_1, e_2 .... e_n are available as voltage analogues from resistance strain gauges connected as Wheatstone bridges and these strains may be read by a system consisting of the following units.

1. A low-voltage DC energising power supply with stable characteristics

and a variable output control which allows the selection of any required value of U.

2. A scanning unit for presenting, in turn, to the voltage measuring equipment, the out-of-balance voltages ΔV_1, ΔV_2, ... ΔV_n from the strain gauge half-bridges 1, 2 ..... n.

3. A DC amplifier which amplifies the input voltages ΔV by a known factor K.

4. An analogue-to-digital convertor for reading the amplified voltage $K \Delta V$ and for presenting it in digital form.

5. A printer to record the digital signals.

(In certain cases item 3 might not be required, as sufficient amplification could be available within the digital voltmeter.)

A typical system

Such a system is in use in the Stress Analysis Laboratory of the Civil Engineering Department in Edinburgh University and it has been successfully operating for over a year. The majority of the units were supplied by Blackburn Electronics Ltd., but several other manufacturers produce similar data-logging equipment and the necessary accessories for use with strain gauges. Originally the system incorporated separate balancing facilities (constructed in the laboratory) in the form of potentiometers for each channel. Unfortunately, it proved impossible to balance the circuits exactly; there was always a small residual out-of-balance, and the balancing circuits frequently gave rise to electronic noise which led to discrepancies in the readings. As a result of these deficiencies the balancing circuits were replaced by a common pair of matched resistors to provide a reference half-

bridge for all strain gauge sets. Stability and accuracy have improved as a result; the only drawback is that an initial set of out-of-balance readings must be subtracted from a final set to get the required results for any particular test.. These initial out-of-balances are caused by the small differences in the resistances of the active and compensating gauges.

The units

A photograph of the complete system is shown in Figure 1 and a diagram of the interconnecting wiring in Figure 3. The various units, some commerical, some constructed in the laboratory, are described below.

Gauge connection boxes

Leads from the strain gauges are soldered to terminals on these boxes and a multi-way lead from each box takes the signal inputs and the power supply to the rest of the equipment. It is useful to have several gauge connections boxes, each capable of taking fifty sets of gauges, since they can be attached to various experimental set-ups and plugged in as required. The boxes may be simply constructed from laminated plastics sheet fitted with turret tags in rows of three; two of the tags are connected internally to the low voltage power supply, the third tag, corresponding to A_1, or A_2 or ..... or A_n (Figure 2) is the common terminal of a set of gauges. Thus the active arms are connected between the positive power terminal and tags, A_1, A_2 .....A_n, the compensating arms between the negative terminal and tags A_1, A_2, ...A_n; a positive reading on the instrument therefore indicates a tensile strain.

Strain gauges may be wired to the box by a three-lead system

(for active and compensating gauges which are physically in juxta-position) or by a four-lead system, when the gauges are far apart or when the compensating gauge is to be used for more than one experiment. The particular scanning unit used in this machine will only select inputs in batches of ten and to avoid overloading the data amplifier, by open circuiting, it is essential to have each input in any set of ten coming from a complete bridge circuit. To achieve this, another pair of matched resistors is incorporated as a half-bridge, with the common point, A_p, connected to tags on the gauge connection box. By taking a lead from any signal tag on the box to one of the A_p tags a full bridge of four precision resistors is completed: in addition to preventing open circuits, this provides a check on the stability of the measuring system as a whole (by noting the output over a period of time).

Reference half-bridge circuits

The two half-bridges in the prototype are composed of $100\Omega \pm 0.1$ per cent precision wire-wound resistors, mounted in a Perspex box, with 4 mm sockets providing connections points. Junction B is taken to the scanning unit and junction A_p to the gauge connection boxes.

Low voltage power supply

The energising voltage for the gauges is supplied by a commercial transistorised power pack, with an isolated DC output which is infinitely variable between 0 and 12 volts. When the voltage U is being set the supply is switched to be in parallel with the bridge circuits and with the digital voltmeter: the latter will read the voltage between points C and D (Figure 2).

Scanning commutator

The commutator selects in turn inputs between points A_1, A_2, ... A_n and input B of the reference half-bridge and conveys the signals to the data amplifier. The switching is done by relays, and information is also sent to the digital voltmeter and to the printer in a pre-determined automatic sequence.

There are three modes of commutator operation:

1. CONTINUOUS The instrument scans all available inputs repeatedly.
2. DEMAND All programmed inputs are scanned in turn when a START switch is depressed.
3. SELECT Any required input is selected and held. No scanning takes place.

The DEMAND mode is the most frequently used, and the START switch initiates the following sequence.

1. Select first input (1, 11, 21 etc. according to programming).
2. Present signal (ΔV_1, ΔV_{11}, ΔV_{21}, etc) to the data amplifier.
3. Instruct the digital voltmeter to read the amplified signal $V(= K \Delta V)$ and display it.
4. Instruct the printer to print out the channel number (1, 11, 21, etc) and the signal displayed by the digital voltmeter.
5. Select second input (2, 12, 22, etc) and repeat the cycle.

This sequence is continued until all available inputs have been scanned once. For this type of measurement the scanning rate is generally kept to about one channel a second.

Timing unit

If it is desired to investigate creep, or some other long-term phenomenon, a timing unit can be connected externally to the commutator which will automatically initiate the DEMAND sequence at set intervals.

Data amplifier

DC signals, applied to the input of this unit through the commutator, are amplified by a known factor before being transmitted to the digital voltmeter. On this instrument the amplification factor K can be set to 10,30,100,300 or 1,000, although when small strains are being studied and the maximum amplification is being used it is possible for electronic noise and extraneous signal pick-up to give false readings of the same order of magnitude as the required signals. In such a case several sets of gauges cemented to unloaded specimens should be used as references to estimate the effect of any error, Stray high frequency signals may be eliminated by a filter built into the amplifier.

Digital voltmeter

The digital voltmeter converts the voltage analogue $K\Delta V$ into digital form, and presents it as a four-digit number with the appropriate decimal point and a positive or negative indicator. One side of any input is earthed, while the other side is compared with earth on a linear ramp circuit; the ramp is set by applying to the instrument's input the known output from a pair of standard Weston cadmium cells.

The signal output may also be displayed on an oscilloscope connected in parallel withthe digital voltmeter and this provides a direct visual aid for, say, demonstration purposes.

Printer

The strip printer is connected to the digital voltmeter and the commutator, and it prints any voltage read by the meter (together

with an appropriate channel identification) on three-inch wide paper tape. The paper may be supplied either in rolls or as flip-flop packs.

Auxiliary switch panel

A small panel was made to take a number of switches for purposes such as calibrating the digital voltmeter, and setting up the low-voltage power supply.

Comments on the use of such equipment

Although the units listed here refer to a specific machine the underlying principles are fairly general. The electronic circuitry is complex but it has been presented here in a much simplified form; in practice, care must be taken to avoid pitfalls (such as earth-loop pick-up), if one wishes to obtain the best results.

Obviously an important factor in the choice of measuring equipment is the degree of sensitivity required, together with considerations of stability, reliability and cost. As described, the data-logger has a high degree of resolution, and with maximum amplification a change of one digit at the first decimal place represents only one-third of a microstrain. Its stability is also excellent, a check on this being provided by the complete precision Wheatstone bridge- which shows that the system's output is constant to within the equivalent of one microstrain over long periods. It has been noticed during actual structural testing that the strain gauges are very sensitive to stray draughts and the influence of direct sunshine, and it is difficult to combat these effects with compensating gauges which are inevitably mounted a little distance

from the test piece. Small environmental temperature changes do not, however, noticeably alter the characteristics of the measuring system.

Finally it may be said that the introduction of data-logging systems is an important asset to stress analysts, who are usually faced with problems whose solutions depend on the accurate recording of a large number of strain gauge results.

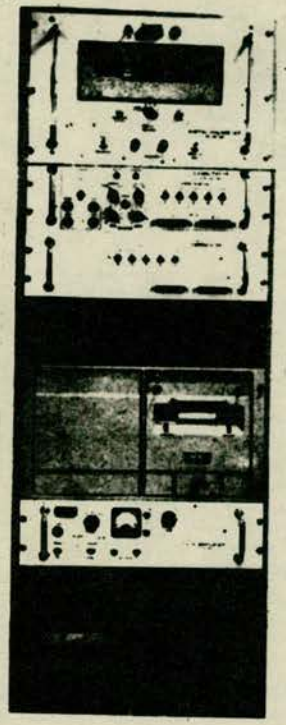

Figure 1: The data logging equipment, showing, from top to bottom, digital voltmeter, 100-channel commutator, reference bridge panel, printer, data amplifier, low voltage power supply and auxiliary switch panel

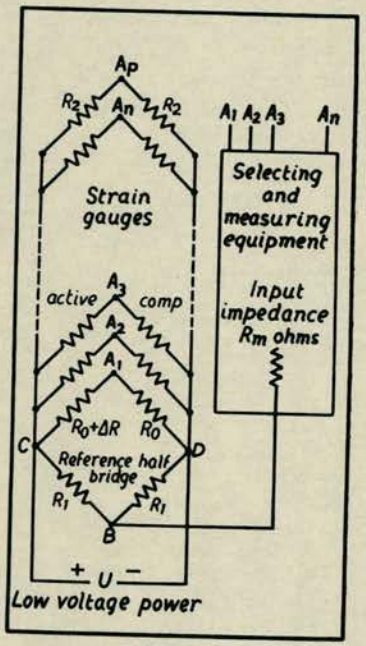

Figure 2: The general arrangement of the Wheatstone bridges formed by the sets of active and compensating strain gauge units. The commutator presents in turn the output from each set of gauges

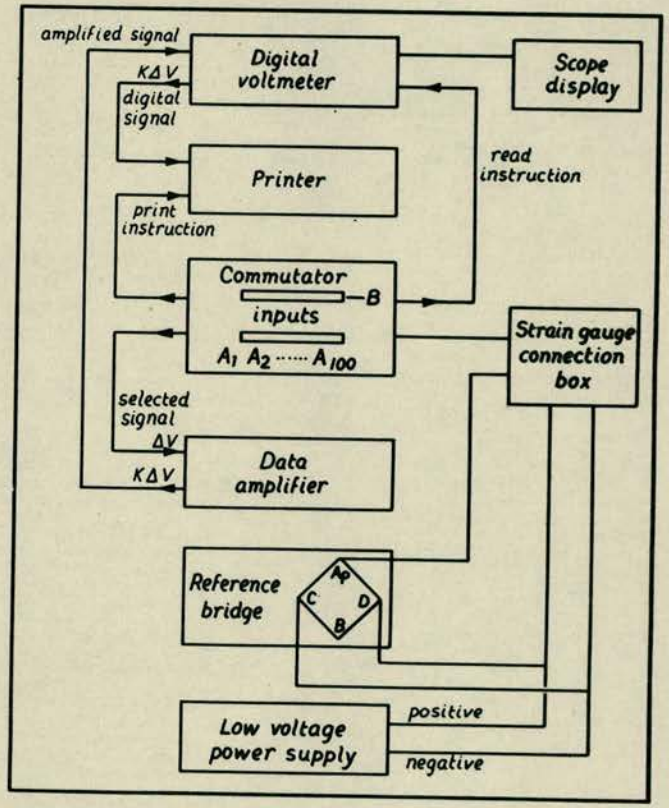

Figure 3: Block diagram of the various units (not in the same vertical order as in Figure 1), showing their inter-connecting wiring

FIG. C

APPENDIX D

EFFECTIVE SLAB WIDTH

As an intermediate form between the skeletal frame and the frameless building comes the structure with slender columns and flat plate floors. Flat slab floors have been used in low rise buildings since 1906 but they have normally been designed for vertical loads only. Under lateral loads the floors serve to distribute forces among the columns and thus act as a type of fixed beam. The behaviour of a column and slab structure is approximately similar to that of rectangular frame but the difficulty is to know what slab width acts as an effective beam. It is possible to consider a slab in terms of a number of discrete elements but a rigorous solution is difficult to achieve, and as a preliminary step tests were carried out on a Perspex model.

A typical reinforced concrete building was designed and the dimensions were reduced in a 40:1 scale to give a model, square in plan, with four 6" x 6" bays each way and four 3" high storeys. The columns were 0.4" square and the slabs (designed by the Chicago method) 0.125" thick. Loading was by dead weights hung from the panel points. Strain gauges were mounted on four of the columns and at various positions on the slabs. A grid of fourteen gauges was set up on the second floor around one of the internal columns (Fig. D.5) to give the strain distribution at a typical column slab junction. Lateral deflections of the columns were measured with variable inductances transducers. The model and its loading frame are shown in Figs. D.1 and D.2.

Several methods were used to determine the effective slab width from the experimental data. Firstly the structure was analysed as a frame by the equivalent column method [1] for different effective slab widths. The theoretical bending moments in the columns were compared with the measured values. No exact fit was found (Fig. D.3) but the best values are given with a ratio of $l_e/l = 0.5$, where l is the slab width between columns and l_e is the effective slab width.

Secondly the measured deflections were compared with deflections computed on the basis of bending only. As may be seen from Fig. D.4, optimum agreement was again obtained for $l_e/l = 0.5$.

The strains on the top surface of a region of the slab at the second floor level are shown in Fig. D.6 . There is a line of inflection at the centre of the span and the strain magnitudes decrease rapidly across the width of the bay. Because axial effects in a frame are small and there is zero measured strain at the centre of the span it will be assumed that the above strains are due to bending only. The third method is based on this assumption and considers the strain energy in the slabs. A plate element of unit width has a flexural rigidity:

$$D = \frac{Eh^3}{12(1 - \nu^2)}$$

and the bending moment at any point is:

$$M = \frac{E\epsilon h^2}{6(1 - \nu^2)} \qquad (D.1)$$

This is only true for a large plate bent into a cylindrical form but

---

(1) Frishmann, W.W., Prabhu, S.S., and Toppler, J.F., Multi-storey frames and interconnected shear walls subjected to lateral loads, Concr. constr. Engng., 58, (6 and 7), 1963.

it will serve as an approximation. The strain energy is such an element of length a is:

$$U_m = \frac{1}{2EI} \int_o^a M^2 \, dx \qquad (D.2)$$

From equation D.1 moments were calculated from the strain gauge readings (ϵ) and these were taken as average moments on 1" wide strips of length a, where 2a is the span between colums (6"). Equation D.2 was then evaluated graphically for each strip and the results were summed to give the strain energy due to bending in a region of slab half a bay long and one bay wide.

The strain energy in a simple beam with end moments is:

$$U_o = \frac{1}{2EI_e} \cdot \frac{M_o^2 \cdot a}{24} \qquad (D.3)$$

where M_o is the total moment in the column at the slab level, and I_e is the effective moment of inertia of the slab. If, therefore, the measured energy in the slabs is compared with the energy in an ideal beam an effective slab inertia can be established. The moment transferred to the slabs (M_o) was measured from the experimental column moment diagram in Fig. D.3. By substitution from equation D.3.the effective slab width ratio was calculated as $l_e/l = 0.622$.

Khan and Sbarounis[2] considered an element of slab as shown in Fig. D.5 to be a grid of intersecting beams. They took into account bending and torsional stiffness and computed effective beam widths for

---

(2) Khan, F.R., and Sbarounis, J.A., Interaction of shear walls and frames, Proc. Am. Soc. civ Engrs, 90, (ST3 Part 1), 1964.

a variety of cases. The theoretical results were checked with experiments on an isolated thin beam subject to central bending moments. Fair agreement was obtained but the boundary conditions were unrealistic and it is to be expected that a portion of a continuous slab will be more rigid than a simple element. From Khan's data the effective ratio for the given example is 0.395.

Results from all of the above methods are summarised in the Table below;

Table D.1

Effective slab width for model (l = 6")

Method	l_e/l	l_e (in)
1. Equivalent column moments	0.5	3.00
2. Frame deflections	0.5	3.00
3. Strain energy	0.622	3.74
4. Khan's data	0.395	2.37

The figures are not conclusive but they provide a tentative guide and it is apparent that the mean value for l_e/l is approximately 0.5. Once the effective slab widths are known the columns can be designed with the aid of any frame technique. It is more difficult to establish the amount of slab reinforcement but appropriate methods are available (3,4).

---

(3) Di Stasio, J., and van Buren, M.P., Transfer of bending moment between flat plate floor and column, J. Am. Concr. Inst., 32, (3), 1960.

(4) Sozen, M.A., and Siess, C.P., Investigation of multiple-panel reinforced concrete floor slabs, Proc. Am. Concr. Inst., 60, (8) 1963.

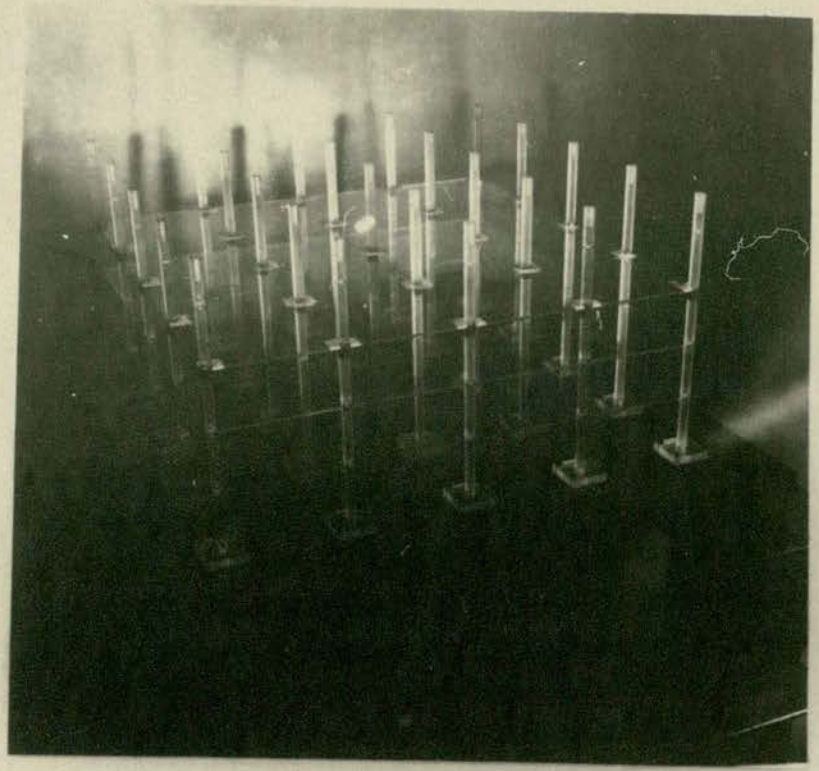

FIG. D.1. The model in the course of construction showing the third floor slab about to be cemented in position.

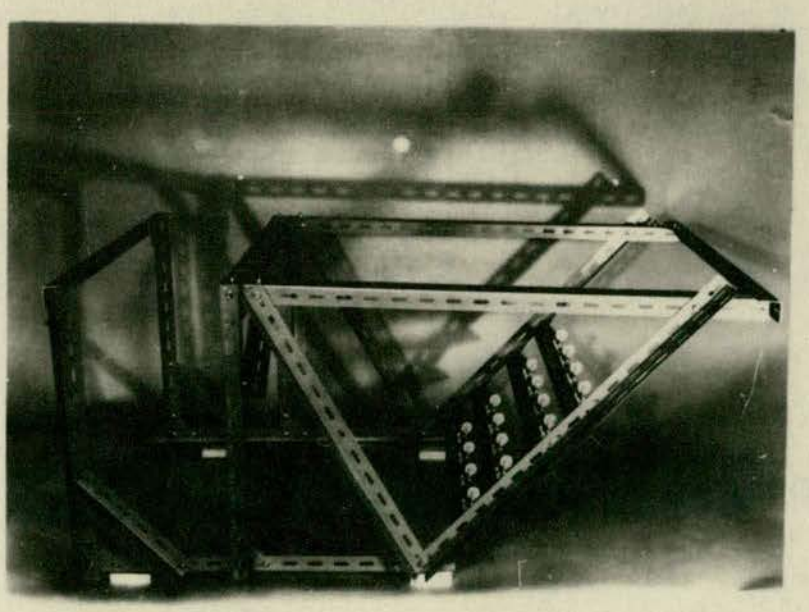

FIG. D.2. Loading frame.

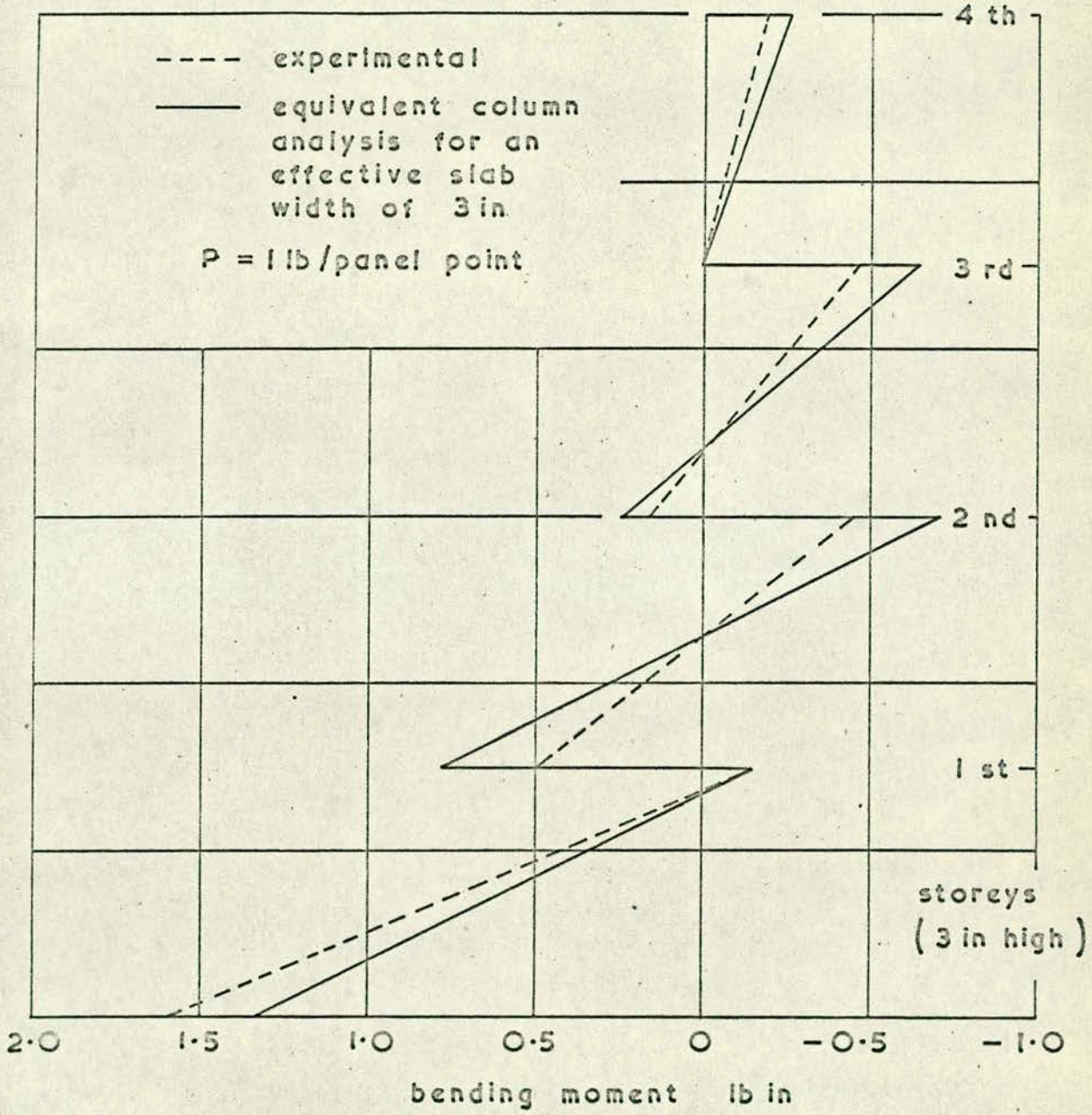

FIG. D.3 COLUMN BENDING MOMENT DIAGRAM

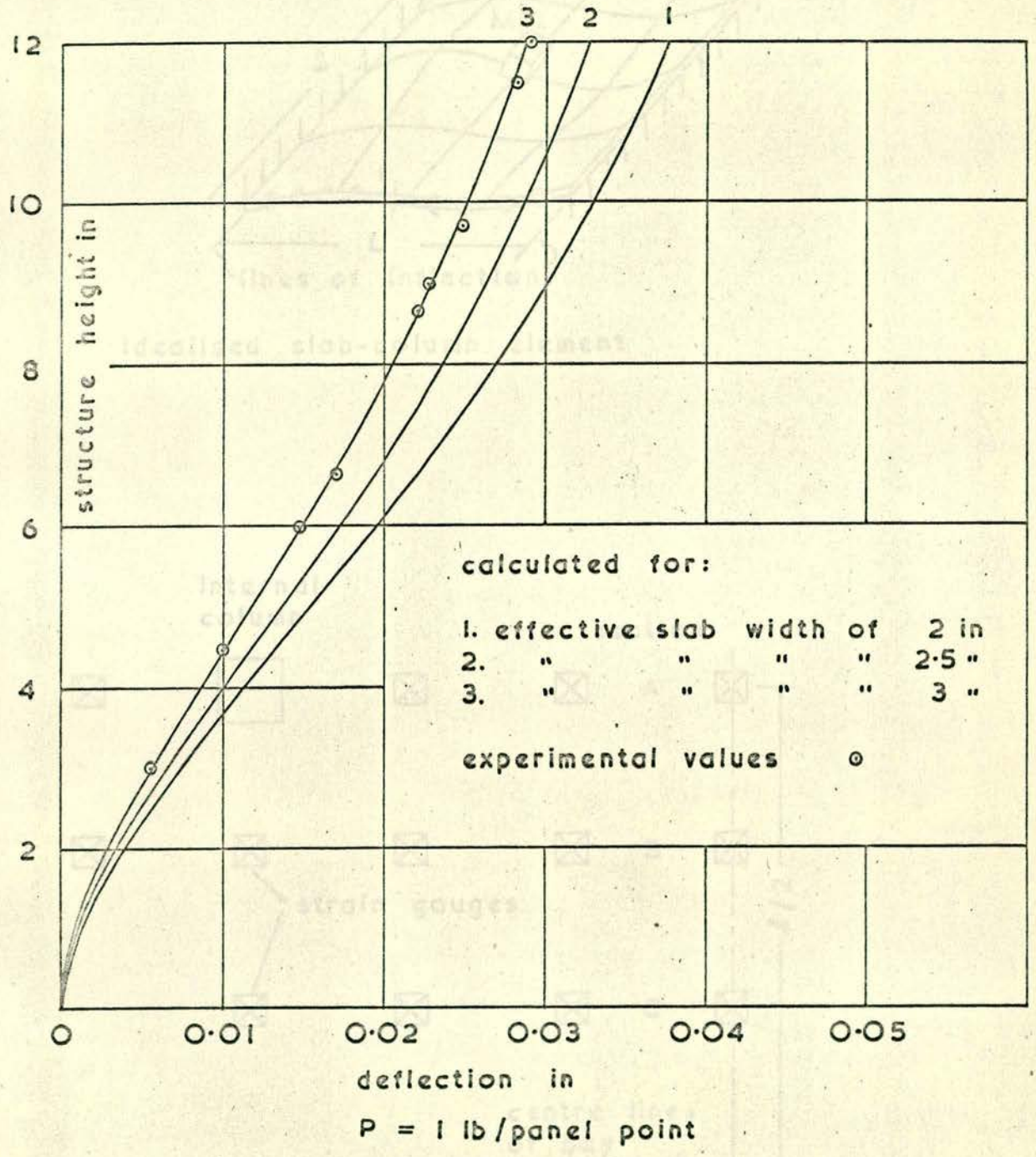

FIG. D.4 DEFLECTION PROFILES

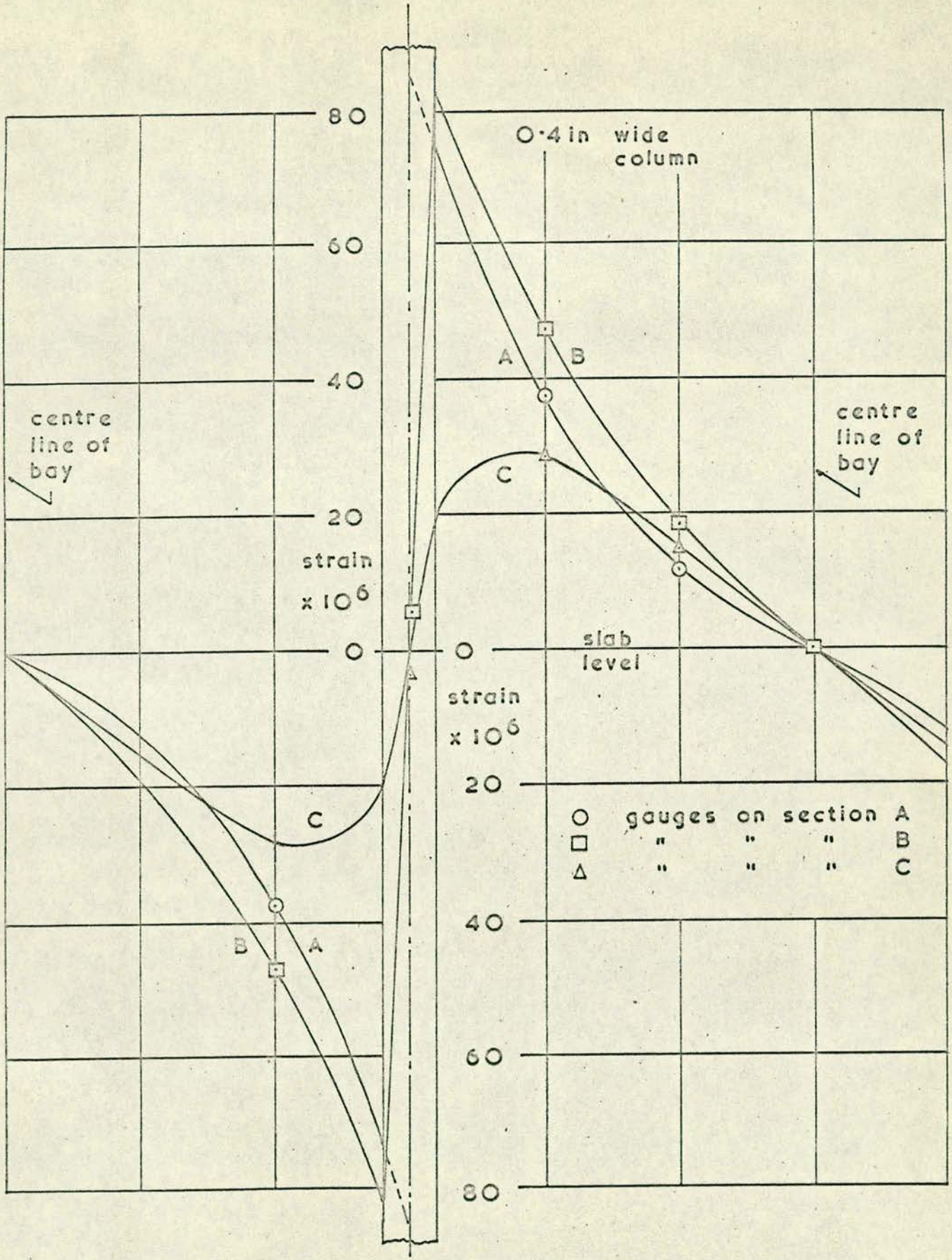

FIG. D.6 STRAIN PROFILES AROUND COLUMN

APPENDIX E

STRESS DISTRIBUTION AROUND A TUNNEL

General

The proposed development of a fourteen storey structure in Liverpool raised unusual foundation problems because the site was directly above part of the Mersey tunnel. This section of the tunnel, which is approximately 29 ft in diameter, runs through sandstone rock strata and the crown is approximately 50 ft below ground level. In order to estimate the distribution of stress around the tunnel the structural consultants, Messrs Bingham Blades and Partners, asked for a photo-elastic investigation. The problem is three-dimensional but it was considered that the analysis of plane stress conditions in a two dimensional model would suffice, although some thought was given to the possibility of using a three dimensional method, such as the technique suggested by Gibson[1].

The models were cast from Araldite MY753 epoxy resin, and, since the tunnel lining is non-structural, each model represented a circular hole in a semi-infinite sheet. The rock was assumed to be elastic and isotropic and because deformations did not alter the action of the external loads the principle of superposition was valid.

Borehole examinations were carried out at the site by Messrs Rock Mechanics Ltd., and their report showed that certain of the rock samples had low tensile strengths (18 lb/in^2 - 80 lb/in^2). The object of the investigation was thereforeto analyse various types of foundation

---

(1) Gibson, J.E., Stress distribution under foundations, Engineering, 180, No. 4680, 1955.

and decide upon a scheme which would produce negligible tension in the region of the tunnel.

Preliminary designs were for a raft foundation (Fig. E.1) but model tests indicated that this would be inadequate so two alternative schemes were proposed. The first of these involved spreading the loads to suitably remote positions on either side of the tunnel by large concrete arches as shown in Fig. E.2a. Although the system was theoretically acceptable it was rejected on economic grounds. Secondly it was suggested that foundation loads could be taken to a suitably deep level by large diameter bored piles. Various pile depths were tested and the final design makes use of 4 ft diameter piles taken to a depth mid-way between the centre of the tunnel and the tunnel bottom (Fig. E.2b).

Self weight stresses

The existing stress state around the tunnel is dependent on the density of the rock and the manner in which the strata were originally deposited, and, because of geological uncertainties, any analysis must be approximate . A theoretical solution was adopted from the work of Savin [2] to find the stresses in a heavy semi-infinite plate of uniform thickness perforated by a hole. The radius of the hole is R and its centre is a distance d from the free surface. A polar co-ordinate system is used with the origin at the centre of the hole and the convention

---

(2) Savin, G.N., Stress concentrations around holes, (translated from the Russian), Pergamon Press, London, 1961.

is as shown in Fig. E.2a. The stresses in the plate due to self weight will be denoted:

$$\sigma_r = \sigma_r^{*} + \sigma_r^{**}$$

$$\sigma_\theta = \sigma_\theta^{*} + \sigma_\theta^{**} \qquad (1)$$

$$\tau_{r\theta} = \tau_{r\theta}^{*} + \tau_{r\theta}^{**}$$

where σ_r is the radial stress (positive compression),

σ_θ is the tangential stress (positive compression),

$\tau_{r\theta}$ is the shear stress.

The stresses with a superscript (*) represent the basic stress state in an infinite sheet with a hole, and the stresses with a superscript(**) represent the particular solution for a semi-infinite plate with a hole.

If γ is the density of the material, ν is Poisson's ratio and λ is a constant whose value will be discussed later, it may be shown that:

$$\sigma_r^{*} = \gamma R \left\{ \left(\tfrac{3}{4} \cdot \frac{r}{R} - \frac{3-2\nu}{4(1-\nu)} \cdot \frac{R}{r} + \frac{\nu}{4(1-\nu)} \cdot \frac{R^3}{r^3} \right) \sin\theta \right.$$

$$\left. + \left(-\tfrac{1}{4} \cdot \frac{r}{R} + \frac{5}{4} \cdot \frac{R^3}{r^3} - \frac{R^5}{r^5} \right) \sin 3\theta \right\}$$

$$\sigma_\theta^{*} = \gamma R \left\{ \left(\tfrac{1}{4} \cdot \frac{R}{r} + \frac{1-2\nu}{4(1-\nu)} \cdot \frac{R}{r} - \frac{\nu}{4(1-\nu)} \cdot \frac{R^3}{r^3} \right) \sin\theta \right.$$

$$\left. + \left(\tfrac{1}{4} \cdot \frac{r}{R} - \tfrac{1}{4} \cdot \frac{R^3}{r^3} + \frac{R^5}{r^5} \right) \sin 3\theta \right\} \qquad (3)$$

$$\tau_{r\theta}^{*} = \gamma R \left\{ \left(\tfrac{1}{4} \cdot \frac{r}{R} - \frac{1-2\nu}{4(1-\nu)} \cdot \frac{R}{r} - \frac{\nu}{4(1-\nu)} \cdot \frac{R^3}{r^3} \right) \cos\theta + \left(-\tfrac{1}{4} \cdot \frac{r}{R} - \tfrac{3}{4} \cdot \frac{R^3}{r^3} + \frac{R^5}{r^5} \right) \cos 3\theta \right\}$$

and:

$$\sigma_r^{**} = \frac{\gamma\lambda R}{4} \left(\left(\frac{r}{R} - \frac{R^3}{r^3} \right) \sin\theta + \left(\frac{r}{R} - 5\frac{R^3}{r^3} + 4\frac{R^5}{r^5} \right) \sin 3\theta \right) - \frac{\gamma d}{2} \left((1+\lambda)\left(1 - \frac{R^2}{r^2}\right) + (1-\lambda)\left(-1 + 4\frac{R^2}{r^2} - 3\frac{R^4}{r^4}\right) \cos 2\theta \right)$$

$$\sigma_\theta^{**} = \frac{\gamma\lambda R}{4} \left(\left(3\frac{r}{R} + \frac{R^3}{r^3} \right) \sin\theta + \left(-\frac{r}{R} + \frac{R^3}{r^3} - 4\frac{R^5}{r^5} \right) \sin 3\theta \right) - \frac{\gamma d}{2} \left((1+\lambda)\left(1 + \frac{R^2}{r^2}\right) + (1-\lambda)\left(1 + 3\frac{R^4}{r^4}\right) \cos 2\theta \right) \qquad (4)$$

$$\tau_{r\theta}^{**} = \frac{\gamma\lambda R}{4} \left(\left(-\frac{r}{R} + \frac{R^3}{r^3} \right) \cos\theta + \left(\frac{r}{R} + 3\frac{R^3}{r^3} - 4\frac{R^5}{r^5} \right) \cos 3\theta \right) - \frac{\gamma d}{2} (1-\lambda)\left(1 + 2\frac{R^2}{r^2} - 3\frac{R^4}{r^4}\right) \sin 2\theta$$

Around the edge of the hole ($r = R$), $\sigma_r = \tau_{r\theta} = 0$ so the tangential stress is :

$$\sigma_{\theta_c} = \left(\sigma_\theta^{*} + \sigma_\theta^{**} \right)_{R=r}$$

$$= \gamma R \left(\left(\frac{1-2\nu}{2(1-\nu)} + \lambda \right) \sin\theta + (1-\lambda) \sin 3\theta \right) - \gamma d \left((1+\lambda) + 2(1-\lambda) \cos 2\theta \right) \qquad (5)$$

Before the hole is made the stress state in the material can be expressed as

$$\sigma_x^{o} = \gamma\lambda (y - d)$$

$$\sigma_y^{o} = \gamma (y - d) \qquad (6)$$

$$\tau_{xy}^{o} = 0$$

The constant λ is thus defined as:

$$\lambda = \frac{\sigma^{\circ}_{x}}{\sigma^{\circ}_{y}}$$

In an elastic isotropic material:

$$\lambda = \frac{\nu}{1 - \nu}$$

It is known [3] that for rocks deposited in a normal manner and not subjected thereafter to horizontal restraints, that $\nu = 0.2$ (approximately), so $\lambda = 0.25$.

There is no evidence of severe vertical cracking from the site tests so the given value of λ (0.25) will be accepted for further calculations.

Equation 5 then becomes:

$$\sigma_{\theta c} = \gamma R \ (0.625 \sin\theta + 0.75 \sin 3\theta) - \gamma \ d(1.25 + 1.50 \cos 2\theta) \qquad (7)$$

The function given by equation 7 was evaluated (Fig. E.3) for a rock density $\lambda = 150$ lb/ft^3 and $d/R = 3.62$ ($R = 14.5$ ft, $d = 52.5$ ft).

Savin states that these equations are accurate for $d/R > 1.5$, however the stress functions were also calculated by an approximate method given by Terzaghi. It may be noted that there are small tensile stresses at the top and bottom of the tunnel while at the sides there are compressive stresses.

Preliminary foundation design

The heaviest superloads come from the central core of the building

---

(3) Terzaghi, K., Measurement of stresses in rock, Geotechnique, X11, (2), June 1962.

and in the preliminary designs these loads were to be transmitted to the 7 ft thick foundation raft through walls. A model was made of a section under two of the walls and it was loaded at two points through a foundation beam as shown in Fig. E.1. Experiments were carried out in a Sharples bench polariscope and tangential stresses around the tunnel were calculated from the fringe patterns given in Fig. E.4. The usual theory of models was used to convert the model stresses to prototype stresses.

$$\sigma_p = \sigma_m \frac{F_d, F_t}{F_p}$$

where σ_p is prototype stresss,

σ_m is model stress,,

F_d is linear scale of model to prototype,

F_t is thickness ratio of model to prototype,

F_p is ratio of load on model to prototype,

and the values were:

F_d = 1:464 ($\frac{3}{4}$" diameter hole representing 29' diameter tunnel)

F_t = 0.25:1 ($\frac{1}{4}$" thick sheet of Araldite representing a 1" thick section of rock)

The experiments showed that the raft foundation would produce tensile stresses (Figs. E.5) at the soffit and invert of the tunnel. When these stresses were added to the exisiting tensile stresses the resultant tension was 80 - 90 lb/in^2 and with measured tensile strength of 1. - 18 to 80 lb/in^2 there was a possibility of failure in the rock at the top and bottom of the tunnel. The experimental stress distribution was checked by an approximate theoretical analysis for the stresses round a hole in a thin plate subject to uniform compression.

Tied arches

On the prototype it would be possible to construct tied arches which would transmit loads from the building as vertical forces to the rock below the abutments on either side of the tunnel. This was simulated on a model by applying, through a stiff beam, two point loads at fixed distances apart. The arches were symmetrical with respect to the tunnel and the spans from centre to centre of the abutments were 2 and 2.5 tunnel diameters, representing to full scale 58 ft and 72.5 ft respectively. To investigate eccentricity effects the point of application of dead weight along the arch was varied. From the experiments it was shown that foundations of this type produce small tensile stresses near the top and bottom of the tunnel when the load is nearly symmetric (Fig. E.6), and tension at skew positions when loading is eccentric. The magnitudes depend on the surface load per inch width below the abutments.

Consider for example a section on either side of the core where there are rows of isolated columns, each approximately 2 ft wide and carrying nearly 1000 tons. Those near the tunnel might be founded on a 58 ft span arch. If the column loads were sited on a 4 ft wide section at the upper level of the abutments and if a 30° spread of load produced uniform compression at rock level 6 ft below this, (i.e. approximately 38 ft above the top of the tunnel with 6 ft deep abutments) then the total load per inch section perpendicular to the tunnel would be:

$$\frac{\text{total load on abutments}}{(\text{effective width of abutment at top} + \text{depth of abutment} \times 2 \sin 30)}$$

$$= \frac{2000}{(48 + 72)} = 16.67 \text{ tons/in}$$

It may be noted from Figs. E.6 and E.7 that with a 2 tunnel diameter arch the maximum tensile stress for symmetric loading is 0.79 lb/in^2 for 1 ton load, and consequently the tensile stress would be 16.67 x 0.79 = 13.2 lb/in^2.

Super load stresses must be added to the self-weight stress system and for λ = 0.25 the existing tension at top and bottom of the tunnel is about 16 lb/in^2, so with this foundation the total would be 29.2 lb/in^2, approximately half of that which would be produced by 2000 ton loading without an arch.

If the loading were not symmetrical then the position would improve because at those points where tension is produced there is already likely to be compression and the net results would be either reduced compression or negligible tension.

Piled foundations.

Preliminary estimates showed that a suitable pile diameter would be 4 ft and that pile centres would be 10 ft from the lateral edges of the tunnel. At those sections where loads would not be directly over the piles post-tensioned concrete beams would be used to span the tunnel region, thus ensuring that all load would be taken to the base of the piles and none would be applied at ground level.

For testing purposes it was assumed that there would be no friction between the piles and the surrounding rock so slots were cut oversize at appropriate distances from the tunnel to take the model piles. Experiments were made for three pile depths to find the shallowest safe level. The minimum tested was for a depth mid-way between the top and bottom of the tunnel, and the maximum at the level of the tunnel bottom.

The section considered for the model was one passing through the diameters of a pair of piles and on the prototype this would carry a load of:

$$F_p = \frac{\text{total load carried by a pair of piles}}{\text{area of pile}} \times \text{diameter of pile} \times \text{width of section.}$$

In all three cases tangential stresses around the tunnel were reduced but the results from the first (i.e. shallowest) showed high stress gradients which meant that there would be undesirably large shear stresses between the pile and the tunnel edge. The other tests were more satisfactory in this respect and there was little difference between them, so it appeared that it would be adequate if piles were taken to a depth three-quarters the way between top and bottom of the tunnel. Super-loads from the piles caused compressive stresses at the sides. If the piles were not loaded equally then skew patterns were produced and a brief study of these indicated that tangential stresses were not serious but a load distribution of the order of 3:1 on a pair of piles could cause high stress gradients. Fringe patterns are shown in Fig. E.8.

Final pile foundation design

After a review of the test results it was recommended that heavy foundation loads should be taken to a suitably deep level by large diameter piles. Prototype calculations, however, showed that in certain regions beneath the tower block the piles would have to be constructed in tandem pairs. The original model results could not therefore be applied directly and a further model had to be tested to simulate the behaviour of the outer pair of piles.

A section was considered through piles 1, 2, 3 and 4 as shown in Fig. E.2b. These piles are staggered in plan so that no section can in fact be drawn through them all. However, the analysis was, of necessity, approximate so the most severe case possible was taken: a line section through the centres of the four piles. The pile loads are unsymmetric but it will be demonstrated that eccentricity effects are negligible.

Table E.1.1

Pile loads

pile	load (tons)
1	800
2	940
3	800
4	627

The stresses caused by the inner pair of piles (2 and 3) were found from the original model tests and at the sides of the tunnel the tensile stress in the prototype is 115 lb/in^2. From the model results for the outer piles it may be seen in Fig. E.9. that the form of stress distribution is similar to that shown in Fig. E.8 but magnitudes are, as expected, lower. The maximum prototype tension from the outer piles is 60 lb/in^2.

By addition the resultant tensile stress from pile super-loads is 175 lb/in^2 and from the estimates of existing conditions due to self-weight the compression at the tunnel sides is 150 lb/in^2. The net tensile stress is therefore (175-150) 25 lb/in^2. The complete stress distribution around the tunnel is shown in Fig. E.10.

The models were also tested eccentrically with pile loads in the ratios of 2:1 and 3:1. The results showed large differences in compression at the foot of each pile but tension at the tunnel sides was not seriously affected. For the 3:1 ratio the stress increase at the heavily loaded side was 20% so the small eccentricity of the prototype (approximately 1.1:1) would be insignificant.

Podium columns

No special precautions had been taken with the foundations for isolated podium columns so the design conditions were checked by model analysis. The row carrying the heaviest load above the tunnel was considered and three columns (denoted B3, B4 and B5) were simulated by point loads at the surface. The model was loaded first above the centre and then above the tunnel edge and super-position was used to obtain the results.

Table E.2

Podium column loads

column	simulated position	load (tons)
B3	vertically above tunnel edge	170
B4	" " " centre	133
B5	" " " edge	115

The reinforced concrete foundation pads are 24" thick and 48" square, the columns being 15" square. A 30° dispersion angle would give approximately uniform pressure over a 42.6" square region at rock level and knowing the column load, the load on a 1" wide slice

at this level could be established.

The model was in effect a two dimensional section and the stresses on this were scaled to give the following results (Fig. E.11).

Table E.3

Podium column stresses

tunnel top

column no.	prototype load on 1" slice (lb)	scaled fringe value	no. of fringes	prototype stress (lb/in^2)
B3	8.94×10^3	5.21×10^{-4}	2.5	11.67
B4	7.00×10^3	7.35×10^{-4}	3.5	18.00
B5	6.05×10^3	5.21×10^{-4}	2.5	7.90

tensile stress at tunnel top: 37.57 lb/in^2

tunnel bottom

B3			1.8	8.40
B4	as above	as above	1.5	7.71
B5			1.8	5.69

tensile stress at tunnel bottom: 21.80 lb/in^2

In practice the load will be spread along the longitudinal axis of the tunnel. No values are known for the angle of dispersion but it is assumed to be rather less than for concrete. Two examples are given below of calculations for net tensile stresses using the estimated values of self-weight tensile stresses at the top and bottom as 12 and 16 lb/in^2 respectively.

Table E.4

Resultant stresses from podium columns

tunnel top (existing tension 12 lb/in^2)

angle of dispersion in rock	stress from Podium columns (lb/in^2)	resultant stress (lb/in^2)
0	38.0	50.0
10°	7.0	19.0
20°	3.7	15.7

tunnel bottom (existing tension 16 lb/in^2)

0	22.0	38.0
10°	4.0	20.0
20°	2.1	18.1

Compressive stresses are produced at the sides of the tunnel but their magnitudes are insuffient to cause trouble. In the absence of severe vertical cracking the loads will be spread at least 20° so it is apparent the effect of the podium loads is negligible in the region of the tunnel.

Conclusions

Two sections have been examined corresponding to the most heavily loaded sections in the designed scheme of foundations. Extreme conditions have been assumed and prototype stresses have been extrapolated from model tests.

Between the double rows of piles the net tensile stress at the sides of the tunnel is 25 lb/in^2. Under the podium columns the net tensile stress at the bottom of the tunnel is 18 lb/in^2. These values

are of the same order as the smallest recorded tensile strength of the rock (18 lb/in^2). The analysis, however, has been severe and in practice the stresses will be considerably smaller than the quoted figures.

It must be emphasised that all of the preceding calculations are based on ideal elastic and isotropic assumptions and therefore will only approximate to the behaviour of the real system. Faulting, layers of differing materials, and uncertainty about the properties of the rock can lead to errors, so the results are a guide rather than an accurate prediction.

A positive method of checking would be to put stress plugs at selected points on the tunnel, probably the bottom, to find the existing stresses and use a second set, adjacent to the first, to observe changes as the structure is erected. However the tests show that there is an adequate factor of safety if the foundations are constructed so that they apply loads to the prototype in the same manner as loads were applied to the models.

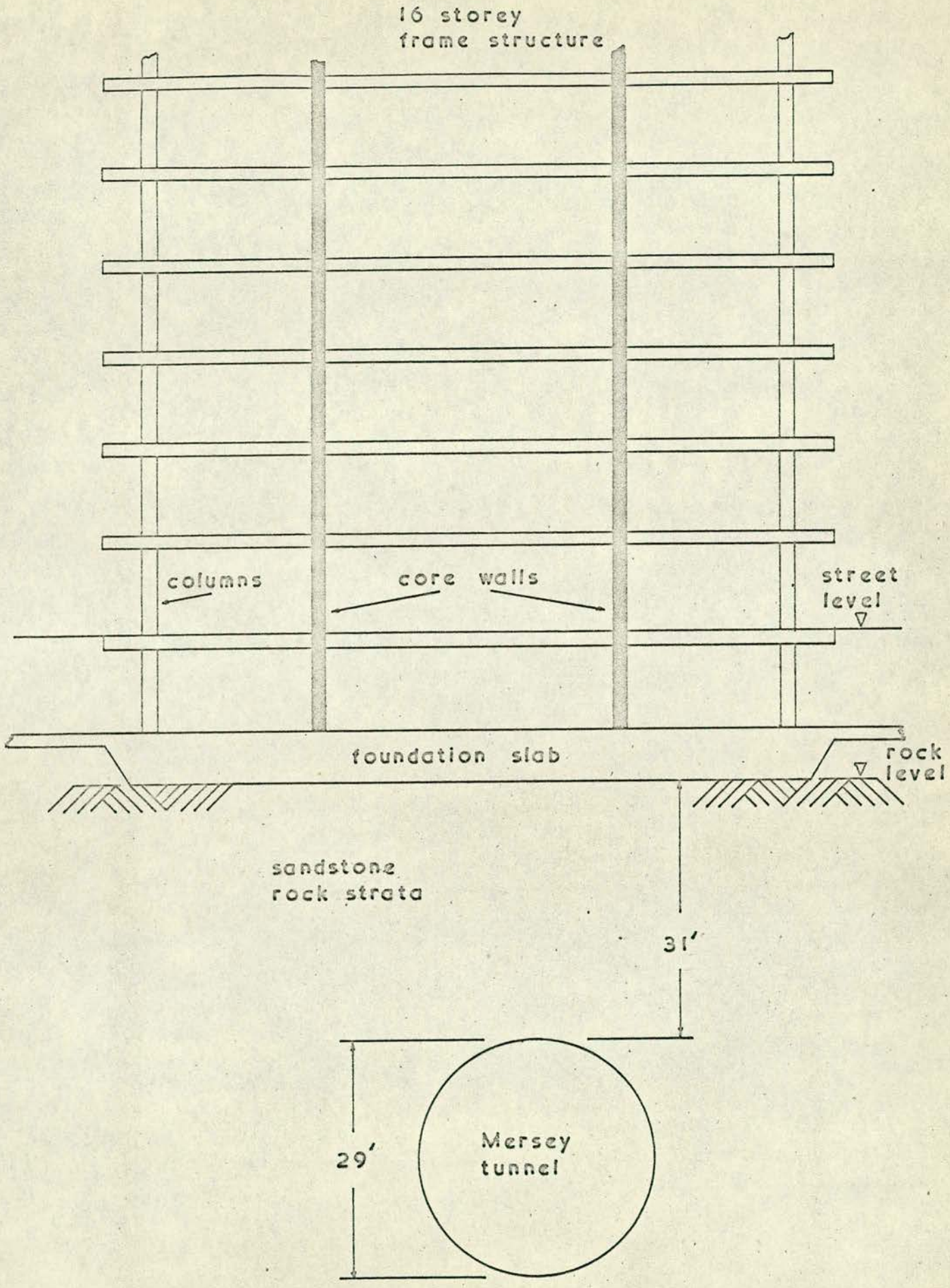

FIG. E.1 ORIGINAL FOUNDATION SCHEME

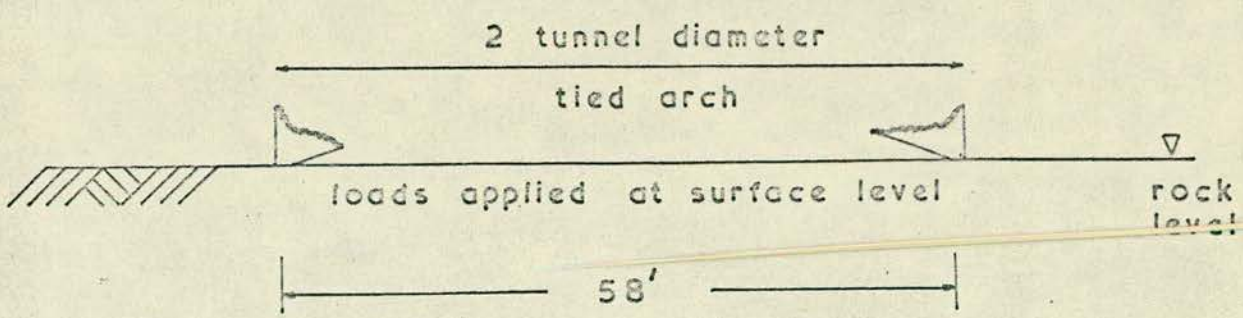

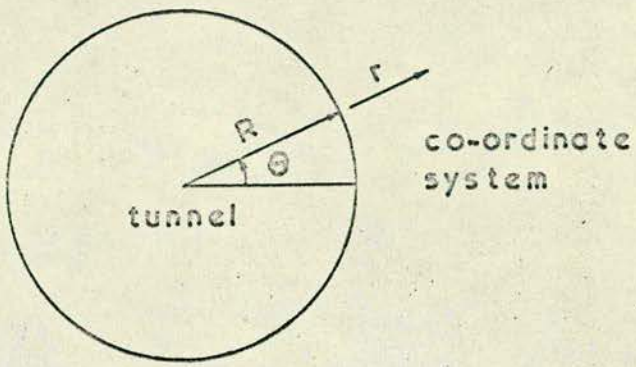

FIG. E.2a TIED ARCH FOUNDATION

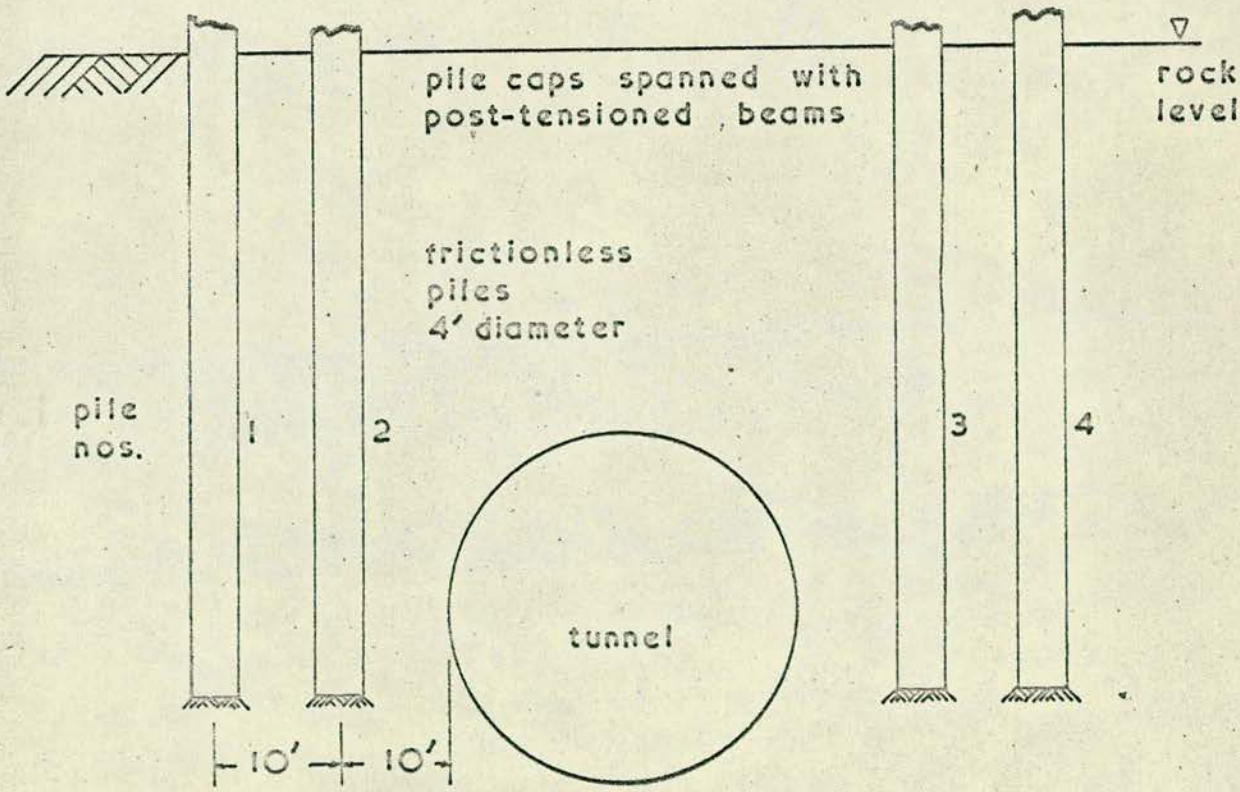

FIG. E.2b PILED FOUNDATIONS

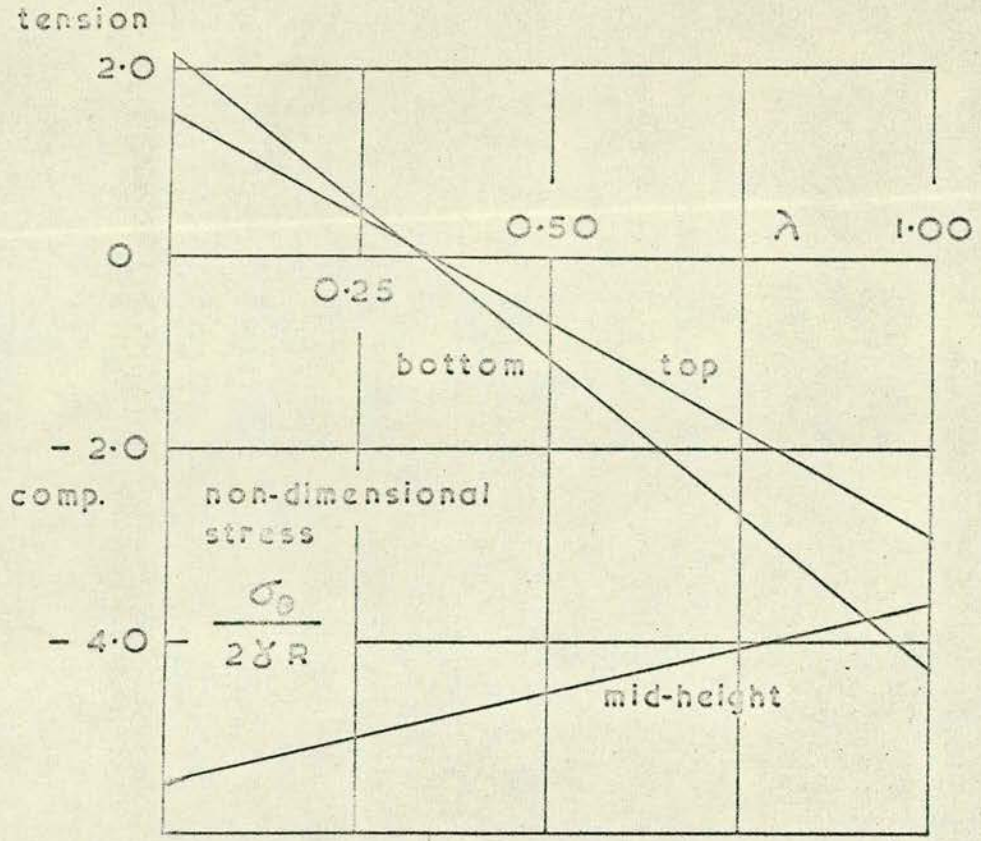

NON-DIMENSIONAL STRESS

$\frac{d}{R} = 3{\cdot}62$

λ is ratio of horizontal initial stress to vertical initial stress

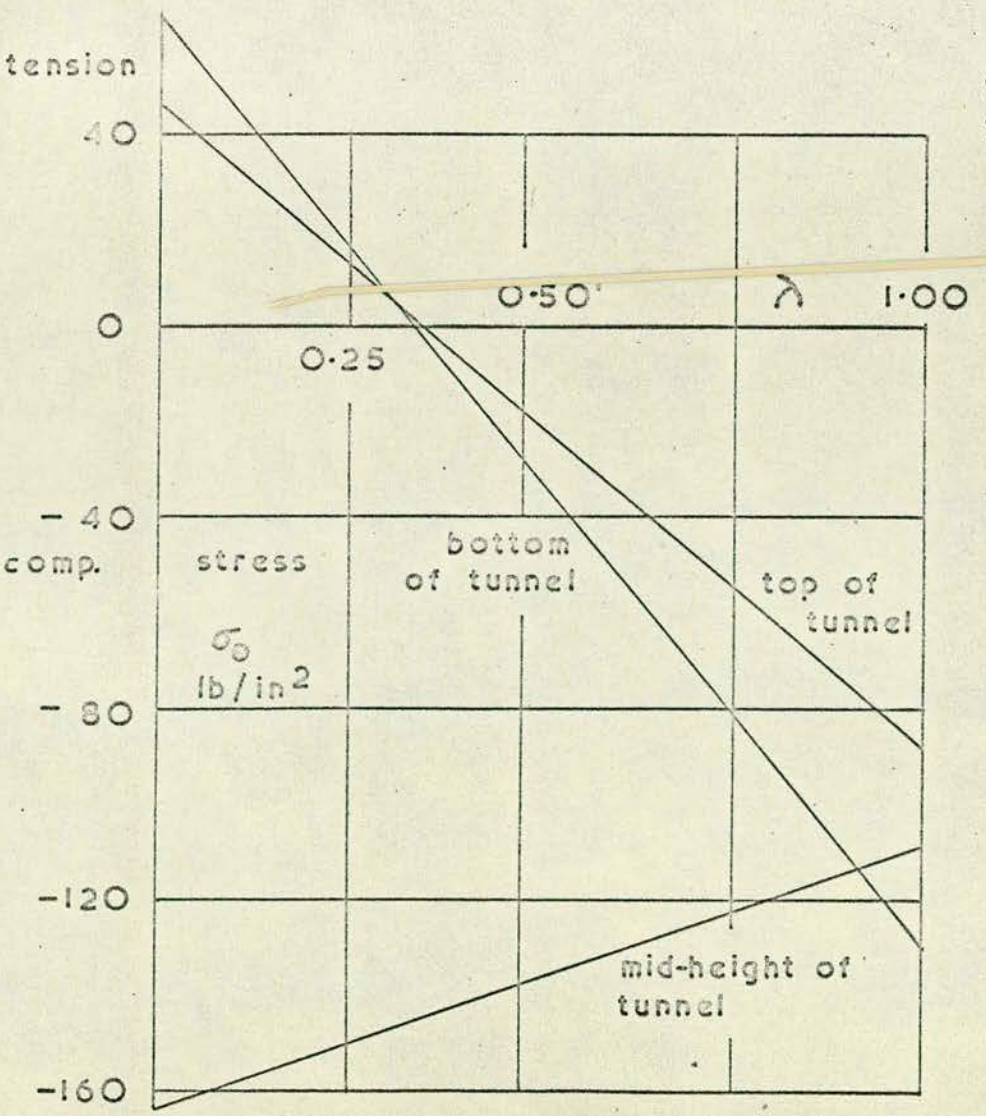

SELF-WEIGHT STRESS

$\nu = 0{\cdot}2$

$\gamma = 150$ lb/ft^3

$R = 14{\cdot}5$ ft

FIG. E.3

FIG. E.4.

Fringe pattern for raft foundation

load 300 lb

model fringe value 180 lb/in^2

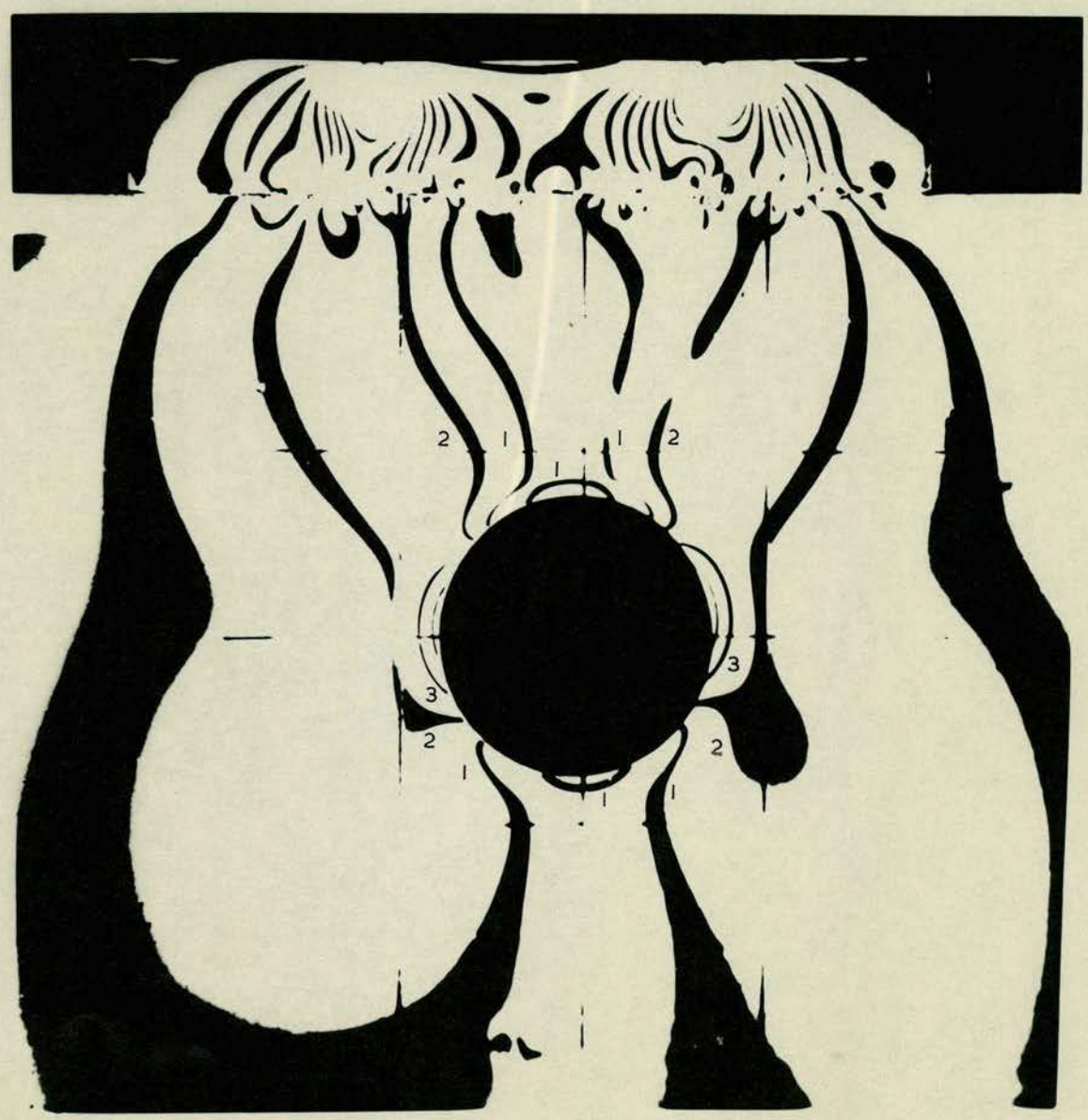

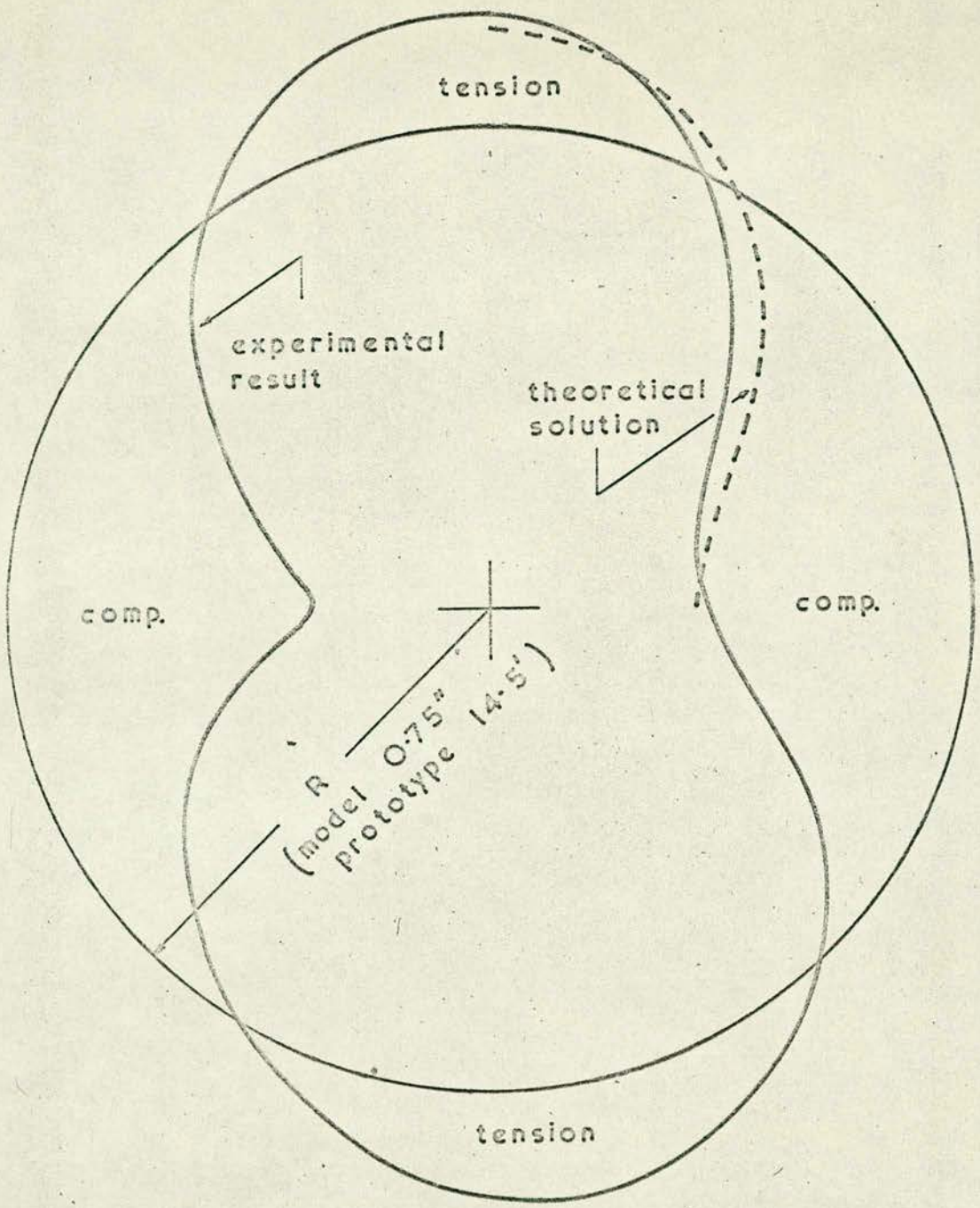

radial plot of boundary stresses

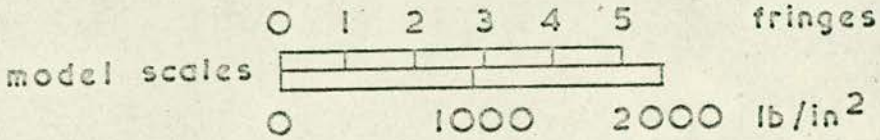

see fig. E.4 for loading

FIG. E.5 STRESS DISTRIBUTION FROM RAFT FOUNDATION

FIG. E.6

Fringe pattern for 2D arch foundation

load 420 lb
(symmetrical)

model fringe value 125 lb/in^2

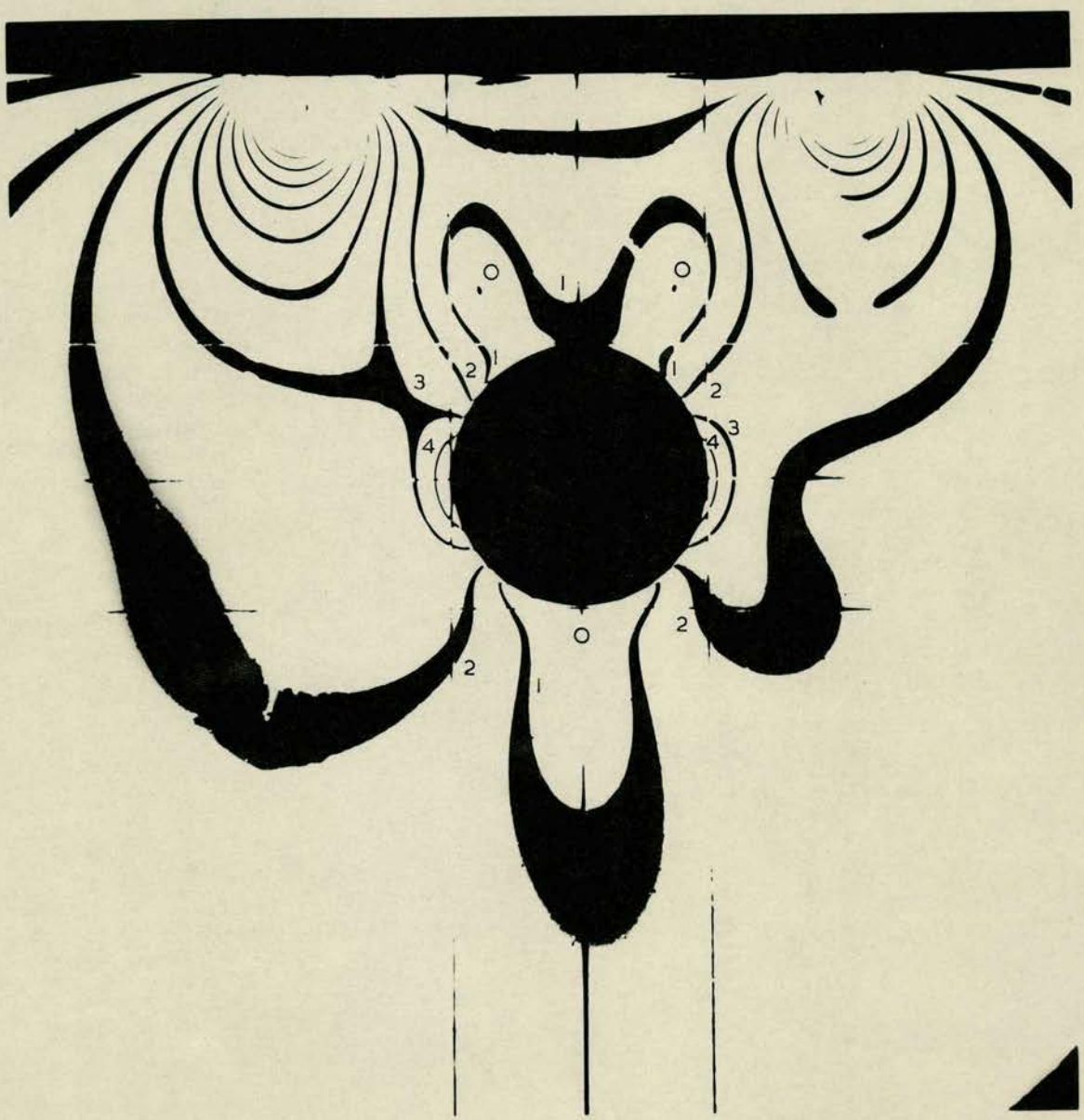

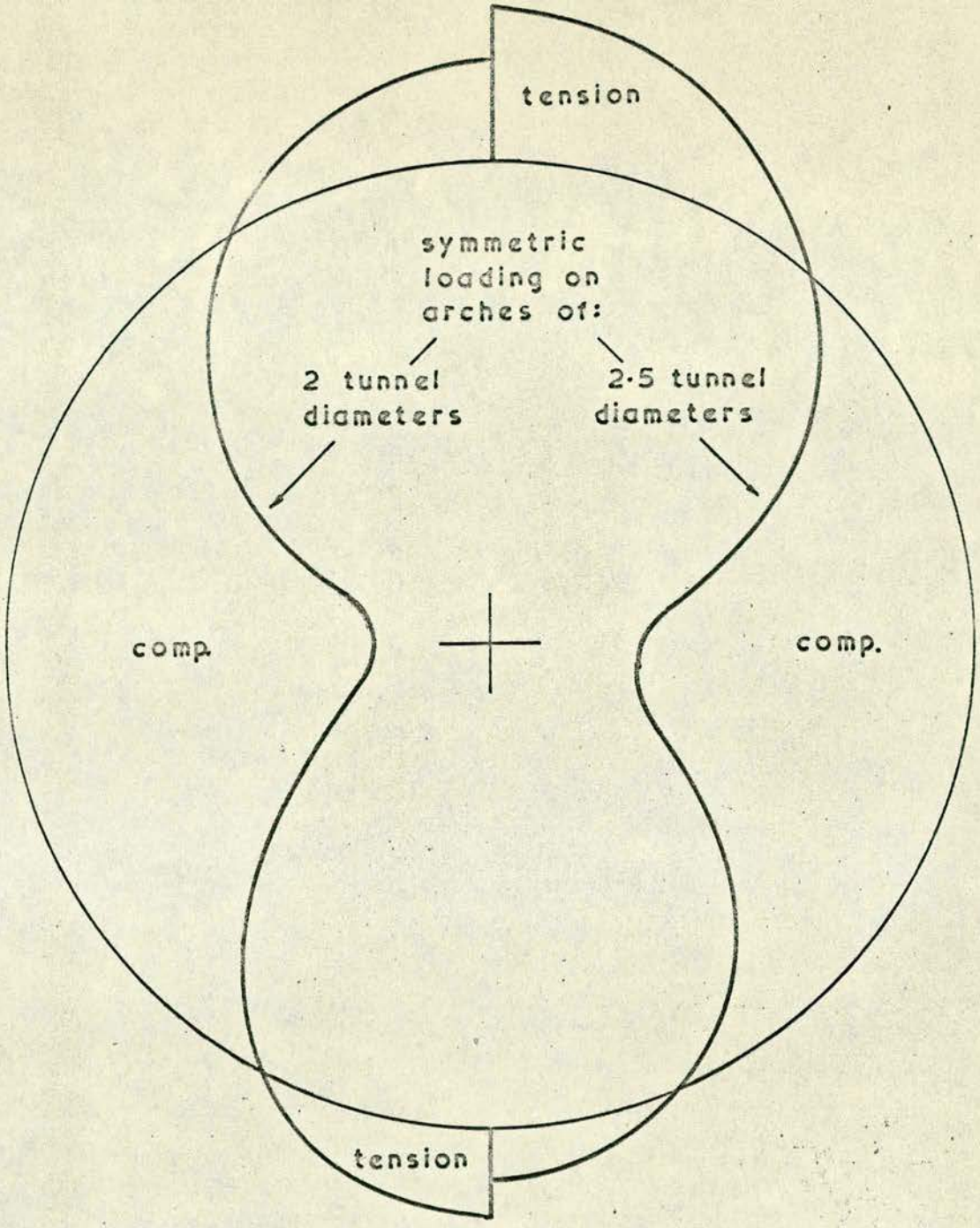

radial plot of boundary stresses

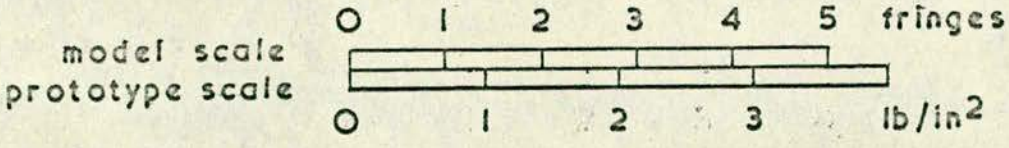

for a load of 1 ton on 1 in wide section

see fig. E.6 for loading

FIG. E.7 STRESS DISTRIBUTION FROM ARCH FOUNDATION

FIG. E. 8

Fringe pattern for
inner pair of piles

load 420 lb
(symmetrical)

model fringe value 125 lb/in^2

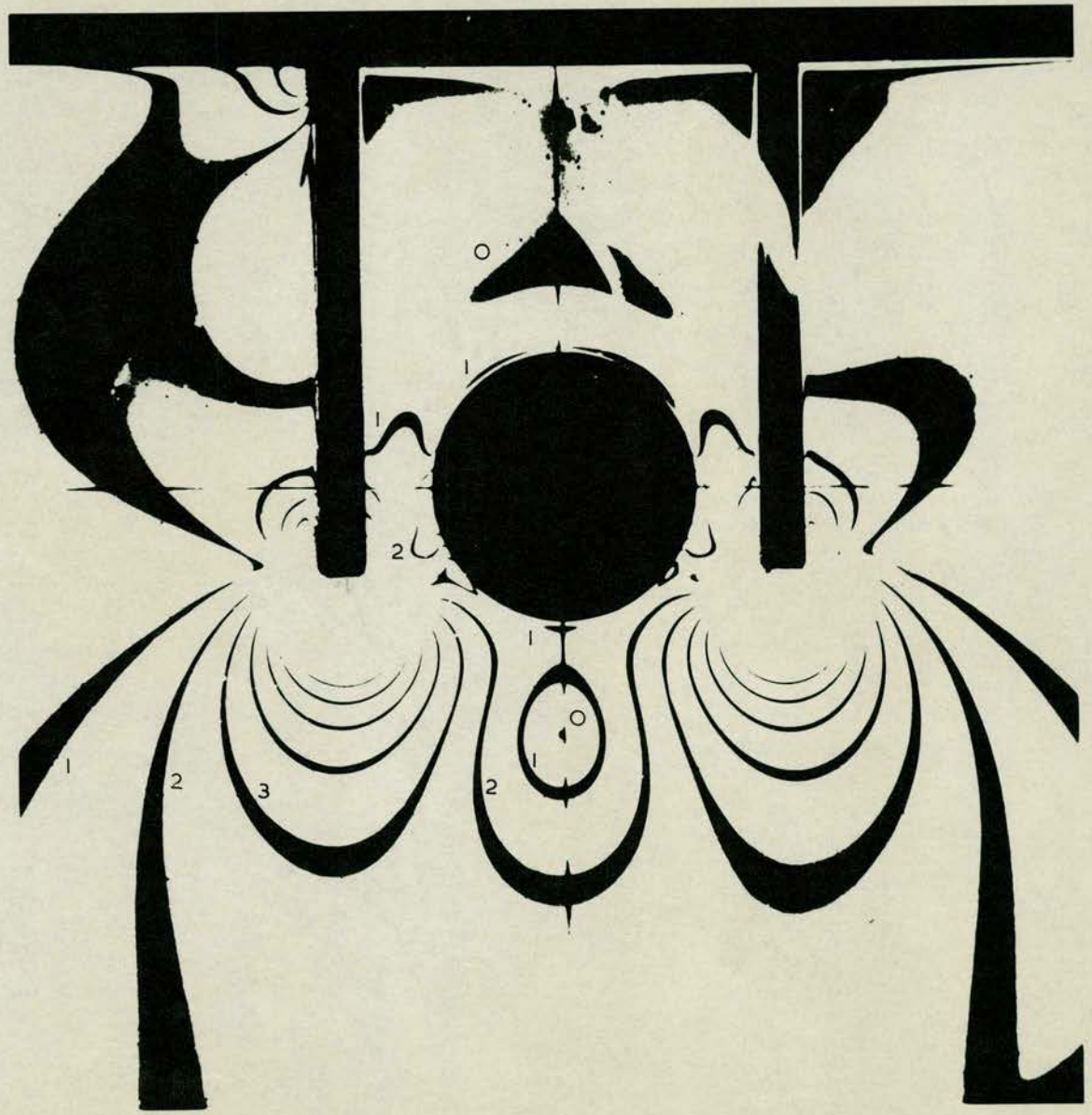

FIG. E.9

Fringe pattern for
outer pair of piles

load 420 lb
(symmetrical)

model fringe value 184 lb/in^2

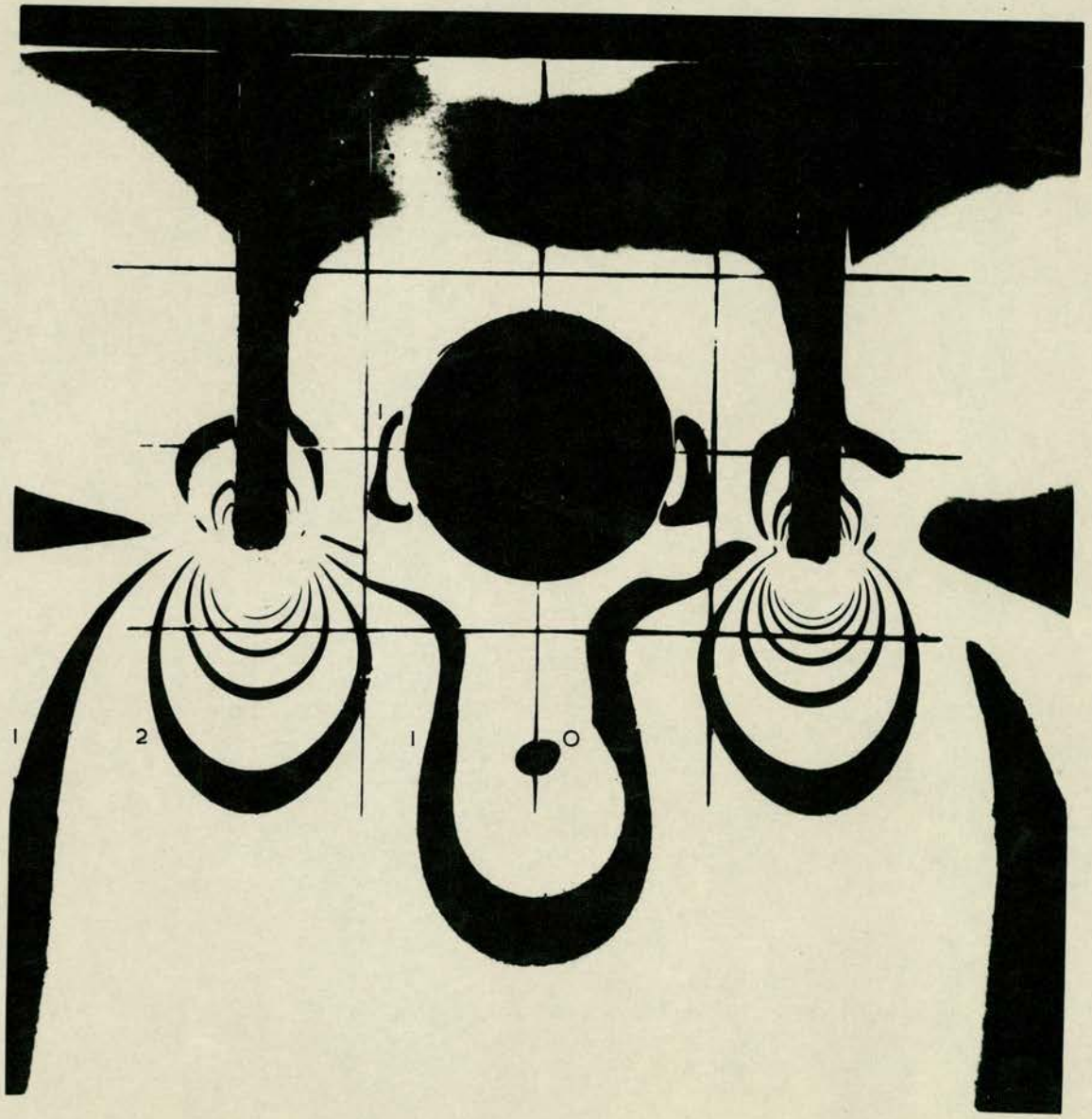

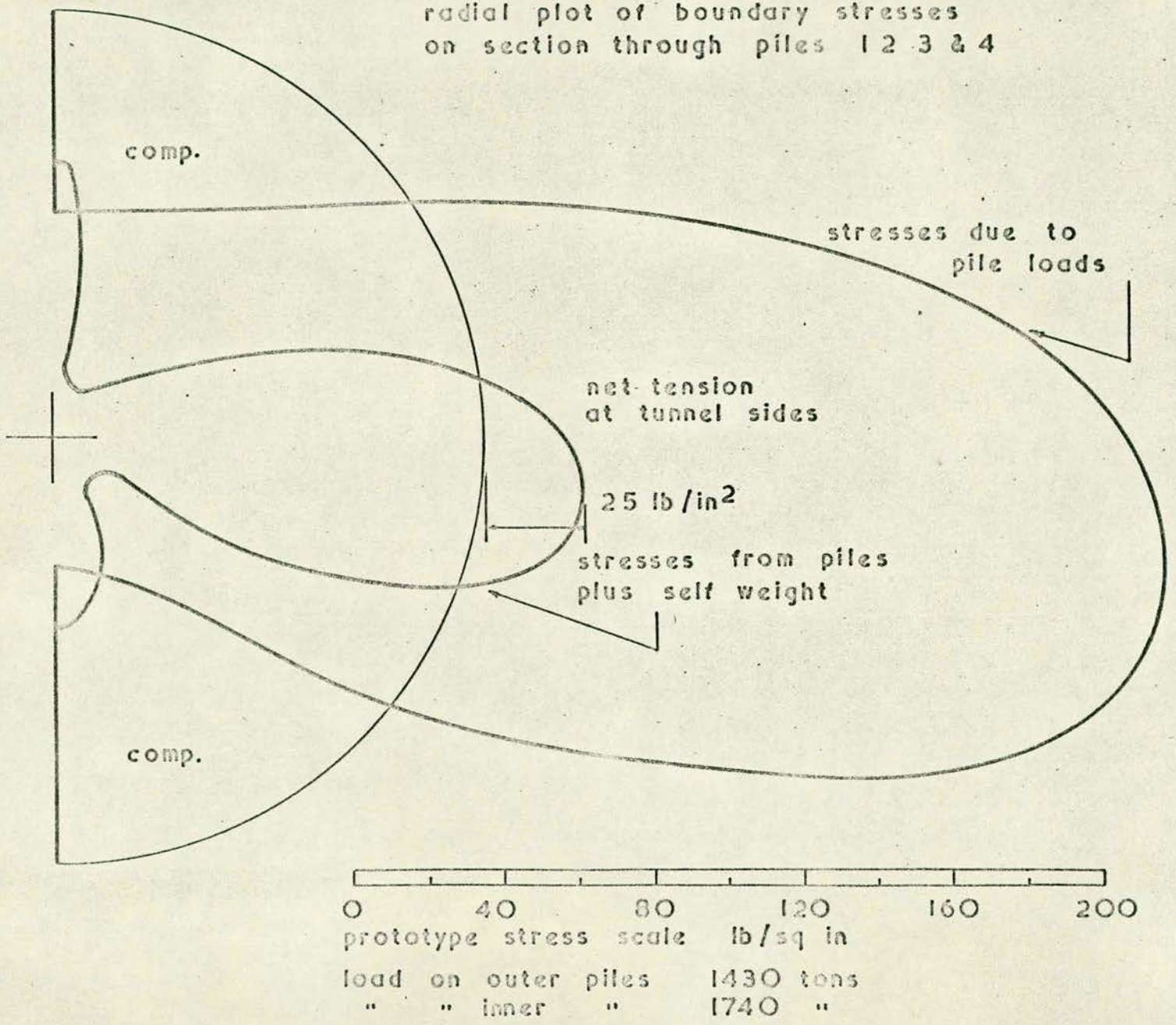

FIG. E.10. RESULTANT STRESSES FROM PILED FOUNDATIONS

FIG. E.11

Fringe pattern for podium column load

load 379 lb
(above tunnel edge)

model fringe value 184 lb/in^2